Universität Hamburg
DER FORSCHUNG | DER LEHRE | DER BILDUNG

Adhesion mediated pre-activation of T cells

Dissertation

Zur Erlangung der Würde des Doktors der Naturwissenschaften des Fachbereichs Biologie der Fakultät für Mathematik, Informatik und Naturwissenschaften der Universität Hamburg

vorgelegt von

Lola Carmen Hernandez Cabrera

Hamburg, 2022

Folgende Gutachter empfehlen die Annahme der Dissertation:

Prof. Dr. rer. nat. Dr. med. habil. Andreas H. Guse

Prof. Dr. rer. nat. Hans-Willi Mittrücker

Datum der Disputation: 19.04.2022

Contents

Abbreviations

ADP	adenosine diphosphate
AP-1	activator protein-1
APC	antigen presenting cell
ATP	adenosine triphosphate
BSA	bovine serum albumin
Ca^{2+}	calcium
cADPR	cyclic adenosine diphosphoribose
CC	coiled-coil
CD	cluster of differentiation
CFP	cyan fluorescent protein
CICR	calcium induced calcium release
Co-IP	co-Immunoprecipitation
CRAC	calcium release activated channels
CRACM	calcium-release-activated calcium modulator
DNA	deoxyribonucleic acid
HRP	horseradish peroxidase
SDS	sodium dodecyl sulfate
SDS PAGE	SDS polyacrylamide gel electrophoresis
PVDF	polyvinylidene fluoride
DAG	diacylglycerol
DM	dichroic mirror
DUOX2	dual NADPH oxidase 2
EM	emission filter
ER	endoplasmic reticulum
FAK	focal adhesion kinase
FAT	focal adhesion targeting
FRET	fluorescence resonance energy transfer
FRNK	FAK-related-non-kinase
GPCR	G protein-coupled receptors
Grb7	growth factor receptor bound protein 7
HN1L	hematological and neurological expressed 1–like protein
ICAM-1	intercellular adhesion molecule-1

I_{CRAC}	store operated calcium current
IFN-γ	Interferon-γ
IL-2	interleukin-2
IP_3	d-*myo*-inositol-1,4,5-trisphosphate
IP_3R	d-*myo*-inositol-1,4,5-trisphosphate receptor
ISM	imaging scanning microscope
ITAM	immuno-receptor tyrosine-based activation motifs
JNK	Jun N-terminal kinase
JPT2	jupiter microtubule-associated homolog 2
LAT	linker for activation of T cells
Lck	lymphocyte-specific protein tyrosine kinase
LFA-1	lymphocyte function-associated antigen 1
MCU	mitochondrial Ca^{2+} uniporters
Mek	MAPK/extracellular protein kinase
MHC	major histocompatibility complex
MLPHA	micro-lens added pinhole array
NAADP	nicotinic acid adenine dinucleotide 2'-phosphate
NAD	nicotinamid adenine dinucleotide
NCLX	$Na^+/Ca^{2+}/Li^+$ exchangers
NCX	Na^+/Ca^{2+} exchanger
NFAT	nuclear factor of activated T-cells
NFκB	nuclear factor-κB
P2RX	purinergic ionotropic receptors
PBS	phosphate – buffered salt solution
PI-3	phosphoinositide-3
PIP_2	phosphatidylinositol 4,5-bisphosphate
PIP_3	phosphatidylinositol (3,4,5)-trisphosphate
PKC-θ	protein kinase C theta
PLC-γ	phospholipase C-γ
PM	plasma membrane
PMCA	plasma membrane Ca^{2+} ATPase
PSF	point spread functions
RasGRP	ras guanyl nucleotide-releasing protein

RNA	ribonucleic acid
RNAi	RNA interference
RT	room temperature
RYR	ryanodine receptor
SAM	sterile α-motif
SE	stimulated emission
SERCA	sarcoplasmic/ER Ca^{2+} ATPase
SH2	Src Homology 2
SH3	Src Homology 3
siRNA	short interfering RNA
SLP-76	SH2 domain containing leukocyte protein
SNR	signal-to-noise ratio
SOAR	STIM-ORAI activating region
SOCE	store-operated Ca^{2+} entry
SoRa	super resolution via optical reassignment
STED	stimulated emission depletion microscopy
STIM	stromal interaction molecule
TCR	T cell receptor
Tg	thapsigargin
T_H cells	helper T cells
TM	transmembrane
TPC	two pore channel
T_{reg} cells	regulatory T cells
TRP	transient receptor potential channels
TRPML	melastatin subfamily of TRP channels
VCAM-1	vascular cell adhesion molecule 1
VLA4	very late antigen-4
WT	wildtype
YFP	yellow fluorescent protein
ZAP-70	zeta-chain-associated protein kinase-70
λ	wavelength

Figure Index

Table Index

Abstract

T cells are an essential part of the adaptive immune system and play a central role in cell-mediated immune response. Their activation leads to an increase of the free cytosolic Ca^{2+} concentration ($[Ca^{2+}]_i$), which can be described by two main pathways: (i) the release of Ca^{2+} from intracellular Ca^{2+} stores into the cytosol and (ii) Ca^{2+} influx from the extracellular space through Ca^{2+} channels located at the plasma membrane (PM). Once activated, T cells proliferate and migrate into the inflamed tissue, thereby binding to other cells or extracellular matrix (ECM) proteins via integrins.

Already in 2018, our lab observed formation of local Ca^{2+} microdomains in the absence of TCR stimulation. However, up to now their detailed molecular mechanism could not be fully elucidated.

In this thesis, the involvement of various components (such as FAK, IP_3R, and SOCE proteins) in adhesion-induced pre-activation of T cells was investigated.

Therefore, we utilized three different advanced optical methods: fluorescence resonance energy transfer (FRET), Super Resolution via Optical Re-assignment (SoRa) and Stimulated Emission Depletion (STED) microscopy. Overall, STED microscopy provided the most accurate information for protein localization due to the achievable spatial resolution of up to 40 nm. Furthermore, the formation of clusters could be determined and it was even possible to dissect them into loose and tight clusters. Here, a tight cluster is defined as an interaction between proteins that is visible as a single spot due to its tight localization. Loose clusters, on the other hand, display an accumulation of these spots in a defined region. Based on the existent crystal structures of individual proteins, we were able to examine individual clusters in more detail. Therefore, it was possible to estimate the number of proteins that accumulate at a site.

Next, for the first time, adhesion-dependent co-localization with ORAI1, as well as clustering of FAK, the three IP_3R subtypes and SOCE proteins (ORAI1 and STIM1/2) could be determined. The increased co-localization and cluster formation of ORAI1, STIM1, FAK and IP_3R1, due to adhesion, suggests an essential role of these proteins in pre-activation of T cells. In addition, the data supports the hypothesis that SOCE activation by STIM1 is critical after adhesion, whereas STIM2 serves to regulate Ca^{2+} levels.

In conclusion, these results demonstrate a pre-activation state of T cells evoked by adhesion to ECM proteins, involving FAK, IP_3R1, and activation of SOCE. Therefore, our findings can be summarized in a three-state model of T cells: (i) quiescent state, (ii) adhesion pre-activated state and (iii) fully activated state upon TCR stimulation.

Zusammenfassung

T-Zellen sind ein wesentlicher Bestandteil des adaptiven Immunsystems und spielen eine zentrale Rolle bei der zellvermittelten Immunantwort. Ihre Aktivierung führt zu einem Anstieg der freien zytosolischen Ca^{2+}-Konzentration ($[Ca^{2+}]_i$, der über zwei Hauptwege beschrieben werden kann: (i) die Freisetzung von Ca^{2+} aus intrazellulären Ca^{2+}-Speichern in das Zytosol und (ii) der Ca^{2+}-Einstrom aus dem Extrazellulärraum durch Ca^{2+}-Kanäle in der Plasmamembran (PM).

Nach ihrer Aktivierung vermehren sich die T Zellen, wandern in das entzündete Gewebe ein und interagieren dabei über Integrine mit anderen Zellen oder Proteinen der extrazellulären Matrix (ECM).

Bereits 2018 wurde von unserem Labor die Bildung lokaler Ca^{2+}-Mikrodomänen in Abwesenheit einer TCR-Stimulation beobachtet. Deren detaillierter molekularer Mechanismus konnte jedoch bisher nicht vollständig aufgeklärt werden.

In dieser Arbeit wurde die Beteiligung verschiedener Komponenten (wie FAK, IP_3R und SOCE-Proteine) an der Adhäsions-bedingten Vor-Aktivierung von T-Zellen untersucht.

Dazu wurden zunächst drei verschiedene hochauflösende optische Methoden verglichen: *Fluoreszenz-Resonanz-Energie-Transfer* (FRET), *Super Resolution via Optical Re-assignment* (SoRa) und *Stimulated Emission Depletion* (STED) Mikroskopie. Dabei lieferte die STED-Mikroskopie, aufgrund der erreichbaren hohen räumlichen Auflösung von bis zu 40 nm, die genauesten Informationen zur Proteinlokalisierung. Darüber hinaus konnte die Bildung von Clustern bestimmt werden, wobei die Möglichkeit besteht zwischen schwachen und starken Clustern zu unterscheiden. Eine starke Cluster-Bildung wird dabei als eine Interaktion zwischen Proteinen definiert, die aufgrund ihrer dichten Lokalisierung als ein einzelner Punkt sichtbar sind. Bei schwachen Clustern hingegen handelt es sich um eine Ansammlung dieser Punkte in einer definierten Region. Anhand der vorhandenen Kristallstrukturen einzelner Proteine waren wir in der Lage individuelle Punkte genauer zu untersuchen und die Anzahl der Proteine abzuschätzen, die sich zu Clustern zusammenfinden.

Im Folgenden wurden erstmals eine adhäsionsabhängige Ko-Lokalisierung mit ORAI1, sowie die Clusterbildung von FAK, den drei IP_3R-Subtypen und SOCE-Proteinen (ORAI1 und STIM1) festgestellt. Die erhöhte Ko-Lokalisierung und Clusterbildung von

ORAI1, STIM1, FAK und IP_3R1 aufgrund von Adhäsion lässt auf eine wesentliche Rolle dieser Proteine bei der Voraktivierung von T-Zellen schließen. Darüber hinaus unterstützen die Daten die Hypothese, dass die SOCE-Aktivierung durch STIM1 nach der Adhäsion entscheidend ist, während STIM2 zur Regulierung des Ca^{2+}-Spiegels dient.

Zusammengefasst deuten die Ergebnisse auf eine Voraktivierung von T-Zellen durch Adhäsion an ECM-Proteine hin, wobei FAK, IP_3R1 und die SOCE Proteine von essenzieller Bedeutung sind.

Aufgrund der erhobenen Daten lässt sich der Zustand von T-Zellen in ein drei-Stadien-Modell zusammenfassen: (i) ruhender Zustand, (ii) durch Adhäsion voraktivierter Zustand und (iii) vollständig aktivierter Zustand nach TCR-Stimulation.

1. Introduction

1.1 The immune system and its cellular components

The immune system consists of a number of different effector cells and molecules, which protect the body from pathogens. It is divided into the innate and adaptive immune system (Bittar et al., 1996). Immediately after infectious organisms enter the body, the innate immune system is activated as the first step in an immune response. The reaction proceeds quickly, widespread and nonspecific, resulting in the release of cytokines and chemokines, which attract further immune cells to the site of infection. In addition, cells of the innate immune system, such as macrophages and dendritic cells, act as antigen-presenting cells (APCs) migrating to the lymphoid tissue. Here, antigenic peptides are presented on major histocompatibility complex (MHC) to naive T cells (Lin and Loré, 2017). Upon binding by the T cell receptor (TCR), a naive T cell gets activated, proliferates and differentiates into specific effector T cells (Broere et al., 2011). At this point, the adaptive immune response is initiated.

While the innate immune response starts immediately, the adaptive immune response takes several days to develop (Lazar, 2002). Mature T cells express, in addition to the TCR, either the Cluster of Differentiation (CD)4 or CD8 receptor. Based on this, the cells are subdivided into two groups. The $CD4^+$ T cells include T helper (T_H) cells, as well as the regulatory T cells. Cytotoxic T cells, on the other hand, belong to the group of $CD8^+$ T cells (Murphy and Weaver, 2018), which induce apoptosis or necrosis in cells infected with viruses or other intracellular pathogens. T_H cells send signals, usually by releasing certain cytokines. These cytokines in turn activate other cells such as B cells (for antibody production) or macrophages (for phagocytosis and killing of pathogens). The T_H cells further develop into a number of different subsets of effector cells. These are defined as T_H1, T_H2 and T_H17 cells (Seder and Paul, 1994; Weaver et al., 2006). The T_H1 cells activate macrophages via Interferon-γ (IFN-γ) secretion and CD40 expression. The T_H2 and T_H17 subsets, on the other hand, produce specific cytokines that stimulate reactions against extracellular bacteria and fungi. Regulatory T cells suppress the activity of other lymphocytes and help control the immune response.

1.1.1 Activation of T cells

T cells are responsible for the cell-mediated immune response (Gowans, 1996). Signalling by the TCR complex alone is not sufficient to activate naive T cells. Full activation requires a co-stimulatory signal mediated by co-receptors like CD28, CD2, LFA-1, CD5 and various interleukin receptors (Rudd et al., 2009). Hence, the activation of naive T cells is a multi-step process involving co-stimulatory proteins: the TCR recognizes the antigenic peptide bound to MHC-II (first signal), followed by a co-stimulation of CD28 on the surface of the T cell via the co-stimulatory glycoproteins B7.1 (CD80) and B7.2 (CD86) on the APC (second signal) (Acuto and Michel, 2003; Rudd et al., 2009). This co-stimulatory process in turn leads to the formation of calcium (Ca^{2+})-mobilising second messengers such as nicotinic acid adenine dinucleotide phosphate (NAADP) (Gasser et al., 2006), cyclic ADP-ribose (cADPR) (Guse, 1999) and d-*myo*-inositol-1,4,5-triphosphate (IP_3) (Streb et al., 1983). The second messengers bind to their respective target Ca^{2+} channels such as ryanodine receptors (RyR) and IP_3 receptors (IP_3R) on the endoplasmic reticulum (ER). This causes an intracellular release of Ca^{2+} from ER Ca^{2+} stores, resulting in a rapid increase in free intracellular cytosolic Ca^{2+} concentration ($[Ca^{2+}]_i$) (Feske, 2007). The depletion of stores activates calcium-release-activated calcium (CRAC) channels, generating a high Ca^{2+} influx across the plasma membrane (PM). This process is called store operated Ca^{2+} entry (SOCE) and is initiated by stromal interaction molecule (STIM) 1 and 2 proteins that are located in the ER membrane. STIM proteins are Ca^{2+} sensors that act as dynamic coordinators of cellular Ca^{2+} signalling (More details in 1.2.4) (Liou et al., 2005; Roos et al., 2005). Once SOCE is activated, a strong Ca2+ influx and subsequent translocation of transcription factors into the nucleus occurs (Fig. 1.1). Leading to transcription of IL-2, which is essential for stimulation of T cell proliferation and differentiation into T effector cells (Kummerow et al., 2009; Soboloff et al., 2012).

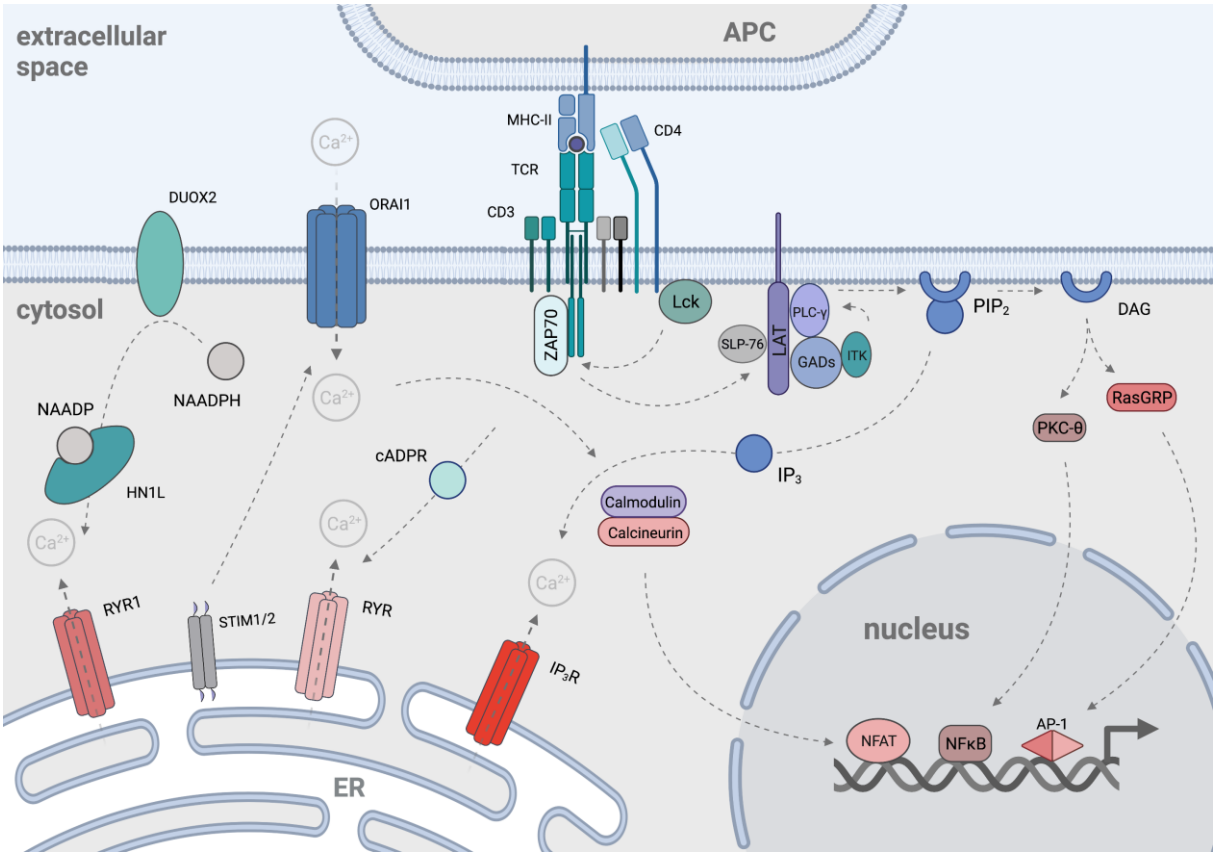

Figure 1.1: Model of T cell activation via antigen receptor signals.

The TCR and co-receptor (here $CD4^+$) bind to the MHC-II complex on the surface of APCs. This leads to phosphorylation of the TCR by the lymphocyte-specific protein tyrosine kinase (Lck). The tyrosine kinase Zeta-chain-associated protein kinase (ZAP)-70 binds to phosphorylated sequences. In this process, ZAP-70 likewise becomes phosphorylated and activated by Lck. The kinase ZAP-70 phosphorylates linker for activation of T cells (LAT) and SH2 domain containing leukocyte protein (SLP)-76, which accumulate at the PM. Phospholipase C (PLC)-γ and Itk are recruited, followed by phosphorylation of PLC-γ by Itk for activation. PLC-γ cleaves phosphatidylinositol-4,5-bisphosphate (PIP_2) into diacylglycerol (DAG) and IP_3. IP_3, as well as other second messengers such as cADPR and NAADP mediate the Ca^{2+} release from the ER by binding to the receptors IP_3R and RYR. The release of Ca^{2+} in the ER leads to aggregation and translocation of STIM to the PM. Here it activates ORAI1 channels and causes extracellular Ca^{2+} influx. A sustained Ca^{2+} increase activates via calmodulin the serine/threonine phosphatase calcineurin, which dephosphorylates nuclear factor of activated T-cells (NFAT). This way it is allowing NFAT to enter the nucleus and activate gene transcription. DAG remains at the membrane and directs Protein kinase C (PKC)-θ and Ras guanyl nucleotide-releasing protein (RasGRP) to the membrane, where they activate different signalling cascades. The activation of RasGRP results in the formation Activator protein (AP)-1, while PKC-θ causes release of nuclear factor kappa-light-chain-enhancer of activated B cells (NFκB). In the cell nucleus, the transcription factors NFκB, AP-1 and NFAT activate the transcription of certain genes (created with Biorender.com, modified from feske2007).

1.2 Ca^{2+}- a versatile signalling molecule

More than 99 % of Ca^{2+} found in the body is present in the form of hydroxyapatite ($Ca_5(PO_4)_3(OH)$) and is located in bones and teeth. Here, Ca^{2+} provides stability and strength. In general, bones serve as one of the main Ca^{2} stores (Yu and Sharma, 2021). Besides its effect on bone structure, Ca^{2+} is essential for cardiac functions, immune responses, muscle contractions and is included in proliferation, apoptosis and cell growth (Brown, 1991; Drake and Gupta, 2021). Therefore, Ca^{2+} is considered the most versatile signalling molecule of all the second messengers. A variation in free cytosolic $[Ca^{2+}]_i$ is required to generate signal transduction. The intracellular Ca^{2+} level is regulated at any time by a balanced influx into the cytoplasm and efflux by a combined action of pumps, exchangers, and transporters (Berridge et al., 2003). Due to their charge, Ca^{2+} ions cannot diffuse independently through the lipid layer, in fact, they require channels for their transport (Cai et al., 2015). T cells express different Ca^{2+}-permeable channels and transporters that control Ca^{2+} influx and efflux through the PM (Feske et al., 2012, 2015; Hogan et al., 2010; Vig and Kinet, 2009), as well as intracellular release into the cytosol and uptake in organelles (ER, mitochondria and endolysosomes) (Berridge, 2016; De Stefani et al., 2016; Foskett et al., 2007; Raffaello et al., 2016; Xiong and Zhu, 2016) (Fig. 1.2). Inside a resting T cell, the free cytosolic $[Ca^{2+}]_i$ is about 100 nM, whereas in the extracellular space, the concentration is 10,000-fold higher in the mM range (Cahalan and Chandy, 2009). When the T cell is stimulated, the cytosolic $[Ca^{2+}]_i$ increases up to 1000 nM (Berridge et al., 2000). There are two main pathways available to increase free cytosolic $[Ca^{2+}]_i$, either Ca^{2+} influx from the extracellular space through the PM into the cytosol and/or via release from intracellular Ca^{2+} stores. In the ER of resting T cells, a $[Ca^{2+}]_{ER}$ of approx. 300 µM-1 mM is present (Parker and Smith, 2010). The increase in free cytosolic $[Ca^{2+}]_i$ via influx or release is coupled to ATP production by providing the formation of cytosolic Ca^{2+} microdomains for uptake via mitochondrial Ca^{2+} uniporters (MCU) (Fig. 1.2) (Berridge, 2016; De Stefani et al., 2016; Prole and Taylor, 2019). ATP acts as an energy source for ion pumps such as PM Ca^{2+} ATPase (PMCA) (Cai et al., 2015; Nikiforov et al., 2015) and sarcoplasmic/ER Ca^{2+} ATPase (SERCA) (Chemaly et al., 2018). They transport Ca^{2+} against the electrochemical gradient and pump the ions from the cytosol into the extracellular space or the ER (Calì et al., 2017; Stafford et al.,

2017) (Fig. 1.2). Free mitochondrial $[Ca^{2+}]_m$ varies between 0.1-10 µM, whereby Ca^{2+} efflux from mitochondria into the cytosol occurs via $Na^+/Ca^{2+}/Li^+$ exchangers (NCLX). These are transporters that use a Na^+ gradient to extrude Ca^{2+} from the mitochondria (Ben-Kasus Nissim et al., 2017; Palty et al., 2010; Sekler, 2015) (Fig. 1.2). Measurements of $[Ca^{2+}]_{ly}$ in endolysosomes indicate a concentration of 400-600 µM. The release of Ca^{2+} from endolysosomes occurs through two pore channels (TPCs) (Morgan et al., 2015) and transient receptor potential mucolipin (TRPML) channels (also located in the PM) (Xu and Ren, 2015) (Fig. 1.2). These channels are thought to regulate exocytosis and endolysosomal fusion, transport, and function (Trebak and Kinet, 2019).

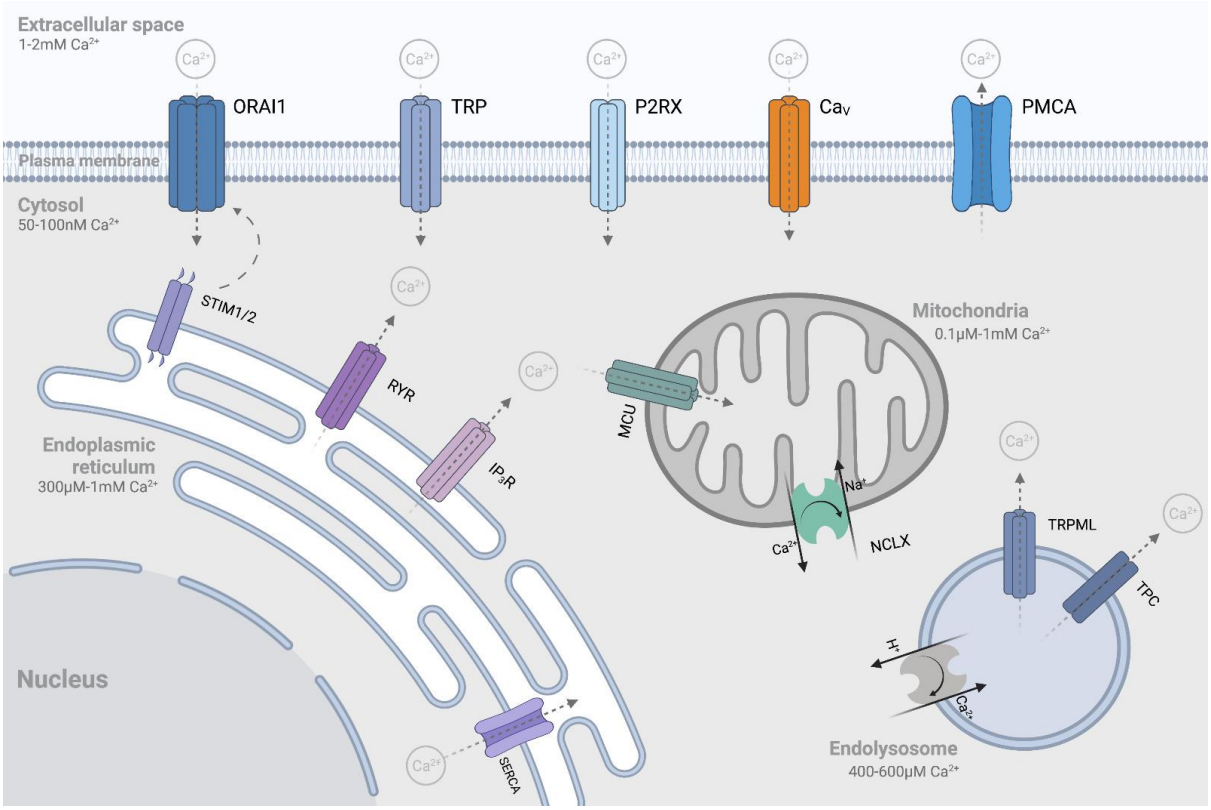

Figure 1.2: Channels, pumps and exchanger involved in Ca^{2+} signalling in T cells.

After initiation of T cell activation, ER channels (IP_3R and RYR) are activated, leading to depletion of the ER Ca^{2+} store. STIM proteins localized in the ER membrane translocate to the PM and activate ORAI channels, resulting in a strong Ca^{2+} influx and Ca^{2+}-mediated signalling. Other PM channels such as non selective transient receptor potential (TRP) channels, purinergic ionotropic receptors (P2RXs) and voltage-activated Ca^{2+} (Cav) channels are also involved in Ca^{2+} signalling during T cell activation. Ca^{2+} release from the ER is partially absorbed by mitochondria via the uniporter MCU. In the endolylsosomes, Ca^{2+} release is regulated by TPCs and TRPML channels. The maintenance of Ca^{2+} homeostasis in the

cytosol and organelles is controlled by transporters and pumps such as PMCAs, SERCAs, NCLXs. (Created with Biorender.com, modified from Trebak and Kinet, 2019).

1.2.1 Ca^{2+}-release by NAADP

NAADP is the most potent Ca^{2+} mobilizing second messenger know to date and was first described by Lee and colleagues in 1987 (Clapper et al., 1987; Langhorst et al., 2004). The transmembrane ectoenzyme CD38, which is associated with intracellular compartments, is able to synthesize at least *in vitro* NAADP from NADP and nicotinic acid via base-exchange reaction (Aarhus et al., 1995; Liu et al., 2017). The catalysis requires an acidic pH, suggesting that NAADP is produced in the endolysosome (Fang et al., 2018). For the formation of Ca^{2+} microdomains, production of NAADP is required within a few seconds (Gasser et al., 2006), indicating another production mechanism outside the lysosome. Recent studies show that NAADPH can be converted to NAADP via the NADPH oxidase DUOX2 in the initial phase of T cell activation (Gu et al., 2021). There are different hypotheses about the Ca^{2+} mobilising activity of NAADP. On one hand, NAADP is supposed to cause Ca^{2+} release from the ER Ca^{2+} store via the activation of RYR1. Furthermore, it is claimed that NAADP stimulates endolysosomal stores via TPCs (Galione, 2019). In addition, it was hypothesized that NAADP regulates various ion channels via a binding protein that targets different channels such as RYR, TPC, and transient receptor potential channel, subtype mucolipin 1 (TRP-ML1) (Guse, 2012). Earlier this year, two research groups demonstrated that NAADP binds to a NAADP-binding protein called hematological and neurological expressed 1–like protein (HN1L) (also known as Jupiter microtubule-associated homolog 2 (JPT2)) (Gunaratne et al., 2021; Roggenkamp et al., 2021). Here, Roggenkamp et al. propose that HN1L is either in a complex with RYR1 and subsequently binds NAADP or is in the cytosol, where it binds with NAADP and then interacts as a complex with RYR1, while Gunaratne et al. observed an interaction of HN1L with TPC1 in endosomes and lysosomes. Later this year, Zhang and colleagues identified the Sm-like protein Lsm12 as a NAADP receptor essential for NAADP-evoked TPC2 activation in acidic stores (Zhang et al., 2021).

In resting T cells, the NAADP concentration is 4.4 +/- 1.6 nM and increases 7.6-fold after TCR/CD3 stimulation (Gasser et al., 2006). Upon T cell activation, the HN1L-NAADP complex causes the activation of RYR1 channels and consequently the

release of Ca^{2+} from the ER Ca^{2+} store (Diercks et al., 20018; Roggenkamp et al., 2021).

1.2.2 Ca^{2+}-release by cADPR

Another important Ca^{2+} mobilising second messenger is cADPR, first described by Lee and colleagues in 1987 in sea urchin egg homogenates (Lee et al., 1989). cADPR is a cyclic adenosine diphospho-ribose (Lee and Aarhus, 1995), a derivative of β-Nicotinamide adenine dinucleotide (β-NAD^+) and is synthesised enzymatically from NAD by ADP-ribosyl cyclases (Nikiforov et al., 2015). These cyclase activities were detected in cytosolic preparations from sea urchin eggs (Graeff et al., 1998) as well as subcellular and soluble fractions from T cells (Guse, 1999). The receptor-mediated increase of cADPR has been demonstrated in various cell systems, such as Jurkat T cells, by stimulation with anti CD3 antibodies (Guse, 1999). In T cells the target channel for cADPR is the RYR (Bourguignon et al., 1995; Guse, 1999) leading to Ca^{2+} release from the ER (Lee, 2001, 2011), thus, in RyR-knock down T lymphocytes a reduced Ca^{2+} signal was detected (Schwarzmann et al., 2002).

1.2.3 Ca^{2+}-release by IP_3

The best-characterised second messenger is IP_3, which was discovered by Schulz and Berridge in 1983 (Streb et al., 1983). In most cell types, the synthesis of IP_3 is a crucial step in the formation of Ca^{2+} signals that are necessary for the regulation of many cellular processes, including cell survival and cell death (Berridge, 1993; Vermassen et al., 2004). IP_3 formation especially involves PLC-γ. PLC-γ activation represents an important step in T-cell activation, as the next step includes the splitting of the PLC-γ signalling cascade into three separate pathways: (i) formation of IP_3 which mediates the influx of Ca^{2+} through ORAI1, (ii) activation of Ras and (iii) activation of PKC-θ. Each of the pathways ends with the activation of different transcription factors (Fig. 1.1).

After TCR stimulation, the activation of PLC-γ (Courtney et al., 2018) leads to the formation of the second messengers IP_3 and DAG (Berridge, 2016). DAG is membrane-bound and activates PKC and Ras-dependent effector mechanisms. IP_3, on the other hand, opens the IP_3R, leading to an increase in $[Ca^{2+}]_i$. This is followed

by the activation of transcription factors NFAT, as well as AP-1 and NFκB, leading to IL-2 expression and subsequently to T cell proliferation as previously stated.

The IP_3R is an intracellular tetrameric channel and is expressed in most mammalian cells (Prole and Taylor, 2011) whereas three different subtypes of IP_3Rs have been described: IP_3R1, IP_3R2 and IP_3R3. They mainly mediate Ca^{2+} release from intracellular stores such as the ER (Berridge, 1993) and the Golgi apparatus (Pizzo et al., 2011; Rodríguez-Prados et al., 2015; Wong et al., 2013). However, the IP_3Rs are also expressed in the nucleus envelope and the nucleoplasmic reticulum (Echevarría et al., 2003). The IP_3Rs form homo or hetero tetrameric Ca^{2+} channels of the receptor subunits (structure is shown in Fig. 1.3). Each subunit can be separated into three principle domains: amino-terminal ligand binding domain, carboxyl-terminal channel domain and a central coupling or regulatory domain with 6 transmembrane domains. IP_3R genes encode a large cytosolic and a small Ca^{2+} channel domain (Furuichi et al., 1989; Mikoshiba, 2007; Patterson et al., 2004). The cytosolic domain contains all key functional sites that confer receptor function and regulation, including an IP_3-binding core (Yoshikawa et al., 1996) and an N-terminal suppressor domain (Yoshikawa et al., 1999). The N-terminal domain reduces the affinity of IP_3 binding and has a large regulatory domain responsible for intracellular effector molecules such as Ca^{2+} (Finch et al., 1991). The IP_3 binding domain, also called internal coupling domain modulates IP_3R channel activity and is involved in the signal transduction of IP_3-binding to channel gating (Mignery and Südhof, 1990; Uchida et al., 2003).
In T cells, all three isoforms of IP_3Rs are expressed, differing in their expression pattern in different tissues, as well as their regulation by Ca^{2+} (Taylor et al., 1999). Differences were observed as well in their affinity for IP_3, with IP_3R2 having the highest and type 3 the lowest affinity for IP_3 (Iwai et al., 2007). The activity of the three IP_3Rs is enhanced by moderate increase in free cytosolic $[Ca^{2+}]_i$ (100-300 nM) and inhibited by more substantial increase ($[Ca^{2+}]_i$ above 300 nM) (Berridge et al., 2000; Foskett et al., 2007). In terms of affinity for Ca^{2+}, interestingly, IP_3R3 shows the highest and type 1 the lowest binding potential (Tu et al., 2005). Activation of the IP_3Rs requires the binding of IP_3 to all four subunits (Alzayady et al., 2016), as well as the binding of Ca^{2+} (Finch et al., 1991; Marchant and Taylor, 1997). Hence, the IP_3Rs are co-regulated by IP_3 and cytosolic Ca^{2+}, with both ligands required for channel opening. Furthermore, the

binding of IP_3 to IP_3R causes two interdependent events: First, Ca^{2+} release from the ER (Mikoshiba, 2007) and subsequently, ER depletion leads to indirect activation of Ca^{2+} influx across the PM via SOCE (Putney, 1986, 1990).

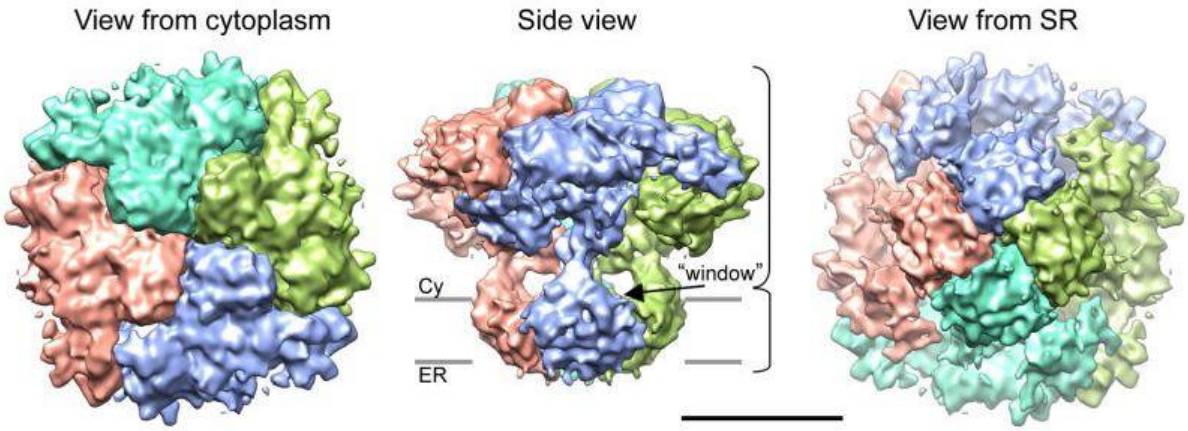

Figure 1.3: Architecture of the IP_3R1 channel depicted in a cryo-EM density map.
Illustration of a 3D structure of IP_3R1 in the closed state. Three orthogonal views are shown: a top view from the cytoplasmic side, a side view, and a bottom view from the luminal side. The identified subunits are colored individually. Gray bars: positions of the cytoplasmic (Cy) and endoplasmic (ER) leaflets of the membrane bilayer. The shape of the IP_3R1 channel forms a ~19 nm high structure. Scale: 10 nm (Ludtke et al., 2011).

This thesis focuses on the Ca^{2+}-releasing pathway via IP_3R activation followed by Ca^{2+} influx through SOCE.

1.2.4 Store-operated Ca^{2+} entry

The Ca^{2+} entry pathway SOCE is activated in response to depletion of Ca^{2+} from the ER and controls regulation and physiological functions in viarous cell types (Ambudkar et al., 2017). SOCE was first discovered by James Putney in 1986 as a capacitive Ca^{2+} influx (Putney, 1986, 2007). Initially, agonist-activated and IP_3-mediated store depletion was thought to be the main pathway of Ca^{2+} influx. This hypothesis was further supported by using the Ca^{2+} indicator fura-2 and the SERCA pump blocker thapsigargin (Tg). The cytosolic Ca^{2+} measurements showed an opening of the membrane ion channels after Tg stimulation and consequently a direct Ca^{2+} influx into the cell (Takemura et al., 1989). Furthermore, in 1992, Hoth and Penner clearly demonstrated the ionic currents through SOCE as "calcium release activated calcium"

(I_{CRAC}) (Hoth and Penner, 1992), which was voltage independent, inwardly directed and defined as selective for Ca^{2+} (Parekh and Penner, 1997). Based on these studies, it was demonstrated that the capacitive Ca^{2+} influx is a store-operated Ca^{2+} entry. Consequently, the name was changed accordingly. In T cells, the amount of Ca^{2+} release is relatively small compared to Ca^{2+} influx (Dolmetsch and Lewis, 1994; Donnadieu et al., 1994; Lewis and Cahalan, 1989). Therefore, the main role of Ca^{2+} release seems to be to modulate the influx. The Ca^{2+} release is caused by the activation of Ca^{2+}-permeable receptors localized in the ER membrane (IP_3R, RYR) via the binding of second messengers (NAADP, cADPR and IP_3) (Berridge, 2016; Parekh and Putney, 2005). The lowering of the Ca^{2+} level in the ER triggers the activation of the SOCE pathway, resulting in the opening of CRAC channels localized in the PM (Hsu et al., 2001; Lewis, 2001; Prakriya and Lewis, 2001; Zweifach and Lewis, 1993). Using high-throughput screens based on RNA-mediated interference, STIM1 and calcium-release-activated calcium modulator (CRACM) 1 were identified as the main SOCE players. STIM1 is a Ca^{2+} sensor that resides in the ER membrane. CRACM1, also called ORAI1, is the pore-forming subunit of CRAC channels (Feske et al., 2006; Liou et al., 2005; Vig et al., 2006; Zhang et al., 2005, 2006). The discovery of STIM1 and ORAI1 has significantly increased our understanding of how Ca^{2+} signalling is regulated in lymphocytes. The sensors STIM1 and 2 detect the abundance of Ca^{2+} storages (Liou et al., 2005; Roos et al., 2005). Upon depletion, there is a conformational change, aggregation and translocation of STIM molecules (Fig. 1.4) to the junctional space where ER and PM come to close contact (9-12 nm) (Lur et al., 2009; Várnai et al., 2007). Due to its low affinity for Ca^{2+}, STIM2 recognises modest depletion of the store, whereas STIM1 activation requires substantial store depletion (Brandman et al., 2007). Maximum CRAC channel activity requires the binding of two STIM proteins to one ORAI protein (Hoover and Lewis, 2011). Ca^{2+} influx into the cytosol through the CRAC channels causes refilling of the Ca^{2+} ER stores by the SERCA pump (Prakriya and Lewis, 2015; Shaw and Feske, 2012). Via the EF domain, STIM1 sense refilling, which leads to deactivation of CRAC channels (Stathopulos et al., 2008). STIM proteins return to their resting state where they are present as a dimer, the EF hands have bound Ca^{2+} and the inhibitory coiled-coil-1 domain occludes the STIM-ORAI activation region (SOAR) (Johnson and Trebak, 2019).

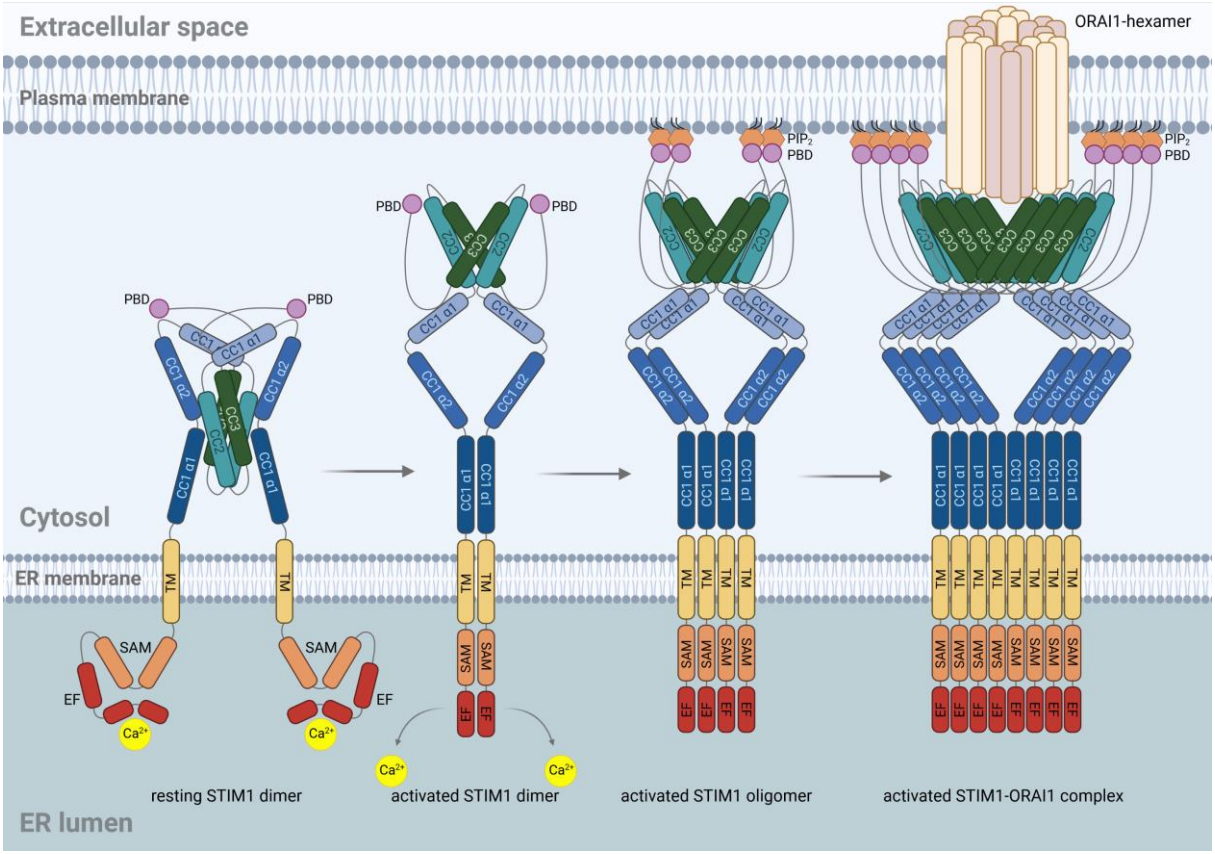

Figure 1.4: Model of STIM1-ORAI1 coupling mediated by store depletion.

In the resting state, STIM1 exists as a dimer and is initially folded and bound to Ca^{2+} (on the EF hands) (left). Upon store depletion, Ca^{2+} ions dissociate from the EF hands and STIM1 gets activated. A conformational change of the cytosolic STIM domain occurs with the SOAR domain being released. The activated STIM1 proteins oligomerize and translocate to the PM, where STIM1 binds to the membrane by binding to PIP_2 via the polybasic domain (PBD). STIM activates ORAI1 by binding via its SOAR domain, leading to Ca influx and increased free cytosolic $[Ca^{2+}]_i$ (created with Biorender.com, modified from Soboloff et al., 2012).

Highlighting the physiological role of SOCE in patients with severe combined immunodeficiency (SCID), a normal Ca^{2+}-release was observed while Ca^{2+} entry and CRAC currents were abrogated (Le Deist et al., 1995; Partiseti et al., 1994), associated with impaired proliferation. Different studies observed impaired cytokine production in ORAI1 and STIM1 deficient cells (Feske et al., 2012, 2015). In STIM1 and 2 double knockout experiments, splenomegaly, lymphadenopathy and inflammation, as well as a complete loss of SOCE was reported (Oh-Hora et al., 2008). These experiments demonstrate the important role of SOCE as an activator mediated by STIM1, 2, and ORAI1. Here, the formation of critical Ca^{2+} microdomains is essential for lymphocyte function.

Ca^{2+} microdomains are formed, when Ca^{2+} enters the cytoplasm either at the cell surface or via internal stores. They are key elements of Ca^{2+} signalling and essential for T cell activation. Here, localized Ca^{2+} domains regulate specific cellular processes in different regions of the cell (Berridge, 2006).

1.2.4.1 STIM proteins

Since the discovery of STIM protein involvement in SOCE, the understanding of the mechanism of SOCE regulation has changed dramatically. Two groups independently identified the function of STIM as a mediator of SOCE by high throughput screening, using short interfering RNA (siRNA) in HeLa cells and RNA interference (RNAi) in Drosophila S2 cells (Liou et al., 2005; Roos et al., 2005). STIM is a 77 kDa single-spanning transmembrane protein localized mainly in the ER membrane (Spassova et al., 2006; Vig and Kinet, 2009; Zhang et al., 2005). It contains a sterile α-motif (SAM) domain and an EF-hand Ca^{2+}-binding domain on the luminal side of the ER as well as a cytosolic coiled-coil (CC) binding domain at the carboxy terminus. In mammals, there are four different isoforms: STIM1, STIM1L, STIM2, and STIM2.1/STIM2β. The isoforms differ in the length of their amino and especially their carboxy-terminal sequences. Otherwise, they are about 61% identical (Derler et al., 2016). STIM proteins are sensors that detect the depletion of ER Ca^{2+} storage via its amino-terminal Ca^{2+}-binding EF-hand domain. Store depletion triggers oligomerization of the STIM proteins by the EF-SAM region. This is followed by translocation to ER-PM junctions (Liou et al., 2007; Stathopulos et al., 2006). In resting cells, the EF-SAM domain was observed to be present as a well-folded dimer. Depletion of the ER causes unfolding of the hydrophobic residue of the EF-SAM region, resulting in oligomerisation of STIM proteins along the ER membrane (Liou et al., 2007; Luik et al., 2006; Zhang et al., 2005) This is followed by the activation of ORAI1 channels via SOAR, which is located in the CC domain of the STIM proteins. This domain additionally stabilises the EF-SAM region, triggers oligomerization and promotes translocation of STIM to ER-PM junctions (Baba et al., 2006). However, the exact mechanism of CRAC channel activation by STIM oligomers remains to be determined. In many cells, STIM1 is more strongly expressed than STIM2 and is the main effector of SOCE (Soboloff et al., 2012). Compared to STIM1, STIM2 is a weak activator of ORAI channels and has a lower affinity than STIM1 for Ca^{2+} (Brandman et al., 2007; Wang et al., 2014; Zheng et

al., 2018). Another isoform of STIM1 is the long isoform STIM1L, which has an additional actin-binding domain at the C-terminus. The precise effect of STIM1L on the stromal properties of ORAI1 is currently unknown. STIM1L is thought to co-localize with ORAI1 channels and interacts with actin. This leads to the formation of permanent clusters (Darbellay et al., 2011) providing a robust and very rapid activation of Ca^{2+} influx by store depletion. On the other hand, STIM1L is reported to slower the recruitment of ORAI1 to ER/PM junctions and the activation rate of Ca^{2+} influx (Saüc et al., 2015). Similar to STIM1L, The function of STIM2 is controversial as well. Some early reports claim that only STIM1 is required for Ca^{2+} oscillation at low agonist concentrations (Bird et al., 2009; Wedel et al., 2007). Other studies, however, observe a main regulation of Ca^{2+} oscillation by STIM2 (Ong et al., 2015; Thiel et al., 2013). Furthermore, there is evidence that in moderate ER Ca^{2+} depletion, STIM2 is responsible for recruiting STIM1 to ER-PM junctions (Son et al., 2020; Subedi et al., 2018). Regulation of STIM1 function is performed by STIM2 splice variants (STIM2.1/STIM2β) as well (Miederer et al., 2015; Rana et al., 2015). A modified SOAR domain in STIM2.1/STIM2β causes reduced interaction with ORAI1. Upon store depletion, STIM2.1/STIM2β binds to STIM1 and inhibits activation of ORAI1. In conclusion, the studies on STIM isoforms suggest that STIM proteins play a more dynamic cooperative role in Ca^{2+} signalling than previously thought. It is for certain that the STIM isoforms are involved in the maintenance and regulation of free cytosolic $[Ca^{2+}]_i$. The exact physiological function, however, seems to be very complex and differs depending on cell type and activation mechanism.

1.2.4.2 ORAI channels

ORAI proteins have a size of 32.7 kDa and consist of four transmembrane (TM) domains, each composed of amino and carboxyl ends, which are directed into the cytosol (Feske et al., 2006; Vig et al., 2006; Zhang et al., 2006). The C-terminal region includes a coiled-coil domain that is required for STIM binding and CRAC channel activation (Muik et al., 2008). ORAI proteins are the pore-forming subunits of CRAC channels, which are primarily required for the activation of Ca^{2+}-dependent transcription factor isoforms of NFAT and subsequently for cytokine production, proliferation and immunocompetence (Feske et al., 2012, 2015; Vig and Kinet, 2009). Already one year after the identification of STIM1, ORAI1 channels were discovered

as store-operated Ca^{2+} channels and thus as the missing link of SOCE. Here, the function of ORAI1 was investigated almost simultaneously and independently by three groups (Feske et al., 2006; Vig et al., 2006; Zhang et al., 2006). For a long time, the tetrameric structure of ORAI proteins was thought to be formed by two dimers each (Vig et al., 2006). In 2012, however, the crystal structure of functional ORAI channels was published, showing that the channel consists of three dimers each, possessing a hexameric structure (Hou et al., 2012) (Fig. 1.5). ORAI1 shares its tetra spanning protein topology with two structurally related paralogues, ORAI2 (CRACM2) and ORAI3 (CRACM3) (Lis et al., 2007). The TM units of the three isoforms have 81-87% matching sequences, with the functional TM1 domain identical in all three channels. The three ORAI isoforms are all activated by STIM1 coupling and exhibit high Ca^{2+} selectivity (Lis et al., 2007). The homologues ORAI2 and 3 mediate smaller Ca^{2+} currents compared to ORAI1 and only sparse information is available on their role in mediating SOCE (Trebak and Kinet, 2019). ORAI2 was proposed to be a negative regulator of ORAI1 (Vaeth et al., 2017). Experiments with ORAI2 deletion indicate enhanced SOCE activity in naïve T cells, but show no effect in effector T cells. It was observed that in effector T cells ORAI2 is downregulated, whereas ORAI1 is upregulated. The isoform ORAI3, on the other hand, is thought to be able to replace the function of ORAI1 in SOCE in its absence (Mercer et al., 2006).

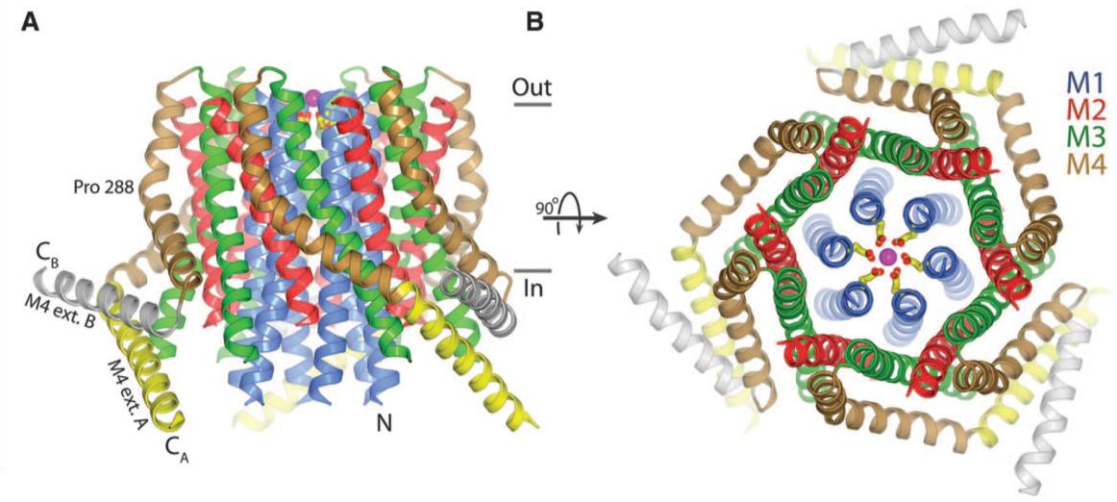

Figure 1.5: Architecture of an ORAI hexamer.

Structure of ORAI. (A) Side view of the tertiary structure: The helices are shown in coloured sections: M1 (blue), M2 (red), M3 (green), M4 (brown), M4 extension (yellow). (B) Top view of the channel from

the extracellular side: here the M4 extension is shown in grey. The structure of an ORAI hexamer has a diameter of ~6-8 nm. Modified from Hou et al., 2012.

1.3 Integrin mediated Ca^{2+} signalling in T cells

Once T cells are activated via the TCR, they migrate from blood vessels to the inflamed tissue, thereby interacting with other structures. These include surface receptors of other cells, cytokines (such as interleukins), as well as components of the extracellular matrix (ECM). T Cell adhesion triggers a cascade, beginning by slow rolling, followed by arrest and strengthened adhesion, and finally crawling and transmigration across endothelial cells (Ley et al., 2007). To initiate transmigration, a weak and transient adhesive interaction between the T cell and the endothelial cell is required. This interaction is mediated by two main adhesion receptor families, selectins (expressed on T cells and endothelial cells) and integrins (expressed on T cells). Integrins are αβ heterodimeric cell surface receptors with more than 30 αβ pairs existing (Herter and Zarbock, 2013; Hynes, 1992). Cell rolling on endothelium is triggered by a short weak binding between the integrins of T cells (e.g. LFA-1, VLA4) and their associated endothelial ligands (e.g. ICAM-1, VCAM-1) (Block et al., 2012; Sriramarao and Broide, 1996; Stadtmann et al., 2011; Zarbock et al., 2008). When T cells interact with endothelium, arrest is mediated by stimulatory signals from the inside out via G protein-coupled receptors (GPCRs) (Alon and Feigelson, 2009; Dixit and Simon, 2012). After arrest, adhesion is strengthened by the recruitment and clustering of diffusive integrins (Constantin et al., 2000; Smith et al., 2005). Adherent T cells transmigrate through the endothelial barrier at paracellular endothelial cell junctions or use their integrins to role along the endothelium in search of exit points (Phillipson et al., 2009). After transmigration through the endothelium, T cells adhere to the basal membrane and matrix of the stroma (called interstitium) via integrins. The basal membrane consists of a thin layer of ECM proteins such as laminins, heparan sulphate proteoglycan perlecan and globular collagen IV and VIII (Paulsson, 1992), while the interstitium contains a different set of ECM proteins such as fibrillar collagen types I, III, V and VI, fibronectin, tenascin and dermatan. Inflammation also causes contact between the T cell and ECM proteins that are upregulated. These include vitronectin (Preissner, 1991) or thrombospondin (Jaffe et al., 1985; Raugi et al., 1982; Sage and Bornstein, 1991;

Weismann et al., 1997). Studies indicate a triggering of signal transduction mechanisms through integrin-mediated adhesion of T cells to ECM proteins. Among other things, an increase in free cytosolic $[Ca^{2+}]_i$ was observed (Weismann et al., 1997; Weiss et al., 1984). Focal adhesion kinase (FAK) is thought to be a key component of the integrin-mediated signalling pathway (Guan, 1997). Hence, upon binding of ECM proteins to integrins, FAK proteins are phosphorylated, leading to the subsequent activation of PLC-γ (Zhang et al., 1999).

1.3.1 Focal adhesion kinase (FAK)

Almost 30 years ago, FAK was first identified and classified as a component of integrin signalling (Guan et al., 1991; Hanks et al., 1992; Kornberg et al., 1992; Schaller et al., 1992). FAK belongs to the non-receptor protein tyrosine kinase family, is expressed in most tissues and cell types and activated by phosphorylation of Tyr397 (Fox et al., 1999; Hanks et al., 1992; Henry et al., 2001). The kinase consists of a central catalytic domain flanked by large N- and C-terminal non-catalytic domains. The N-terminal domain shows sequential similarities with the so-called FERM domain and also mediates interaction with the activated epidermal growth factor (EGF) receptor (Girault et al., 1999; Sieg et al., 2000; Sun et al., 2002). *In vitro*, the FERM homology domain of FAK binds to sequences of the cytoplasmic domain of β-integrin (Schaller et al., 1995). In this way, FAK is directed to sites where integrin or growth factor receptors cluster, thereby regulating the interaction with other potentially activating proteins. In contrast, the C-terminal region is rich in protein-protein interaction sites, with the focal adhesion targeting (FAT) region directing FAK to newly formed and pre-existing adhesion complexes (Martin et al., 2002). Clustering of integrins causes rapid phosphorylation of FAK at Tyr397, as well as other sites in the kinase and C-terminal domain (Calalb et al., 1995). This is followed by increased catalytic activity of FAK and the formation of the phosphotyrosine binding site for various signalling molecules (Schaller et al., 1994; Xing et al., 1994). Phosphorylation of Tyr397 creates, among other things, high-affinity binding sites for SH2 domains and thus recruits phosphoinositide-3 (PI-3) kinase, PLC-γ and the adapter proteins Grb7 (Akagi et al., 2002; Chen and Guan, 1994; Chen et al., 1996).

1.4 Advanced light microscopy methods to visualize co-localization of proteins

In this work different light microscopy methods have been used to determine the spatial distribution and interaction of proteins within T cells. In the following section a detailed description of these methods will be presented.

1.4.1 Fluorescence Resonance Energy Transfer (FRET)

FRET is a non radiative energy transfer mechanism that can occur between two fluorescent molecules. It was first described in 1946 by Theodor Förster as a physical phenomenon in which a donor fluorophore in the excited state transfers its excitation energy without the emission of any quantum of light to an acceptor fluorophore. This results in emission from the acceptor (Forster, 1946). Donor and acceptor form a so-called FRET pair. A fluorescent molecule is eligible to be a donor only if its emission spectrum overlaps the excitation spectrum of the acceptor. For this phenomenon to occur, the excited states of the donor and acceptor have to be close to each other, i.e., there should be a physical overlap. In other words, FRET can only occur when the distance between donor and acceptor varies between 2 and 10 nm (Selvin, 1995; Stryer and Haugland, 1967).

FRET is often used in biology to monitor different biochemical activities that depend on changes in molecular proximity. These include protein-protein interaction, conformational changes, intracellular ion concentration, enzyme activity and many more (Lam et al., 2012; Miyawaki, 2011). A FRET bio sensor is made by a FRET pair designed to monitor the above-mentioned biological interactions. Depending on how the fluorophores are bound, the FRET biosensor can be divided into two categories: (i) the intramolecular type, where donor and acceptor are located on the same molecule and conformational changes of the molecule cause changes in the FRET signal. (ii) the intermolecular type, where the donor and acceptor fluorophore are located on different molecules and the FRET signal is triggered only when the molecules are in close proximity to each other (Stryer and Haugland, 1967).

One advantage of FRET biosensing over biochemical assays is that it is performed optically, allowing non-destructive and minimally invasive examination of living cells (Miyawaki, 2011). Thus, FRET can be used to detect dynamic events during live cell imaging experiments if the microscope set up supports image acquisition to be rapid

enough (Broussard and Green, 2017). FRET based experiments, however, are limited by several factors related to the physical process as well as the technology used to measure FRET (Leavesley and Rich, 2016). For example, low signal-to-noise ratio (SNR) associated with FRET imaging is a major limiting factor. Moreover, many light microscopy methods to measure FRET suffer from the photobleaching (donor photobleaching) that can occur during the acquisition.

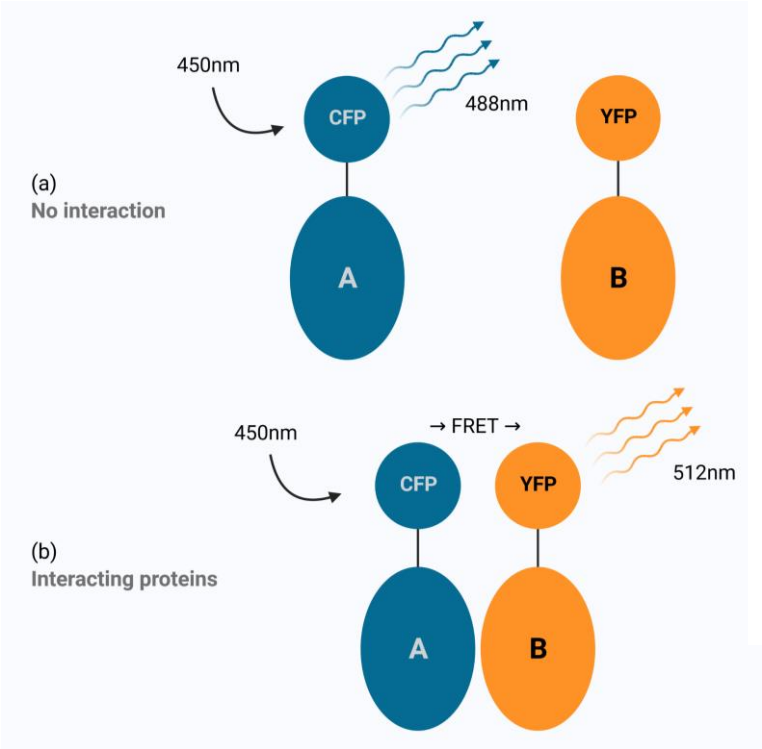

Figure 1.6: Description of the principle of CFP-YFP FRET biosensor.
Proteins of interest (Protein A and B) are attached to different fluorophores, CFP (donor) and YFP (acceptor), respectively. (a) Proteins do not interact, no energy is transferred in a not radiative way from CFP to YFP. (b) Proteins interact, the energy absorbed by CFP is transferred in a not radiative way and excites YFP. FRET can be observed (created with Biorender).

1.4.2 Super resolution Confocal Microscopy

Sheppard proposed in 1988 that in a special configuration also confocal microscopy can overcome the diffraction limit and enables the so-called super resolution (Sheppard, 1988). Sheppard's theory was realized practically in 2010 by Mueller and Enderlein, who developed the Imaging Scanning Microscope (ISM) (Müller and Enderlein, 2010).

The principle of confocal laser scan microscopy (CLSM) is not to illuminate the entire specimen as in wide field microscopy. On the contrary in CLSM the excitation light is focused in one point and by scanning the laser through the sample an image is formed by collecting light point by point.

The image of a point like source i.e. a fluorescence object smaller than the diffraction limited focal spot is called point spread function (PSF) of the system for a given objective and excitation wavelength. The PSF of the system for a given objective and excitation wavelength is in general the product of the excitation and detection PSFs. In CLSM the excitation PSF is defined as intensity distribution of the focused excitation beam (Inoué, 2006). While, in confocal microscopy the intensity distribution of the light when is passing over the pinhole plane is called detection PSF. In imaging, the excited light is focused through a lens, while the emitted light is detected through the same or a different lens. As a result, reducing the detection or emission PSF can lead to higher resolution (Azuma and Kei, 2017). The excitation PSF due to the diffraction limit of the focusing objective lens cannot be reduced at will. In other words, there is no way to decrease the total PSF and increase the resolution beyond the diffraction limit by working on the excitation PSF. This limitation can be overcome, for example, by narrowing the emission PSF.

1.4.2.1 Super resolution by optical Re-assignment (SoRa) Microscopy

As alternative way to overcome the diffraction limit in confocal microscopy, Sheppard and colleagues have developed a novel approach to reduce the emission PSF known as "photon reassignment" (Sheppard, 1988; Sheppard et al., 2013). To achieve photon reassignment the acquired light will pass through an intermediate magnification while being re-scanned on the camera. If the intermediate being expansion is 1/m (intermediate magnification) the position of the focused light would be r+s x (1-m) whereby (r+s) is the position of the scanned excitation light with respect to the effective position of a fluorescence object. For example, if the intermediate magnification of the detected beam 1/m = 2, this would lead to a relocation of the detected beam 50% closer to its real position. In this way, the captured photons of the excited sample are shifted closer to the location from which they are most likely to originate. For each scan position, this reassignment is performed, resulting in increased maximum resolution (Azuma and Kei, 2015). This principle shown in figure 1.7. The peak of the excitation PSF is located at point r, while the peak of the imaging PSF is located at position r+s. Consequently, the two PSFs do not overlap perfectly. Ideally, the imaging point would have to be shifted from r+s to r+s/2, which would result in a 2x higher spatial resolution than limited diffraction. This re location was initially done computationally, which

resulted in significantly slower image acquisition. In the last years, the method was improved by optically remapping the photon using lenses. In this thesis, a Yokogawa spinning disk microscope is used which is capable of high-resolution optical realignment (SoRa) (York et al., 2013).

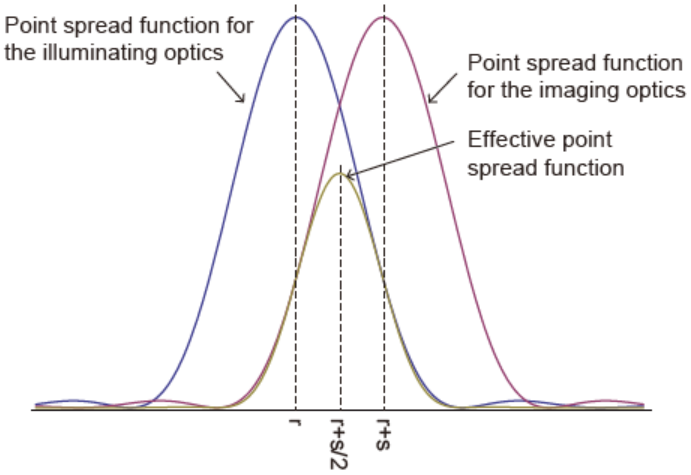

Figure 1.7: Effective PSF of a confocal microscope.
Position r represents the illumination PSF peak, r+s the imaging PSF peak. The position r+s/2 defines the point where the imaging PSF peak should be shifted to achieve the goal of photon reassignment (Azuma and

SoRa uses a two-disk system (lens and pinhole disk) where the excitation microlens disk is located above the primary pinhole disk used for detection. To reassign the detected photons microlenses are added to the bottom of the pinhole disk (Fig. 1.8). This causes a new optical assignment of the photons and thus the achievement of super-resolution. The advantage of this system is the combination of the high acquisition speed given by the spinning disk and high-resolution imaging. The rotation of the disk is 4000 rounds per minute that make possible an acquisition of up to 200 images per second. SoRa can reduce to a lateral resolution down to 150 nm (improving of a factor 1.4 with respect to a normal spinning disk) (Azuma and Kei, 2015). After deconvolution the SoRa spinning disk microscope used in this work can achieve up to 120 nm optical resolution.

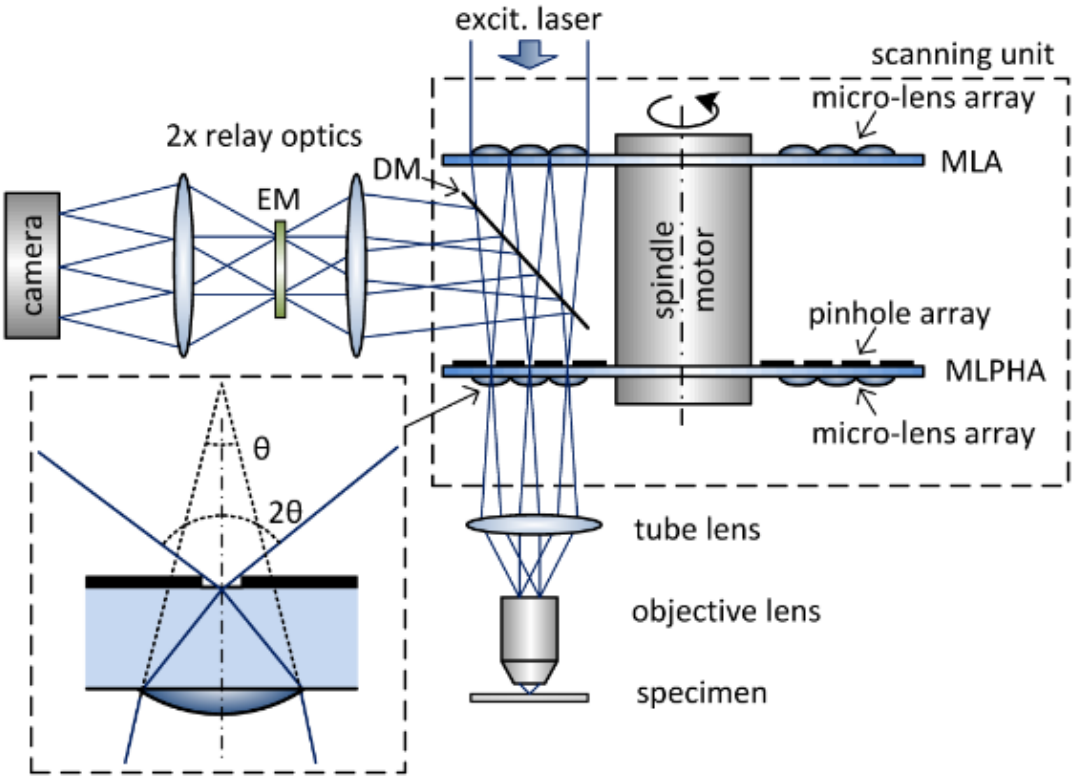

Figure 1.8: Simplified diagram of the optical path of a super-resolution Spinning disc confocal microscope.

The excited light passes through the micro lens disk and is focused on the sample through an objective lens. In the detection is placed a micro-lens pinhole array (MLPHA) disk before the acquired light is separated from the excitation via a dichroic mirror (DM). The collected emission is imaged by the camera through an emission filter (EM). (Azuma and Kei, 2015).

1.4.2.2 Stimulated Emission Depletion (STED) Microscopy

STED microscopy is a super resolution technique based on the confocal laser scanning microscopy. The method was developed in 1994 by Stefan Hell and Jan Wichmann (Hell and Wichmann, 1994). However, first experiments were demonstrated by Stefan Hell and Thomas Klar in 1999 (Klar and Hell, 1999). Due to diffraction limit, it is not possible to focus the light to below 200 nm. Using STED microscopy, they were able to exceed this diffraction limit by reversibly switching off (depleting) fluorophores at predefined positions of the diffraction-limited excitation area (Wei and Min, 2013). STED microscopy requires an excitation beam and a depletion (STED) beam, whereby the excitation beam excites the probe and the STED beam causes stimulated emission (SE) of the excited fluorophore. The STED beam is engineered to produce a doughnut-shaped focal intensity distribution with zero-intensity point in the centre (Hell, 2009).

The process of stimulated emission begins when the fluorophore absorbs an excitation photon and enters a higher energy state. Once it reaches this state, the STED beam is activated, causing the fluorophore to emit photons at the wavelength of the depletion beam and return to the ground state. The wavelength of the STED beam differs from the fluorescence wavelength so that a filter can be used to block the STED beam wavelengths and only the fluorescence wavelength can pass. Since the donut-shaped STED beam only captures fluorophores near the centre of the emission PSF, a smaller effective PSF is generated. This results in a higher image resolution whereby details in the range of 20-40 nm can be resolved, producing a tenfold improvement in resolution over traditional fluorescence microscopy (Hell and Wichmann, 1994; Klar and Hell, 1999).

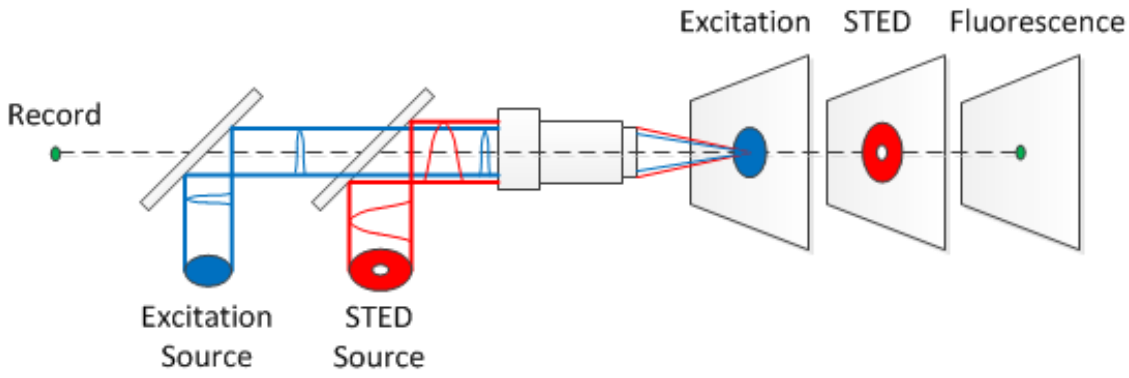

Figure 1.9: Light path of a STED microscope.

The excitation light is switched off in the outer region of the excitation focus by stimulated emission using a depletion beam (Beeson et al., 2015).

2. Study Objective

The activation of T cells is initiated by binding of the TCR to an antigenic peptide. This is followed by Ca^{2+} release from Ca^{2+} stores and subsequent Ca^{2+} influx via SOCE, which lead to an increase in global cytosolic Ca^{2+} concentration and finally proliferation of T cells. Once activated, they migrate into inflamed tissue, interacting with other cells or components of the ECM via integrins (located on the T cell surface). Studies already indicated that integrin-mediated Ca^{2+} signalling in T cells also results from the interaction of integrins with ECM proteins even in the absence of TCR stimulation. Hence, we hypothesised that Ca^{2+} microdomains occurring without TCR stimulation are the initial elements of T cell pre-activation and are caused by ECM protein binding. The main objective of this thesis was to analyse the interaction of components likely involved in adhesion-dependent pre-activation of T cells under control and adhesive conditions, like FAK, the IP_3R and SOCE proteins. Therefore, in the first part of this work, different advanced optical methods were optimized and compared to achieve the best possible spatial resolution to characterize clustering and co-localization of proteins. Here, FRET biosensing, SoRa and STED microscopy were utilized and co-localization between proteins compared.

In the second part, the best suited method (STED microscopy) was then used to study the interaction and clustering of FAK and the IP_3R isoforms as well as SOCE proteins STIM1/2 and ORAI1 during adhesion.

3. Materials and methods

3.1 Cultivation of Jurkat T cells

The Jurkat cell line was isolated in 1976 from the peripheral blood of a 14-year-old boy with acute lymphoblastic leukaemia (Schneider et al., 1977). Jurkat cells are an immortalised cell line of T lymphocytes and play an important role in the analysis of signalling processes involved in the activation of T cells (Abraham and Weiss, 2004). In the following experiments, the subclone JMP was used. The cells were cultured at 37 °C and 5 % CO_2 in a CO_2 incubator. Every 2 to 3 days the cell density was determined and adjusted to a concentration of $0.3x10^6$ cells/mL with fresh culture medium (Jurkat JMP medium).

3.1.1 Buffer and solutions

- Jurkat JMP Medium: RPMI medium 1640 + GlutaMAX™-I + 25 mM HEPES and phenol red, supplemented with 1 % (v/v) PenStrep (final concentration: 100 U/mL) and 7.5 % (v/v) NCS.

3.2 Transfection of Jurkat T cells

To determine the interaction between ORAI1 and STIM1 or STIM2, Jurkat T cells were transfected by electroporation. Electroporation is a method of temporarily permeabilising cell membranes in order to transfer macromolecules, such as DNA or proteins, into cells or tissues (Neumann et al., 1982; Shi et al., 2018). Here, electrical impulses are used to create temporary pores in the cell membrane. In this experiment, a plasmid containing protein sequences coupled with dyes were transferred into the cell. This enables to determine the interaction between the three different proteins using FRET analysis (3.7.1). For transfection, a Neon™ transfection system (Invitrogen) and the associated Neon transfection system 100 µL kit was used. Initially, 2×10^6 Jurkat T cells were pelleted by centrifugation (1200 rpm, 5 min, RT) and washed with PBS. The cells were centrifuged (1200 rpm, 5 min, RT) again and dissolved in 120 µL R-buffer. 10 µg DNA was added to the cells. The sample was included in the electroporation pipette and electroporated (Pulse: 1400 V; Width: 20 s;

Pulse number: 2) using the electroporation device. After transfection the cells were placed in culture medium and incubated overnight.

Table 1: Plasmids for transfection of Jurkat T cells

Vector	Supplier
EGFP-N1, ORAI1 CFP	Addgene #19757
MO91, STIM1 YFP	Addgene #19754
MO91, STIM2 YFP	produced by using in Fusion Kit

3.2.2 Buffer and solutions

- Transfection medium: RPMI medium 1640 + GlutaMAX™-I + 25 mM HEPES, supplemented with 10 % (v/v) FBS.
- FBS: Biochrom, Germany
- PBS (Ca^{2+}/Mg^{2+}-free): Gibco, Life Technology, USA
- Neon Transfection system 100 µl kit: Invitrogen, USA

3.3 Isolation of primary T cells

Primary T cells were isolated from spleens and lymph nodes of C57BL/6 (black 6) mice. The black 6 mouse is the most commonly used mouse as a model of human diseases. The mouse model was created in 1921 by Clarence Cook Little at the Bussey Institute at Harvard University (Åhlgren and Voikar, 2019). At the beginning, the spleen and lymph nodes were embedded in RPMI medium, mashed with the plunger of a syringe and pressed through a strainer. The cells were washed with further medium through the strainer and centrifuged (1200 rpm, 5 min, 4 °C). To lyse the red blood cells, the cells were resuspended in Ack buffer and incubated on ice for 5 min. Afterwards, the suspension was centrifuged (1200 rpm, 5 min, 4 °C) and the supernatant discarded. For the isolation of $CD4^+$ T cells an EasySep Mouse $CD4^+$ T Cell Enrichment Kit was used. Here the $CD4^+$ T cells are separated from the remaining cells by negative selection. In this process, unwanted cells are specifically removed with biotinylated antibodies directed against non-$CD4^+$ T cells and bound to streptavidin-coated magnetic particles (RapidSpheres™). These magnetic particles,

together with bound cells, are separated from the solvent via a magnet. The targeted $CD4^+$ T cells remain in the solution.

3.3.1 Buffer and solutions

- PBS (Ca^{2+}/Mg^{2+}-free): Gibco, Life Technology, USA
- Ack buffer: 4.3 g ammonium chloride; 0.5 g KHCO3; 0.0186 g Na2-EDTA adjust volume to 400 mL with H_2O, pH 7.2–7.4.
- EasySep™ Mouse $CD4^+$ T Cell Isolation Kit: STEMCELL Technologies, Canada

3.4 Membrane preparation

To analyse the interaction of certain proteins, P10 membrane was prepared from Jurkat T cells. In order to grow a large amount of cells, they were cultured in a spinner flask. Initially, cells were centrifuged (1.200 rpm, 5 min, room temperature (RT)) and washed with Ca^{2+} measuring buffer. Afterwards, the cells were resuspended in Ca^{2+} measuring buffer and incubated at 37 °C for 20 min. One part of the cells were stimulated for 5 min with 1.67 µM thapsigargin (Tg) while the other part remained in an unstimulated state (about 2×0^7 lymphocytes per experiment). Cells are centrifuged again (1200 rpm, 5 min, RT), resuspended in RSB buffer and placed on ice for 10 min to swell. Afterwards, the cells were lysed with 30 strokes in a douncer. To exclude the cell nuclei the preparation was centrifuged (2.500 rpm, 5 min, RT) and the supernatant was transferred to a new tube. The pellet with the cell nuclei was discarded. In the final step, the supernatant was centrifuged (10.000 rpm, 30 min, 4 °C) and the resulting pellet - the P10 fraction – was dissolved in RSB buffer. Additionally, the experiment was also performed with primary T cells as described above, but the cells were lysed with a sonicator (3 x 6 s, 70 Hz, on ice).

For the determination of the protein content 250 µL Bradford reagent was added to the fractions in microtiter plates. Different dilutions of Bovine Serum Albumin (BSA) were prepared as a standard series. After 5-30 min incubation at RT, the evaluation was performed with a microtiter plate photometer at a wavelength of 595 nm. All samples were measured as triplicates.

3.4.1 Buffer and solutions

- Ca^{2+} measuring buffer: 20 mM HEPES; 5 mM KCl; 140 mM NaCl; 1 mM NaH_2PO_4; 1 mM $MgSO_4$; 1 mM $CaCl_2$; 5.5 mM Glucose; in dest. H_2O, pH 7.4
- RSB Buffer: 20 mM HEPES; 10 mM $CaCl_2$; 3 mM $MgCl_2$; protease inhibitor; in dest. H_2O, pH 7.2
- Protease inhibitor: Roche, Switzerland
- Tg: Merck, EMD Millipore Corp., Billerica, MA USA
- BSA: SIGMA Life Science, USA
- Bradford reagent: SIGMA Life Science, USA

3.5 Co-Immunoprecipitation (Co-IP)

Co-IP is a technique to identify protein-protein interactions by using protein-specific antibodies (Kaboord and Perr, 2008). In this process, specific proteins are isolated from complex samples using beads coated with specific antibodies against the target protein. Co-IP uses the antibody-protein complex to isolate unknown proteins that bind to the target protein (Qoronfleh et al., 2003). Here, binding between two proteins at different stimulation states of T cells were analysed.

In the first step, magnetic beads (50 µL) were coated with 4 µg of target-specific antibodies (Incubation rotating, overnight, at 4 °C). The following day, the beads were washed three times with PBS-TWEEN and 400 µg of P10 membrane (3.2) was added. The sample was incubated for at least 1.5 hours (rotating, 4 °C). After incubation, the beads were separated from the solvent and washed again three times with PBS-TWEEN. The target protein with its binding partner were bound to the beads.

3.5.1 Buffer and solutions

- PBS-TWEEN: PBS with 0.1 % (w/v) Tween 20
- Protein G magnetic beads: EMD Millipore, PureProteome™ Protein G Magnetic Beads, USA
- 6x Sodium dodecyl sulfate (SDS) sample buffer: 350 mM tris pH 6.8; 30 % (v/v) glycerol; 10 % (w/v) SDS; 0.5 M DTT; 0.0012 % (w/v) bromphenol blue; in bidest. H_2O.
- Sample buffer: 74% (w/v) 6x SDS sample buffer; 4.2% (w/v) SDS; 5% (v/v)

mercaptoethanol

Table 2: Antibodies for Co-IP

Antibody	Origin	Supplier
anti-STIM1 (CDN3H4)	Mouse	Invitrogen, USA
anti-ORAI1	Rabbit	Thermo Scientific, USA

3.6 Western Blotting

3.6.1 SDS polyacrylamide gel electrophoresis (SDS PAGE)

The electrophoretic system developed by Ulrich K. Laemmli is used to analyse proteins via the separation according to their molecular mass (Gallagher, 2012; Laemmli, 1970). In preparation for SDS PAGE, 20 µL H_2O and 5 µL Laemmli sample buffer were added to the magnetic beads described in 3.5. The proteins were denaturated and detached from the beads via incubation with shaking on a heating block at 94 °C for 10 min. In the next step, the sample was separated from the beads, using a magnet and was applied to the gel. In order to be able to assign the proteins to a molecular weight, 10 µL of a protein marker (Multicolour Broad Range Protein Ladder, Thermo Scientific) was additionally applied to the gel. Afterwards, the proteins of the P10 fractions were separated in a polyacrylamide gel, by SDS-PAGE. Whereby the electrophoresis was run at 200 V for about 40 min. Here, precast gradient gels were used with a gradient of acrylamide content of 4-20 %.

3.6.2 Transfer of proteins onto polyvinylidene fluoride (PVDF) membrane

Western blot is a molecular biological method to transfer proteins onto a carrier membrane (Renart et al., 1979). Transferred proteins can specifically detected via protein specific antibodies (Moritz, 2020). For the transfer of the proteins to a PVDF membrane, semi-dry Western blot methods was used (1.5 h, 200 mA, on ice). Therefore, the PVDF membrane was first activated in methanol for 1 min, followed by

a 5 min incubation in water and then a 5 min incubation in transfer buffer. The SDS-polyacrylamide gel was equilibrated in transfer buffer for 10 min. The acrylamide gel, membrane and filter papers were then stacked in the blot apparatus as follows:

Semi dry Blot:

(+) Anode
3x Whatman filter paper
PVDF membrane
Acrylamide gel
(-) 3x Whatman filter paper

The transfer was verified using Ponceau S solution

3.6.3 Immunodetection

After staining with Ponceau S, the membrane was incubated for 1 hour at RT in blocking solution to avoid unspecific binding of the used antibodies. Afterwards, the membrane was incubated over night at 4 °C with the primary antibody diluted in block solution. To remove excess antibody, the membrane was washed three times with TBS-T buffer (10 min each time). Finally, incubation with a HRP (horseradish peroxidase)-conjugated antibody (1:5000 in block solution) was conducted for one hour and washed again three times with TBS-T buffer. For the detection of peroxidase activity the membrane was covered with ECL reagent for 4 min and the chemiluminescence was detected using the ImageQuant LAS4000.

3.6.4 Buffer and solutions

- SDS electrode buffer: 3 g Tris; 14.4 g glycine; 1 g SDS adjust volume to 1 L with H_2O
- Transfer buffer: 5.8 g Tris; 2.9 g glycine; 0.37 g SDS, 200 mL methanol; adjust volume to 1 L with H_2O
- TBS: 150 mM NaCl; 100 mM Tris-HCl; in bidest. H_2O, pH 7.5
- TBS-T: TBS with 0.1 % (w/v) Tween 20
- Methanol: Avantor, USA

- Ponceau S Staining solution: AppliChem, USA
- Block solution: TBS-T with 5 % (w/v) low-fat milk powder
- ECL reagent: 90 % (v/v) Super Signal West Dura Trial Kit (Thermo Scientific), USA mixed with 10 % (v/v) Super Signal West Pico Chemiluminescent Substrate Kit (Thermo Scientific), USA
- Protein standard (260 kDa – 10 kDa): Thermo Scientific Spectra™ Multicolor Broad Range Protein Ladder, Lithuania
- 4-20 % Precast gel: Mini-PROTEAN® TGX™ Gels, USA
- PVDF Membrane: Merck Millipore Ltd., Immobilon®-P Transfer Membrane, Germany

Table 3: Antibodies for Western Blot

Antibody	Origin	Dilution	Supplier
anti-STIM1 (CDN3H4)	Mouse	1:1000	Invitrogen, USA
anti-ORAI1	Rabbit	1:1000	Thermo Scientific, USA
HRB	Goat anti rabbit	1:5000	Thermo Scientific, USA
HRB	Goat anti-mouse	1:5000	Biozol, Germany

3.7 Fluorescence microscopy

3.7.1 Förster resonance energy transfer (FRET)

FRET is a physical process of energy transfer and is first described by Theodor Förster in 1946 (Förster, 1946). In this process, the energy of an excited dye (donor) is transferred to a second dye (acceptor), whereby the energy is not exchanged via a release (emission) and absorption (absorption) of photons (Bajar et al., 2016). The energy transfer only takes place when the fluorescent molecules have a distance of

less than 10 nm. Therefore, the FRET method can be used to determine a protein-protein interaction.

The Jurkat T cells, transfected with ORA1-CFP and STIM1- or STIM2-YFP (described in 3.2) were centrifuged (1200 rpm, 5 min, RT) and washed with Ca^{2+} measuring buffer. After the washing step the cells were centrifuged (1200 rpm, 5 min, RT) again and dissolved in 2 mL Ca^{2+} measuring buffer. Cells were placed on slides coated with either BSA (5 mg/mL) or BSA (5 mg/mL) and poly-L-lysine (PLL) (5 mg/mL). After the cells settled on the slide, the FRET signal was recorded either directly or after two minutes of stimulation with OKT3 (1 µg/ml) or Tg (1.67 µM). Images were acquired using a super resolution spinning-disk (Visitron) equipped with a CSU-W1 SoRa Optic (2.8 x, Yokogawa), a 100 x magnification objective (Zeiss) and a sCMOS camera (Orca-Flash 4.0, C13440-20CU Hamamatsu). The different fluorophores were excited with lasers [CFP: excited with a 405 nm laser, detected with a 445/50 emission filter and YFP: excited with a 515nm laser, detected with a 540/30 emission filter. FRET images were corrected for spectral cross-talk (bleedthrough) of the donor and acceptor signal into the FRET channel. Bleedthrough correction was determined by expressing the donor (ORAI1 CFP) and acceptor (STIM1 YFP and STIM2 YFP) separately, and the resulting bleedthrough (CFP, 92 %; YFP, 13 %) was subtracted from the FRET channel image of double-transfected cells to get the true FRET image. The ImageJ plugin pixFRET was used to determine the FRET signal (FRET Calculation).

3.7.2 SoRa Imaging

Co-localization between ORAI1 and STIM1 or STIM2 was determined using SoRa microscopy. The SoRa microscope has a spinning disc, which enables fast imaging in confocal mode. Using a relatively high post-magnification and by applying micro lenses, the spinning disk mode provides an approximate 1.4-fold improvement in lateral resolution beyond the optical diffraction limit (Azuma and Kei, 2015).

Initially, primary mouse wild type (WT) T cells were stimulated with Tg (1.67 µg/ml) for 5 min or remained in an unstimulated state. After stimulation, the cells were seeded on slides coated with BSA (5 mg/ml) or BSA (5 mg/ml) and PLL (0.1 mg/ml) and fixed with 4 % (w/v) paraformaldehyde (PFA) for 15 min. To permeabilise the cells, they were incubated with 0.05 % (w/v) saponin for 15 min. The next step is to block non-specific binding sites. Therefore, the cells were incubated with 10 % (v/v) fetal bovine serum

(FBS) over night at 4 °C. Primary antibodies (see table below) were diluted in 3 % (v/v) FBS and incubated for 1 hour at room temperature. Secondary antibodies [anti-rabbit Alexa Fluor 488, 1:400 (A21206, Life Technologies) and anti-mouse Alexa Fluor 568, 1:400 (A11004, Thermo Fisher Scientific)] were likewise diluted in 3 % (v/v) FBS and incubated for 1 hour at room temperature. After staining the slides were washed four times with 3 % (v/v) FBS. In the last step, coverslips were mounted with Abberior Mount Solid over night at 4 °C. Images were acquired using a super resolution spinning-disk microscope (Visitron) equipped with a CSU-W1 SoRa Optic (2.8 x, Yokogawa), a 100 x magnification objective (Zeiss) and a sCMOS camera (Orca-Flash 4.0, C13440-20CU Hamamatsu). The following lasers and filters were used for the respective dyes and fluorophores [Alexa Fluor 488: ex 488 nm laser, em 525/50 nm; Alexa Fluor 568: ex 561 nm laser, em 609/54 nm]. To analyze protein co-localization, a deconvolution script was used (Openlab5; PerkinElmer). Subsequently, in FIJI (version 1.52p) the trainable weka (Waikato environment for knowledge analysis) segmentation plugin and a watershed segmentation was used to obtain a more detailed segmentation of the detected proteins. To calculate and quantify the co-localization, a Matlab script (described in (Nauth et al., 2018)) was adopted

3.7.3 STED Imaging

To obtain a higher resolution of the individual proteins the co-localization between ORAI1 and STIM1 or STIM2 was determined by STED microscopy. STED microscopy creates super-resolution images by selectively deactivating fluorophores (Westphal et al., 2008). With the STED method it is possible to achieve a resolution of up to 20-40 nm. For this purpose, the specimen is not only illuminated with the excitation beam, but simultaneously with a second laser beam, the "depletion beam". This depletion beam has a doughnut-shaped profile so that only the area of the excitation beam with maximum brightness remains visible (Yang et al., 2021).

The primary mouse WT T cells were prepared as described for SoRa imaging. In contrast, the secondary antibodies [anti-rabbit STAR RED, 1:200 (STRED-1001-500UG, Abberior Instruments) and anti-mouse Alexa Fluor 594, 1:200 (A11037, BioLegend)] were used instead. Images were acquired with the Abberior Expert Line fourchannel easy3D STED equipped with a 775 depletion beam (Abberior Instruments), a Nikon 60x, 1.4-numerical aperture objective and a QUAD beam

scanner. Alexa Fluor 594 was excited with a pulsed 561-nm diode beam, depleted with a pulsed 775-nm STED beam and detected with a 615 ± 20-nm emission filter. Star red 640 was excited with a pulsed 640-nm diode beam, depleted with the 775-nm STED beam and detected with an avalanche photo diode (APD) with in front 685 ± 70-nm band pass filter. In all experiments the pixel size was set to 20 nm. The initialising step of the analysis is a background correction by using a deconvolution script (Richardson-Lucy algorithm, Abberior). The segmentation plugins and the Matlab script described above were used to analyse the co-localization, as well as tight and loose cluster formation (described in 4.2) of the different proteins.

Table 4: Antibodies for Immunostaining

Antibody	Origin	Dilution	Supplier
ORAI1	Mouse	1:50	Proteintech, USA
STIM1	Rabbit	1:100	Cell Signaling, USA
STIM2	Rabbit	1:600	ProSci, USA
FAK	Rabbit	1:100	Abcam, England
IP_3R1	Rabbit	1:100	Invitrogen, USA
IP_3R2	Rabbit	1:100	Alomone, USA
IP_3R3	Rabbit	1:100	Invitrogen, USA

3.7.5 Buffer and solutions

- Ca^{2+} measurement buffer: 140 mM NaCl; 5 mM KCl; 1 mM CaCl2; 1 mM MgSO4; 1 mM NaH2PO4; 20 mM HEPES; 5.5 mM glucose; in bidest. H_2O, pH 7.4
- Saponin: Fluka, Germany
- Tg: Merck, EMD Millipore Corp., Billerica, USA
- PLL: Sigma-Aldrich Co, USA or Sigma-Aldrich Chemie GmbH, Germany
- BSA: SIGMA Life Science, USA
- PFA 4%: Alfa Aesar, USA
- PBS (Ca^{2+}/Mg^{2+}-free): Gibco, Life Technology, USA
- FBS: Biochrom, Germany
- Mount solid: Abberior, USA

3.8 Devices

- Blotting-Chamber semi-dry: Bio-Rad, Trans-Blot® SD Semi-Dry Transfer Cell, USA
- Blotting-Chamber wet-Blot: Bio Rad, Mini Trans-Blot® Cell, USA
- CASY TT1 cell counter: Schärfe Systeme, Germany
- Cellspin: Integra Biosciences, Cellspin, Switzerland
- Centrifuge 5810 R: Eppendorf, Germany
- Chamber: Bio-Rad, Mini PROTEAN® Tetra Cell, USA
- Chemiluminescence documentation system: Image Quant LAS4000, GE Healthcare, Great Britain or Vilber GmbH, Fusion FX, France
- CO2 incubator: Thermo, Heraeus Instruments, Germany
- Douncer: GPE scientific, Ireland
- Haemocytometer with division according to Neubauer: Hellma, Germany
- Heating Block: Eppendorf, Thermomixer 5436, Germany
- Light microscope: OLYMPUS CK2, Japan
- Magnet: BD Biosciences, BD IMag™, USA
- Microtiter plate photometer: Thermo Scientific, USA
- Neon™ Transfection System: Invitrogen, USA
- Power Supply: Bio-Rad, PowerPac™, USA
- Rocker: Biometra, WT12, Germany
- Rotor: Ika, Ika® Trayster digital, China
- Sonicator: BANDELIN electronic, UW 70, Germany
- SoRa Microscope: Visitron GmbH, Germany
- Spinner-Flasks: Integra Biosciences, Cellspin 1000, Switzerland
- STED Microscope: Abberior instruments, USA
- Sterile workbench: BDK GmbH, Germany
- Ultracentrifuge: Sorvall, RC 5C Plus, USA

4. Results

The aim of this study was to analyse the adhesion mediated signalling pathway activated by the binding of T cells to PLL. Therefore, the first part of this work was to find the optimal advanced optical method to determine the localization of proteins.
The second part of the study focuses on the pathway of adhesion-dependent T cell activation upstream of SOCE activation.

4.1 Analysis of the interaction between ORAI1 and the STIM proteins during T cell activation

As already described above our group discovered that Ca^{2+} microdomains acquired in the absence of TCR/CD3 stimulation are dependent on Ca^{2+} influx.
Initially, it was tested whether a binding between ORAI1 and STIM1 in the unstimulated state of T cells was detectable. Therefore, a Co-IP experiment was performed (Fig. 4.1). Beads were labeled with anti-ORAI1 or anti-STIM1 antibodies and incubated with membrane fragments of Jurkat T cells. In this case, the cells were in solution without contact to adhesive surfaces before fragmentation. (Fig. 4.1a-c). Using membrane fragments from unstimulated T cells, STIM1 was detected in ORAI1 precipitates and *vice versa* (Fig. 4.1b+c). As positive control samples were stimulated with Tg (1.67 µM). As expected, much stronger signals compared to unstimulated T cells were obtained (Fig. 4.1b+c). Similarly, in unstimulated primary WT T cells, a weak but clearly detectable binding between ORAI1 and STIM1 was determined in STIM1 Co-IPs (Fig. 4.1d+e).

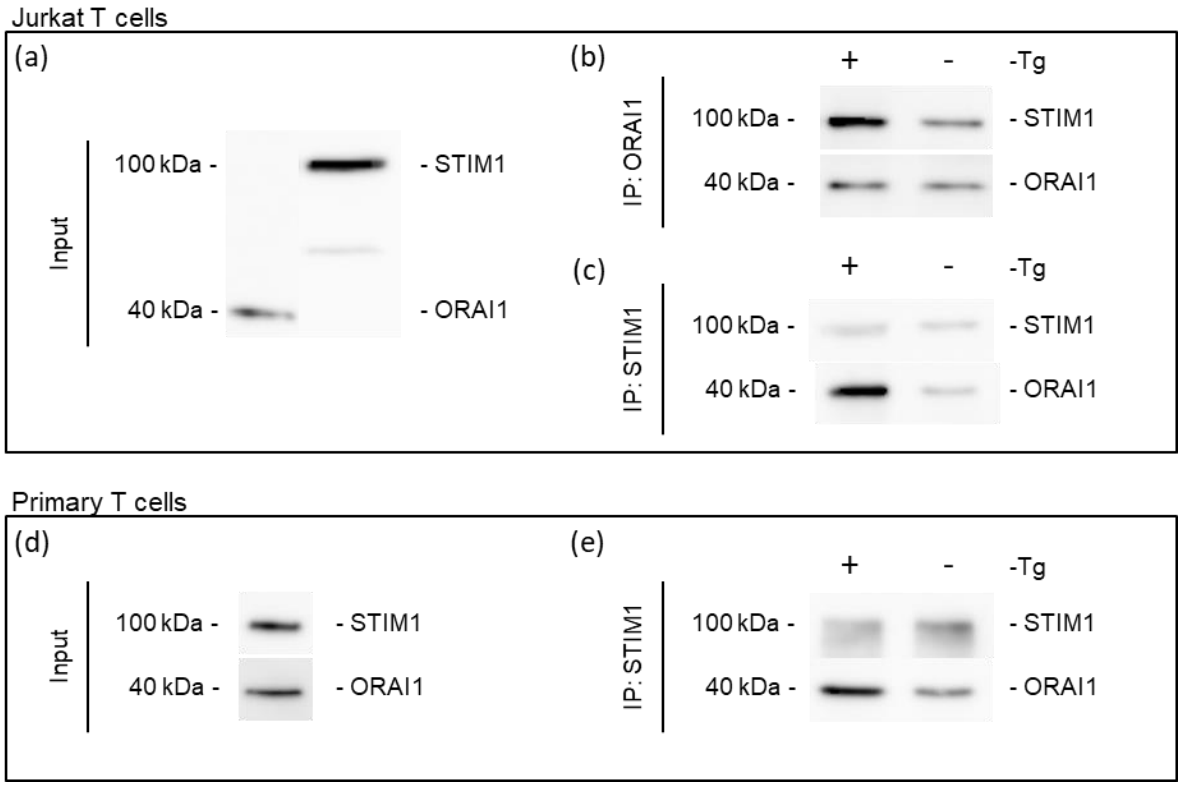

Figure 4.1: Detection ORAI1 and STIM1 binding in non-stimulated Jurkat and primary murine T cells by Co-IP.

Binding between STIM1 and ORAI1 was determined in (a-c) Jurkat T cells and in (d-e) primary mouse WT T cells. A representative Western Blot experiment (n=3) shows the detection of STIM1 and ORAI1 in (a) membranes of Jurkat T cells and (d) in the whole cell lysate of primary murine T cells. A representative Co-IP of fragmented membranes obtained from unstimulated or stimulated with Tg (1.67 µM) (positive control) Jurkat T cells (n=3) using beads coupled with either (b) anti-ORAI1 or (c) anti-STIM1 antibody. (e) Pull-down of whole cell lysate obtained from unstimulated or stimulated primary WT T cells (n=3) using beads coupled with anti-STIM1.

Taken together, weak but detectable binding between STIM1 and ORAI1 was observed by Co-IP in Jurkat T cells as well as in primary mouse T cells without TCR/CD3 stimulation.

4.1.1 Adhesion-dependent interaction between ORAI1 and STIM proteins using advanced optical methods

To mimic adhesion of the T cells, the experiments were performed on a PLL coating. By weakening the adhesive force acting on T cells, e.g. by replacing PLL by bovine serum albumin (BSA) coating, a significant decrease in the number of Ca^{2+} microdomains was observed (communicated by Dr. Mariella Weiß, Department of

Biochemistry and Molecular Cell Biology, University Medical Center Hamburg-Eppendorf, unpublished data). Based on these results, it was investigated whether there is an adhesion-dependent increase of co-localization between ORAI1 and STIM proteins. Therefore, the interaction was measured under three different conditions:
(i) Without adhesion (cells on BSA coated slides), (ii) weak adhesion (cells on PLL coated slides) and (iii) weak adhesion plus activation of T cells (stimulation of TCR by anti-CD3 antibody (OKT3) or SOCE activation by Tg).
The anti-CD3 antibody activates T cells by binding to the TCR, while Tg induces ER depletion which stimulates SOCE via inhibition of SERCA (Rogers et al., 1995).
The adhesion-dependent interaction between ORAI1 and STIM proteins were determined using three different advanced optical methods, (i) FRET, (ii) SoRa and (iii) STED imaging.

4.1.2 Analysis of the interaction between ORAI1 and STIM proteins using FRET

To determine the degree of co-localization between ORAI1 and the STIM proteins, Jurkat T cells were transfected with ORAI1-CFP and STIM1-YFP or STIM2-YFP constructs and the FRET signals were analyzed. The images were recorded using SoRa microscopy, hence a spatial resolution of images of approximately 120 nm was achieved. This feature enables comparison of FRET signals in T cells at high resolution either adhesion-dependent and or non-adhesion-dependent. As a positive control, T cells were stimulated with anti-CD3 antibodies (OKT3) (1 µg/ml) or Tg (1.67 µM). In all the different conditions, FRET signals were observed between ORAI1 and STIM1 (Fig. 4.2), as well as between ORAI1 and STIM2 (Fig. 4.3) at the plasma membrane.

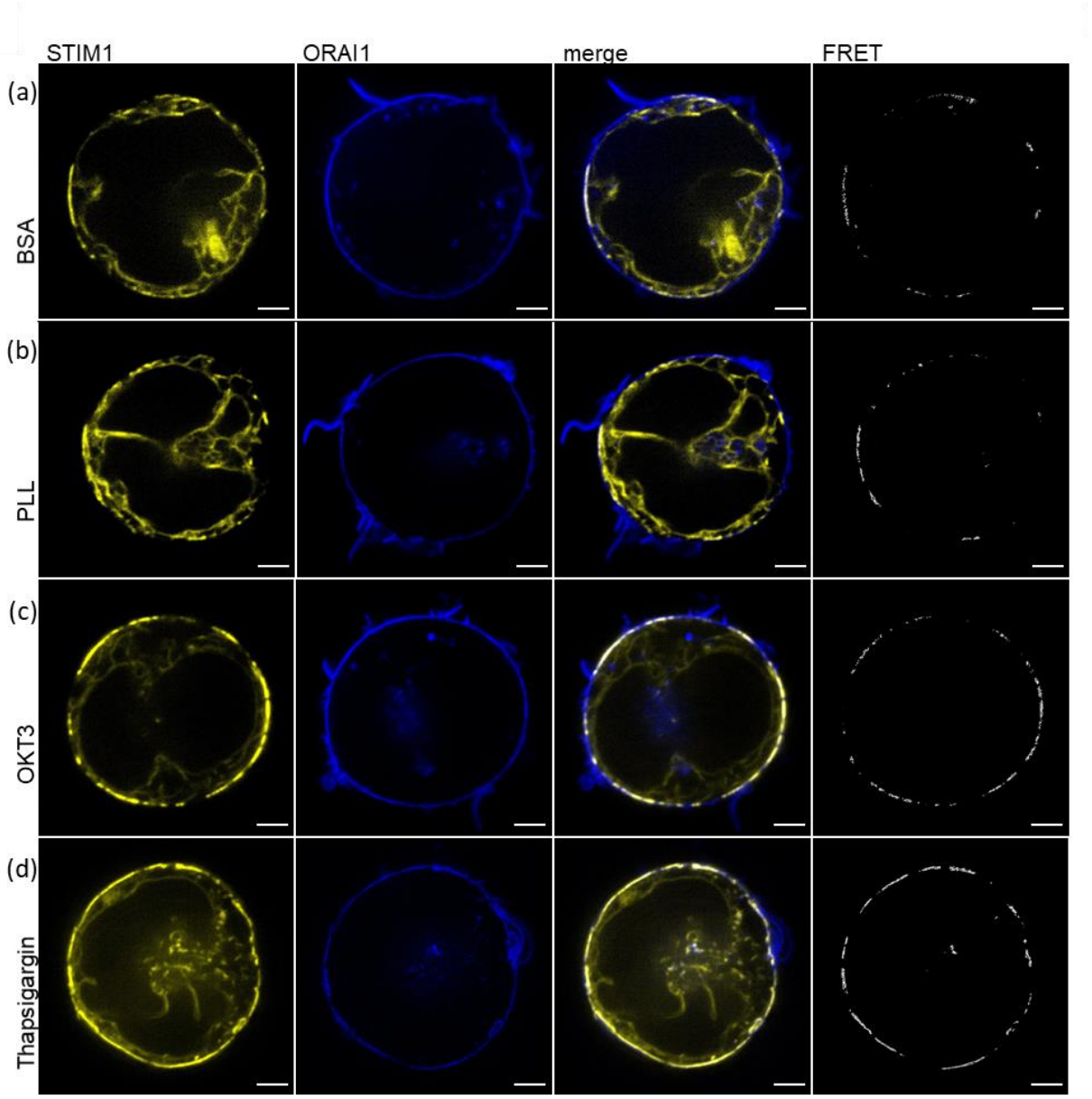

Figure 4.2: Determination of the degree of co-localization of STIM1 and ORAI1 by different stimulations and conditions in Jurkat T cells.

Co-localization of STIM1 and ORAI1 was determined by FRET experiments, using SoRa microscopy at approx. 120 nm spatial resolution. Jurkat T cells transfected with ORAI1-CFP and STIM1-YFP constructs were seeded on slides coated with (a) BSA or (b) PLL and were stimulated with (c) OKT3 (1 µg/ml) or (d) Tg (1.67 µM). Representative images of Jurkat T cells after background correction; STIM1 labelled in yellow, ORAI1 in blue, the merged image and the FRET signal between STIM1 and ORAI1 are shown. Scale bar: 2 µm.

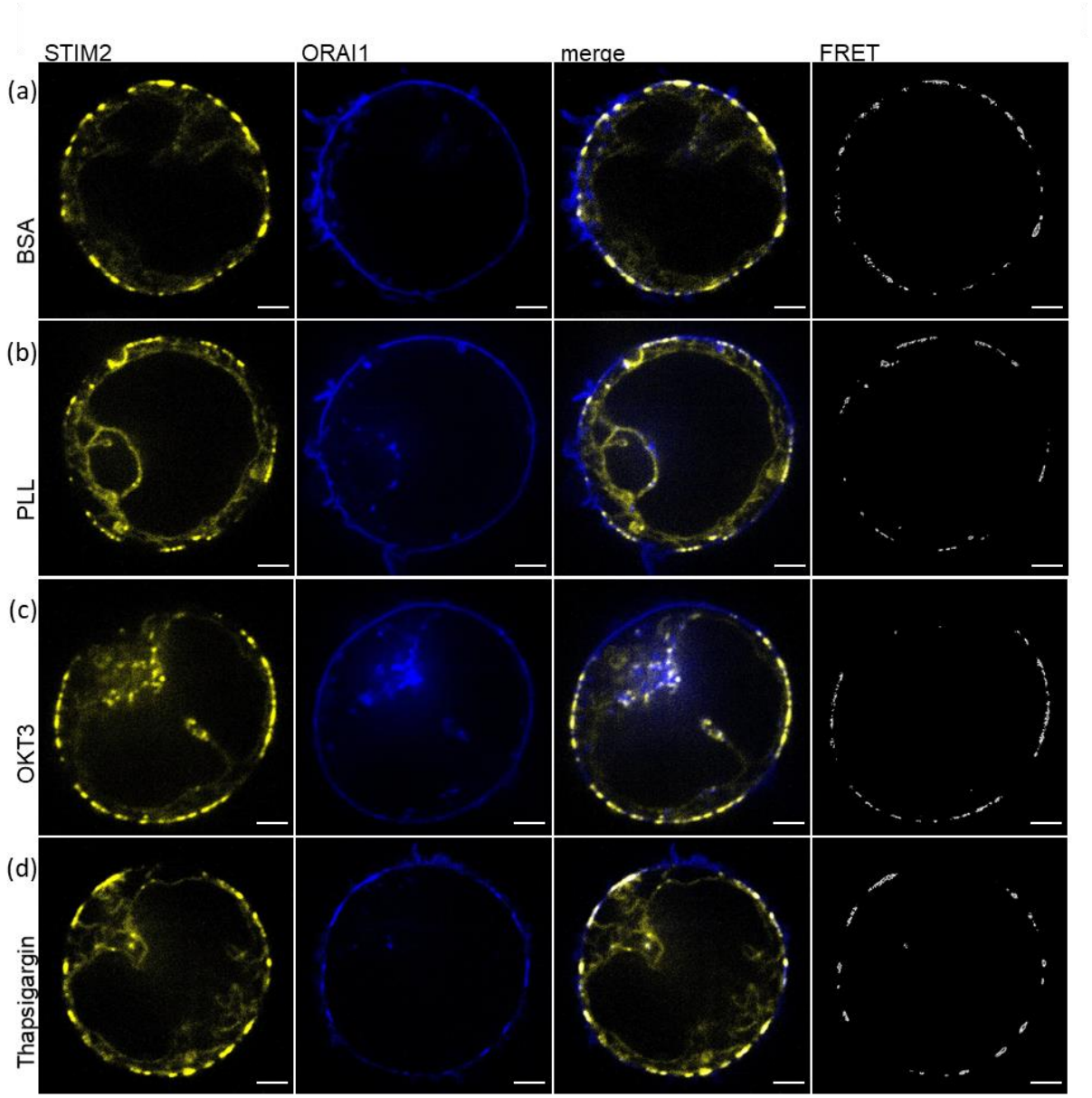

Figure 4.3: Determination of the degree of co-localization of STIM2 and ORAI1 by different stimulations and conditions in Jurkat T cells.

Co-localization of STIM2 and ORAI1 was determined by FRET experiments, using SoRa microscopy at approx. 120 nm spatial resolution. Jurkat T cells transfected with ORAI1-CFP and STIM2-YFP constructs were seeded on slides coated with (a) BSA or (b) PLL and were stimulated with (c) OKT3 (1 µg/ml) or (d) Tg (1.67 µM). Representative images of Jurkat T cells after background correction; STIM2 labelled in yellow, ORAI1 in blue, the merged image and the FRET signal between STIM2 and ORAI1 are shown. Scale bar: 2 µm.

Statistical analysis revealed a slight but not significant increase in FRET signals between ORAI1 and STIM1 from non-adhesion in comparison to adhesion and after T cell activation (Fig. 4.4a). No difference in FRET signal was detected in the interaction

between ORAI1 and STIM2 in the different conditions (Fig. 4.4b).

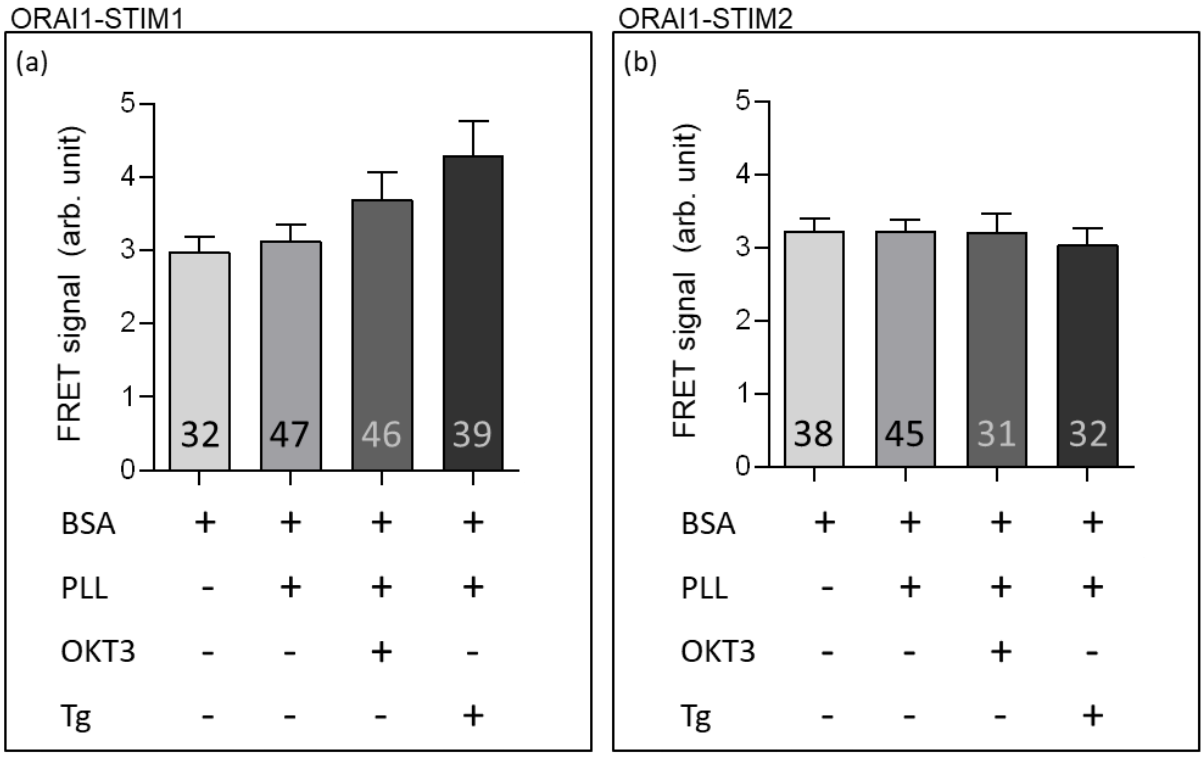

Figure 4.4: Statistical Analysis of ORAI1-STIM1 and ORAI1-STIM2 co-localization in Jurkat T cells.

Figure shows the statistical analysis of the co-localization between (a) ORAI1 and STIM1 or (b) ORAI1 and STIM2 determined by FRET experiments using SoRa microscopy at approx. 120 nm spatial resolution. Jurkat T cells were seeded on slides coated with BSA or with PLL and the FRET signal was determined without stimulation and after 2 min of incubation with OKT3 (1 µg/ml) or Tg (1.67 µM). Statistical test: one-way ANOVA, Bonferroni correction.

4.1.3 Analysis of the interaction between ORAI1 and the STIM proteins by using SoRa microscopy

In the next chain of experiments, the adhesion-dependent co-localization between ORAI1 and the STIM proteins was analyzed using immunofluorescence microscopy. Primary murine T cells were fixed on slides, stained with antibodies against ORAI1, STIM1 and STIM2 and the images were recorded by the SoRa microscope at a spatial resolution of approx. 120 nm. In addition to the adhesion-dependent measurements, T cells were stimulated with Tg (1.67 µM), which functions as a positive control. Comparison of representative T cells showed co-localization between ORAI1 and STIM1 (Fig. 4.5) or STIM2 (Fig. 4.6) at the plasma membrane in all conditions.

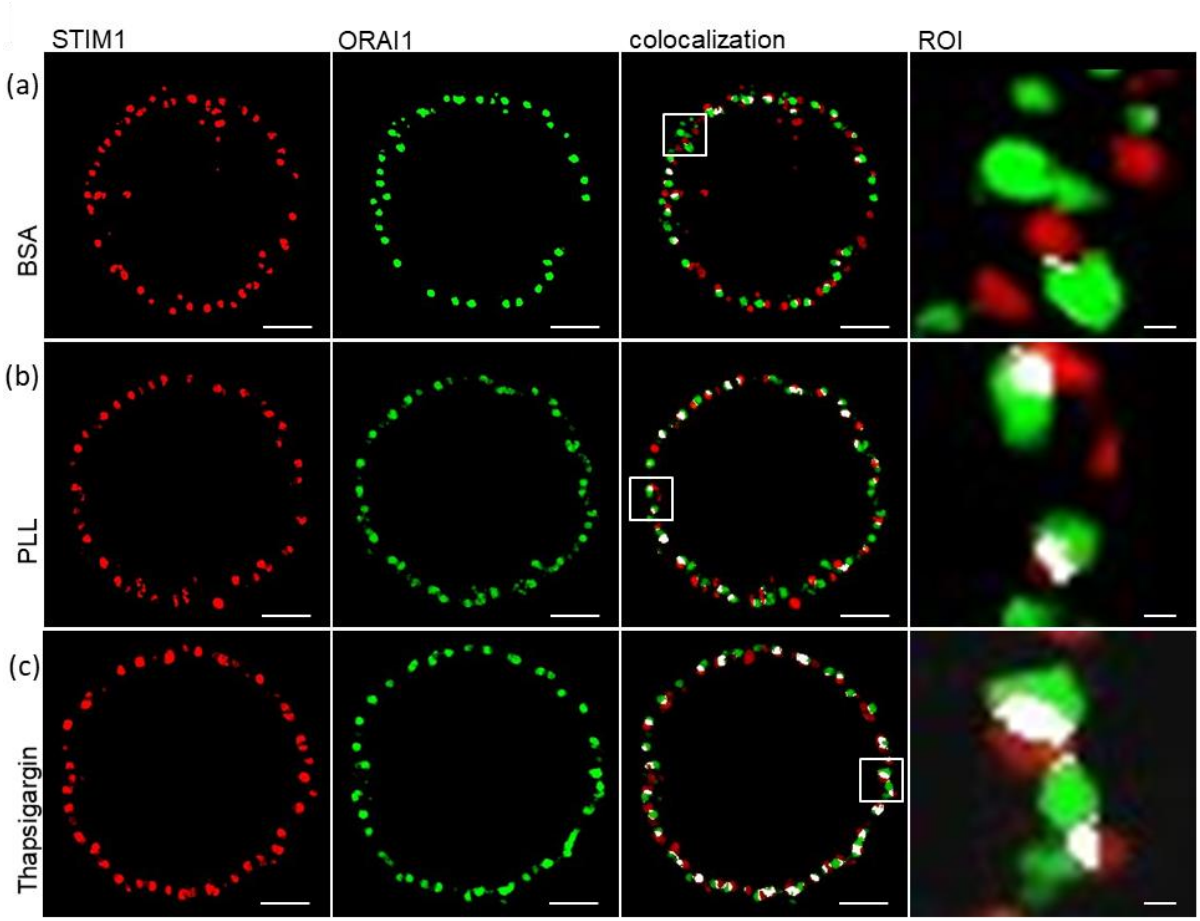

Figure 4.5: Co-localization of ORAI1 and STIM1 in primary murine T cells using SoRa microscopy.

Primary murine T cells were seeded without TCR stimulation on either (a) BSA or (b) PLL coated slides or were (c) incubated for 5 min with Tg (1.67 µM) before fixation. The distribution of protein and co-localization in representative primary murine WT T cells after weka (Waikato environment for knowledge analysis) segmentation, recorded by SoRa microscopy at approx. 120 nm spatial resolution are shown; STIM1 labelled in red, ORAI1 labelled in green, co-localization in white. The magnification (ROI) shows a region of co-localization at the plasma membrane. Scale bar: 2 µm; ROI: 100 nm.

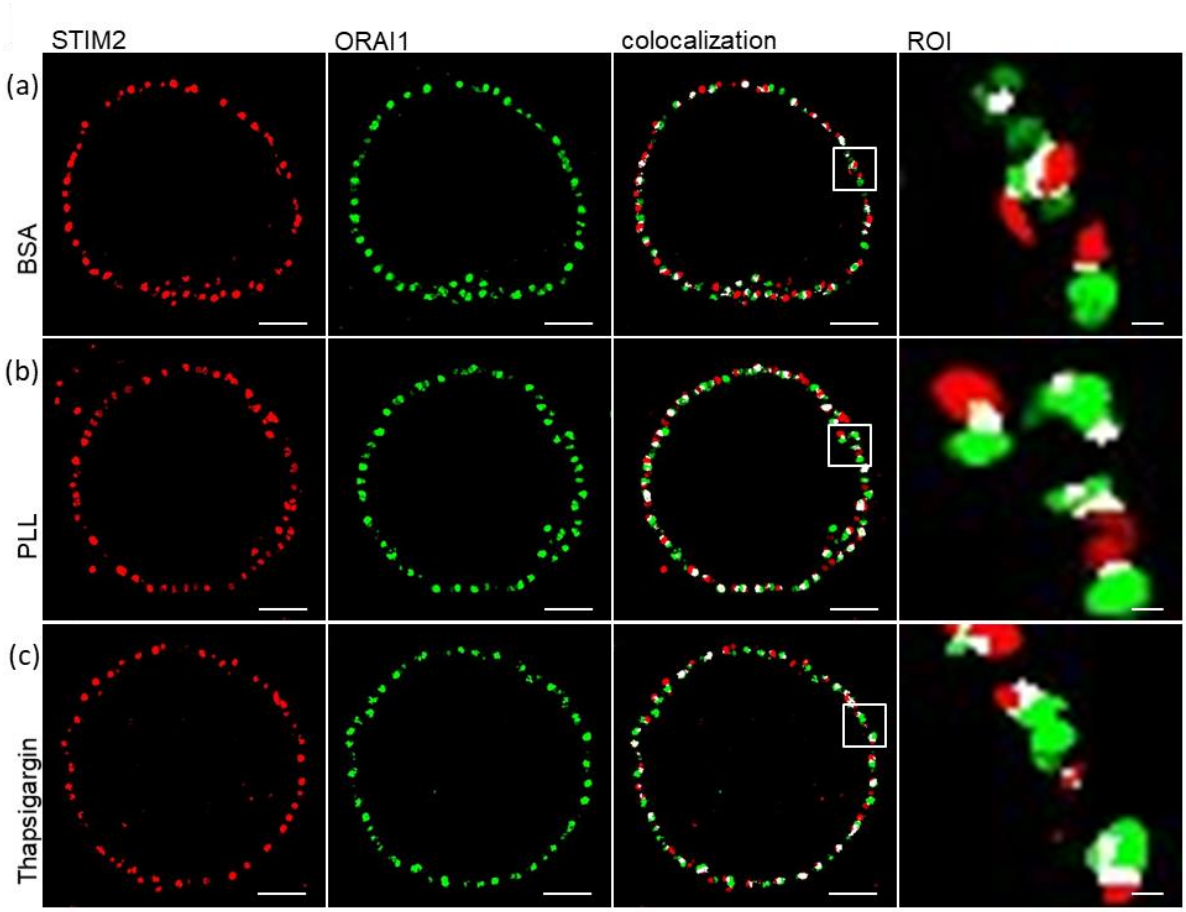

Figure 4.6: Co-localization of ORAI1 and STIM2 in primary murine T cells using SoRa microscopy.

Primary murine T cells were seeded without TCR stimulation on either (a) BSA or (b) PLL coated slides or were (c) incubated for 5 min with Tg (1.67 µM) before fixation. The distribution of protein and co-localization in representative primary murine WT T cells after weka (Waikato environment for knowledge analysis) segmentation, recorded by SoRa microscopy at approx. 120 nm spatial resolution are shown; STIM2 labelled in red, ORAI1 labelled in green, co-localization in white. The magnification (ROI) shows a region of co-localization at the plasma membrane. Scale bar: 2 µm; ROI: 100 nm

30.6 % of the ORAI1 proteins were determined to co-localize with STIM1 in non-adhesion conditions (BSA-coated slides) (Fig. 4.7a). Co-localization increased to 33.8 % after slight stimulation using PLL-coated slides (Fig. 4.7a). A significant increase to 40.7 % was observed from slightly stimulated to activated T cells (Fig. 4.7a). The co-localization between ORAI1 and STIM2 was similar in all conditions. It was observed that 34.4 % of ORAI1 proteins co-localize with STIM2 in non-adherent conditions, 34.8 % in adherent conditions and 32.7 % after T cell activation (Fig. 4.7b).

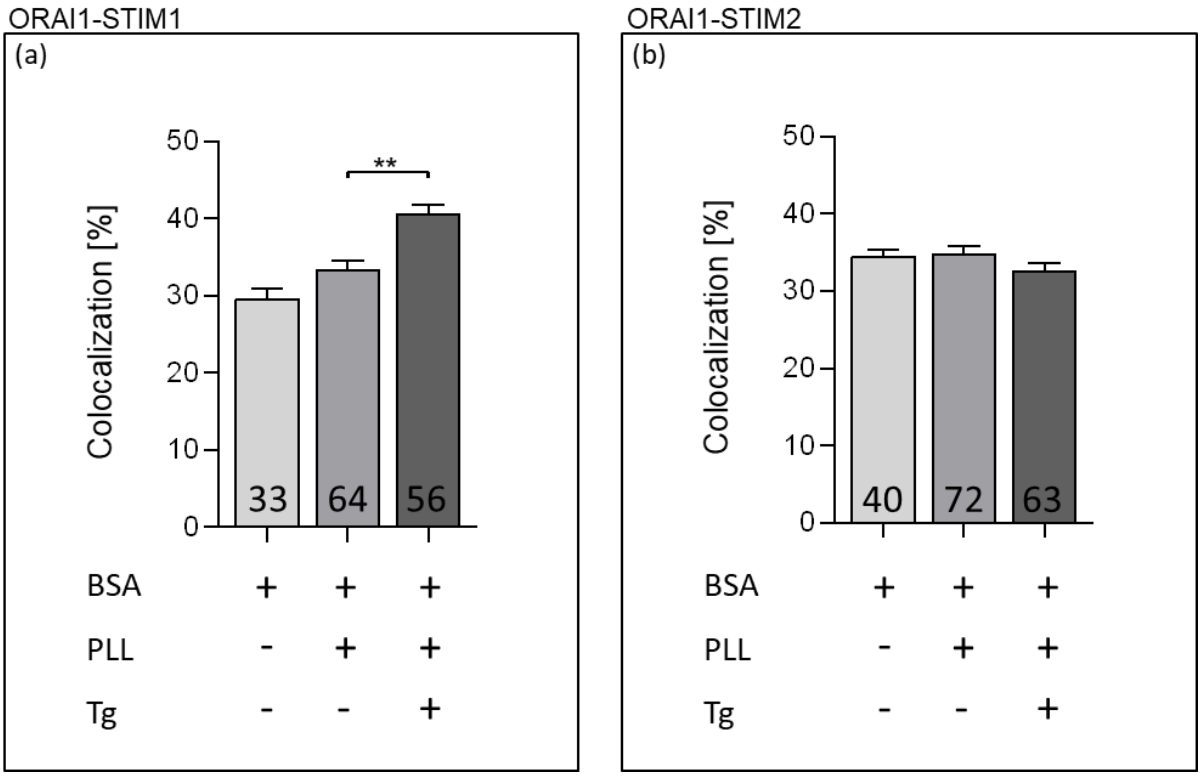

Figure 4.7: Statistical Analysis of the co-localization between ORAI1 and STIM1 or STIM2 determined by SoRa microscopy.

Shown are the statistical analyses of the percentage of ORAI1 proteins that co-localize with (a) STIM1 or (b) STIM2. The localization was determined at approx. 120 nm spatial resolution using SoRa microscopy. Primary murine T cells were seeded on slides coated with BSA or with PLL and the co-localization was determined without stimulation or after 5 min of incubation with Tg (1.67 µM). Statistical test: one-way ANOVA, Bonferroni correction: **: $p<0.01$.

Altogether, using SoRa microscopy, an increase in the co-localization between ORAI1 and STIM1 was observed during progressing T cell activation, with a significantly higher increase after stimulation than on PLL-coated slides. The co-localization between ORAI1 and STIM2 remained constant in all conditions.

4.1.4 Analysis of the interaction between ORAI1 and the STIM proteins using STED microscopy

Next, the adhesion-dependent co-localization between ORAI1 and the STIM proteins was determined by STED microscopy, achieving a resolution of 40 to 50 nm. With this method, we obtained the best resolution and hence we detected the precise localization of the individual proteins. Primary murine T cells were fixed, labeled with

antibodies and the images were analyzed under the same conditions. As in the experiments before, co-localization between ORAI1 and STIM1 (Fig. 4.8) or STIM2 (Fig. 4.9) at the plasma membrane was observed in all conditions.

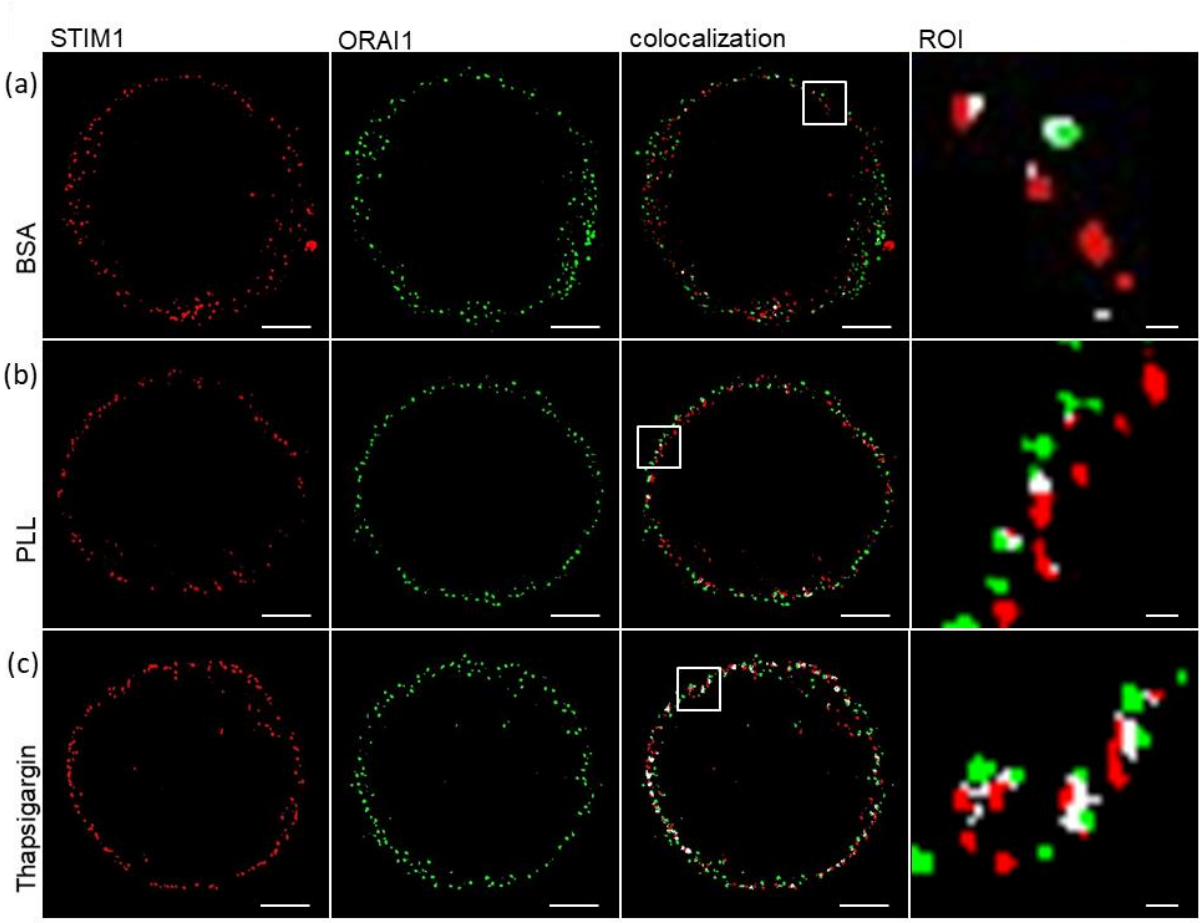

Figure 4.8: Co-localization of ORAI1 and STIM1 in primary murine T cells using STED microscopy.

Super resolution STED images at approx. 40 nm spatial resolution were used to determine the localization of proteins on slides coated with either BSA or with PLL. Representative primary murine T cells, (a and b) without stimulation or (c) after 5 min of incubation with Tg (1.67 µM) are shown. The protein distribution and co-localization is depicted after weka (Waikato environment for knowledge analysis) segmentation. The STIM1 proteins are marked in red, ORAI1 in green and the co-localization in white. The magnification (ROI) shows a region of the plasma membrane with average co-localization between ORAI1 and STIM1. Scale bar: 2 µm; ROI: 100 nm.

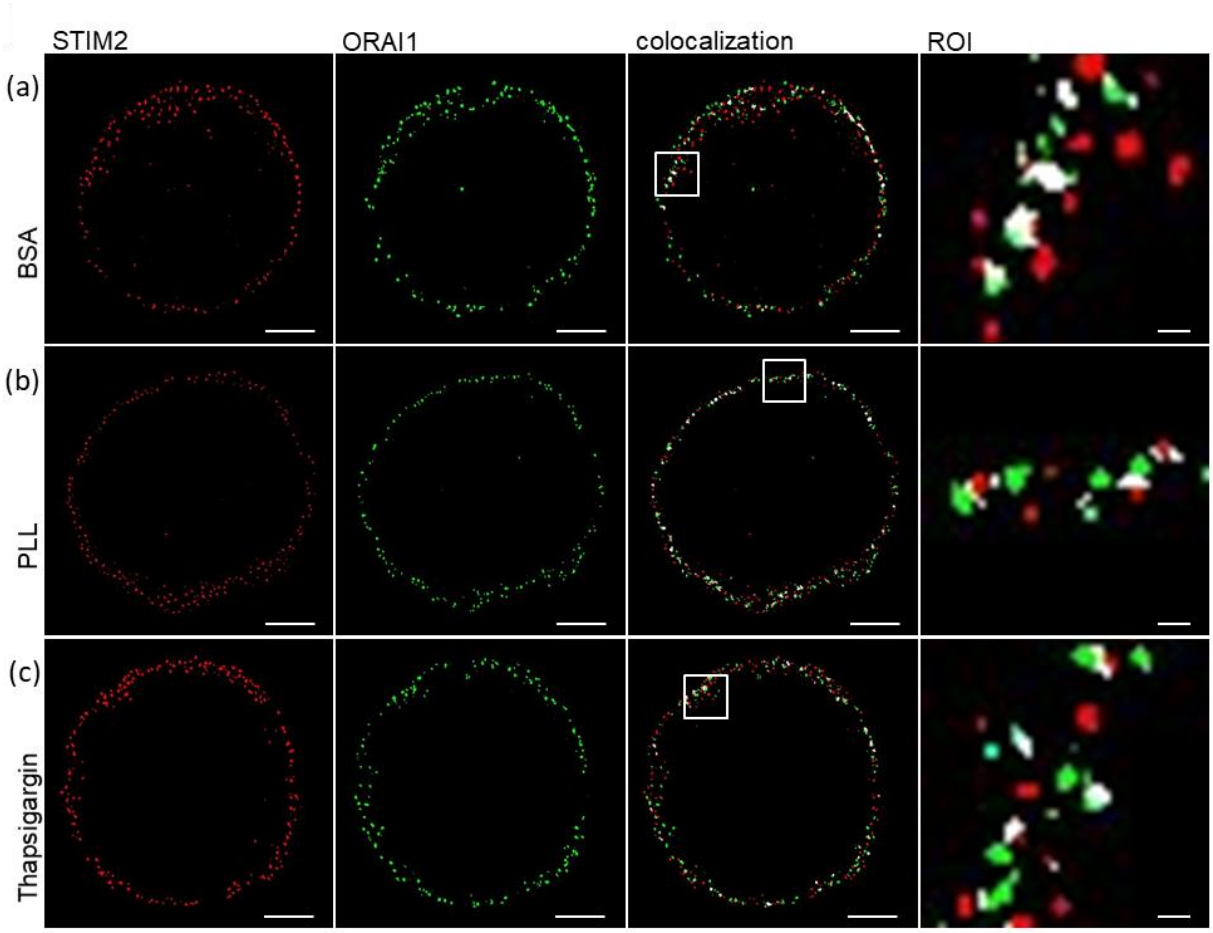

Figure 4.9: Co-localization of ORAI1 and STIM2 in primary murine T cells using STED microscopy.

Super resolution STED images at approx. 40 nm spatial resolution were used to determine the localization of proteins on slides coated with either BSA or with PLL. Representative primary murine T cells, (a and b) without stimulation or (c) after 5 min of incubation with Tg (1.67 µM) are shown. The protein distribution and co-localization is depicted after weka (Waikato environment for knowledge analysis) segmentation. The STIM2 proteins are marked in red, ORAI1 in green and the co-localization in white. The magnification (ROI) shows a region of the plasma membrane with average co-localization between ORAI1 and STIM2. Scale bar: 2 µm; ROI: 100 nm.

9.9 % of ORAI1 proteins co-localized with STIM1 in non-adherent conditions (BSA-coated slides). After adhesion of -coated slides, a significant increase in co-localization (18 %) was detected. Compared to slight stimulation, a significant increase in co-localization of ORAI1 proteins with STIM1 corresponding to 32.9 % was observed after stimulation with Tg (1.67 µM) (Fig. 4.10a). The co-localization between ORAI1 and STIM2 showed only marginal changes in all conditions. It was shown that 40.3 % of ORAI1 proteins co-localize with STIM2 in non-adherent conditions, 43.2 % in adherent conditions and 40.3 % after T cell activation respectively (Fig. 4.10b).

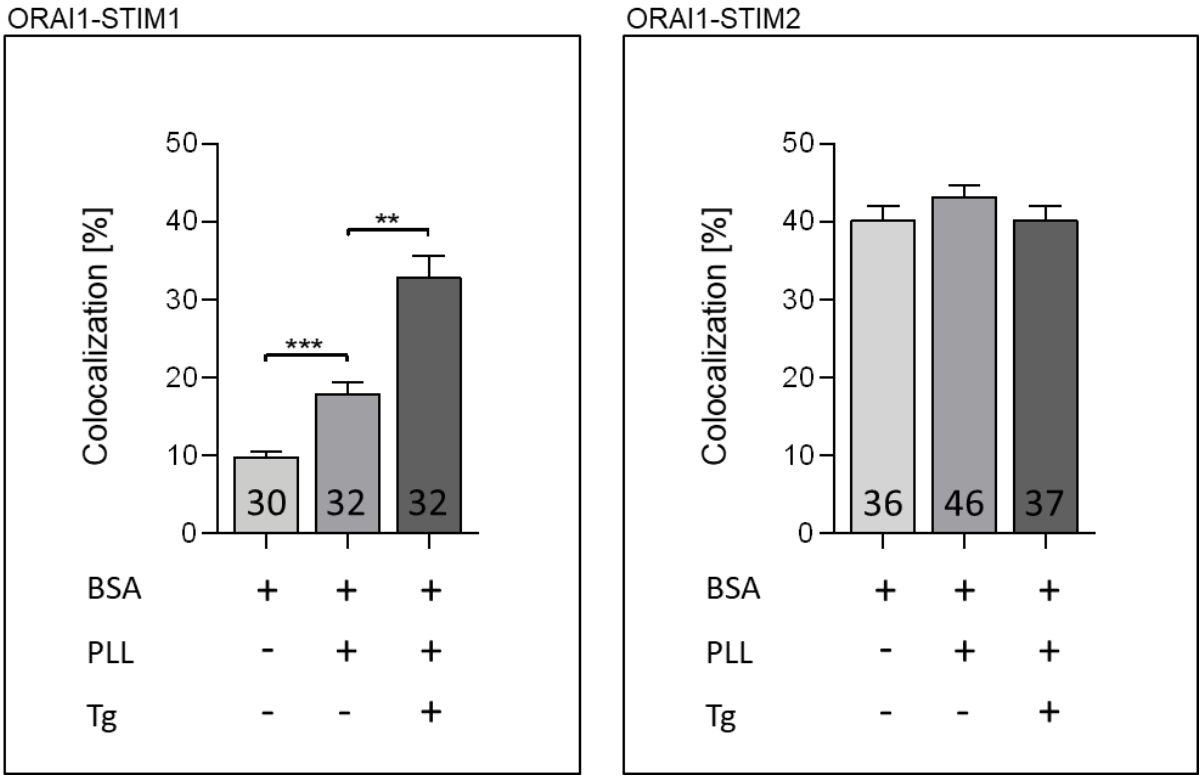

Figure 4.10: Statistical Analysis of the co-localization between ORAI1 and STIM1 or STIM2 determined by STED microscopy.

Figure shows the statistical analysis of the percentage of ORAI1 proteins that co-localize with (a) STIM1 or (b) STIM2. The localization was determined at approx. 40 nm spatial resolution using super-resolution STED microscopy. Primary murine T cells were seeded on slides coated with BSA or with PLL and the co-localization was determined without stimulation or after 5 min of incubation with Tg (1.67 µM). Statistical test: one-way ANOVA, Bonferroni correction: **: $p<0.01$, ***: $p<0.001$.

Using STED microscopy, a reduced percentage of interaction between ORAI1 and STIM1 was observed as T cell activation progressed compared with SoRa measurements. However, a significant increase was obtained under all conditions. In contrast, the co-localization between ORAI1 and STIM2 remained constant as before. In conclusion, with increasing spatial resolution (FRET<SoRa<STED), a lower co-localization rate was observed between ORAI1 and STIM1, but a significant increase in the difference between non-adherent and adherent conditions. STIM2 and ORAI1, on the other hand, showed an unchanged interaction for each condition and spatial resolution.

4.2 FAK/PLC-y signalling pathway and SOCE evokes pre-activation of T cells

The pathway of adhesion-dependent Ca^{2+} microdomains is mediated by FAK and PLC-γ. To further investigate this in T cells, FAK, as well as PLC-γ were individually inhibited, whereby a significant reduction of Ca^{2+} microdomains was observed (communicated by Dr. Mariella Weiß, Department of Biochemistry and Molecular Cell Biology, University Medical Center Hamburg-Eppendorf, unpublished data). Based on these results, tight and loose cluster formation of the individual protein spots potentially involved in this pathway were determined.

Here, a tight cluster is defined as an interaction between several proteins that are close to each other, so that the individual fluorophores of the proteins overlap and are visible as a single spot. Loose clusters, on the other hand, are defined as an accumulation of spots located in the clustering region. This region is calculated by multiplying the radius of a fluorescence spot by 1.3 (Fig. 4.11).

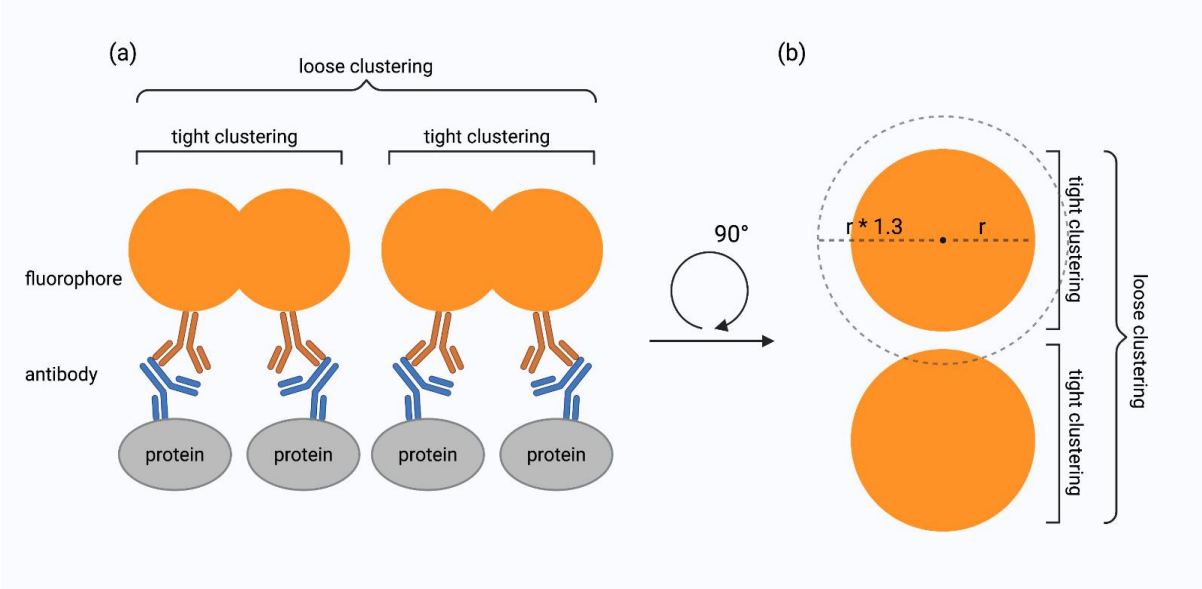

Figure 4.11: Schematic representation of tight and loose clustering.

The interaction of proteins determined by antibody staining is displayed. (a) Tight clustering is defined as proteins close to one another that the fluorophores overlap and are detected as one signal. Loose clustering describes the interaction between spots, with a distance such that the fluorophores do not overlap and are detected separately. (b) Top view (rotated 90°) of spots. Here the definition of loose clustering is shown, where all spots within the radius of a spot multiplied by 1.3 belong to one cluster. Created with Biorender.com

The experiments were performed in primary murine T cells under non-adherent (BSA-coated slides) and adherent conditions (PLL-coated slides). In order to obtain the most precise information possible, STED microscopy was used.

4.2.1 Adhesion-dependent Cluster formation and spot size analysis

The main focus of this work was to elucidate the function of ORAI1 especially in adhesion-dependent T cell pre-activation. The representative images of ORAI1 proteins showed that they are localized in the region of the plasma membrane at non-adherent (BSA-coated slides) (Fig. 4.12a) as well as adherent conditions (PLL-coated slides) (Fig. 4.12b). Interestingly, the average number of spots in a loose cluster significantly increased from 6.1 spots per cluster on BSA-coated slides to 9 spots per cluster on PLL-coated slides (Fig. 4.12c). Furthermore, a significant increase in the mean radius from 45 nm to 51 nm was determined in the size of the spots of tight clusters from non-adherent to adherent conditions (Fig. 4.12d).

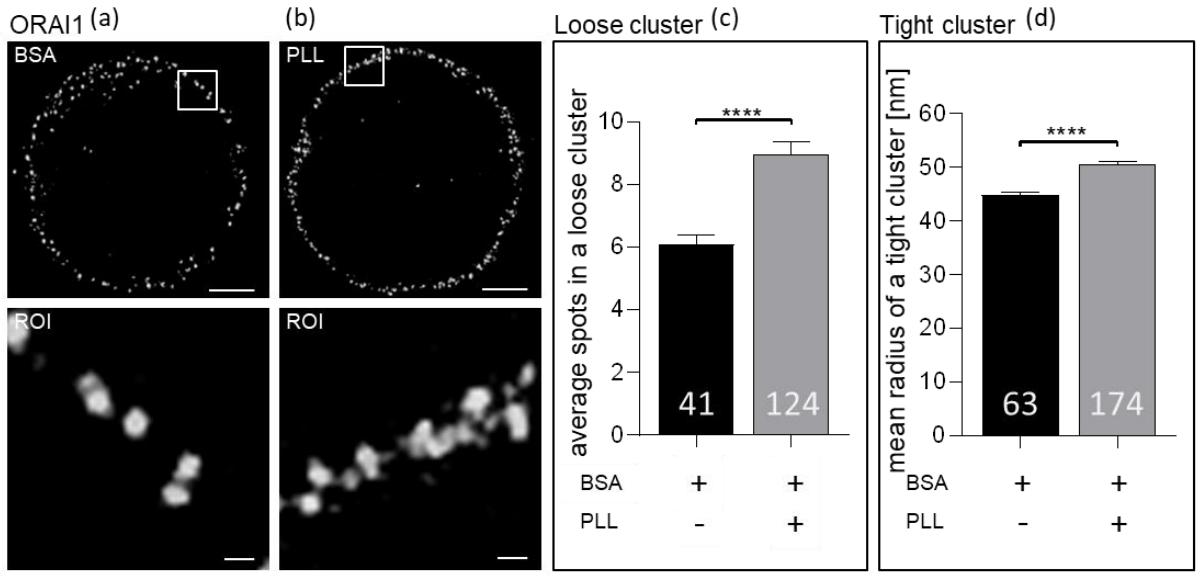

Figure 4.12: Analysis of cluster formation and mean radius of ORAI1 protein spots in primary murine T cells.

The distribution of ORAI1 proteins was determined by super resolution STED microscopy, at approx. 40 nm spatial resolution. Cells were fixed on slides coated with (a) BSA or (b) PLL and the (c) average cluster formation and (d) mean size of the individual spots were determined. Representative primary murine T cells after weka (Waikato environment for knowledge analysis) segmentation are shown. Upper row: Distribution of ORAI1 proteins throughout the cell; scale bar: 2 µm. Lower row: Magnification (ROI) of a region of the plasma membrane, showing an average distribution; scale bar: 100 nm. The bar

charts show the statistical analysis of the (c) average loose cluster formation and (d) the average mean value of the spot size of tight clusters. Statistical test: two-tailed Mann-Whitney U-test, ****: p<0.0001.

Moreover, the localization, clustering and spot size of STIM1 and 2, the other main players of SOCE were investigated. It is known that the STIM proteins are located in the ER membrane (Dziadek and Johnstone, 2007). STED microscopy was used to determine the distribution of the STIM1 (Fig. 4.13a+b) and STIM2 (Fig. 4.13e+f) proteins under non-adherent (Fig. 4.123a, 4.13e) and adherent conditions (Fig. 4.13b, 4.13f). Considering loose cluster formation, a significant increase of 6 spots per cluster in non-adherent conditions in comparison to 7 spots per cluster in adherent conditions was observed for STIM1 proteins (Fig. 4.13c). The size of the spots of tight clusters of STIM1 proteins also increased significantly from a radius of 49 nm by non-stimulated conditions to 53 nm by adherent conditions (Fig. 4.13d). In contrast, the loose clustering of the STIM2 proteins remained unchanged in both conditions. On BSA-coated slides 8.9 spots per cluster were determined, whereas 8.5 spots per cluster of PLL-coated slides were detected. (Fig. 4.13g). Similar to the loose cluster formation, the size of the spots of tight clusters remained almost unchanged for the STIM2 proteins. A radius of 47 m was observed for BSA-, as well as for PLL-coated slides (Fig. 4.13h).

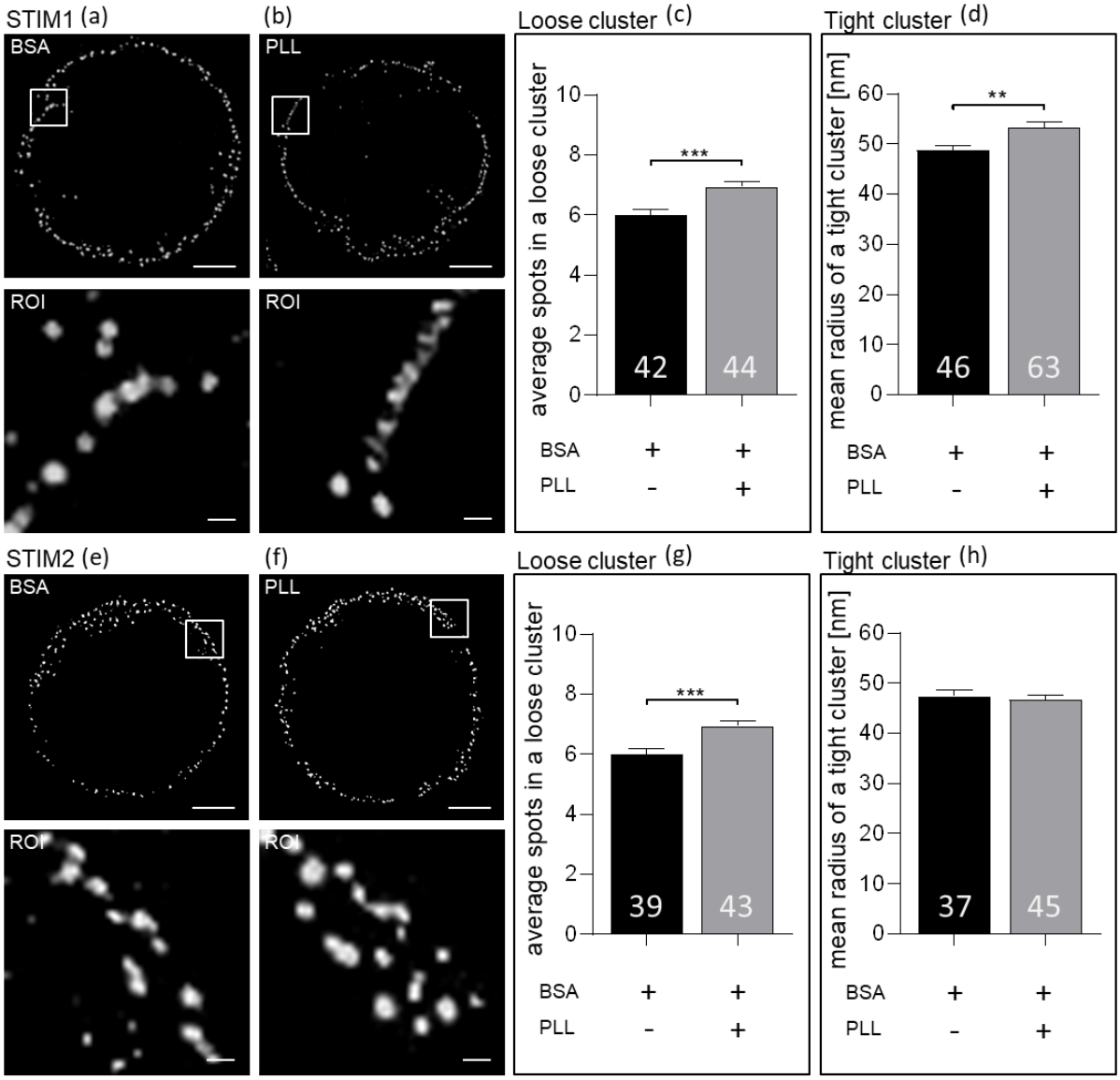

Figure 4.13: Analysis of cluster formation and mean radius of STIM1 and STIM2 protein spots in primary murine T cells.

The distribution of the STIM proteins was determined by super resolution STED microscopy, at approx. 40 nm spatial resolution. Cells were fixed on slides coated with (a+e) BSA or (b+f) PLL and the (c+g) average cluster formation and (d+h) mean size of the individual spots were determined. Representative primary murine T cells after weka (Waikato environment for knowledge analysis) segmentation are shown. Upper row: Distribution of (a+b) STIM1 or (e+f) STIM2 proteins throughout the cell; scale bar: 2 µm. Lower row: Magnification (ROI) of a region of the plasma membrane, showing an average distribution; scale bar: 100 nm. The bar charts show the statistical analysis of the average loose cluster formation and the average mean value of the spot size of tight clusters (c+d) STIM1 or (g+h) STIM2. Statistical test: two-tailed Mann-Whitney U-test, **: $p<0.01$, ***: $p<0.001$.

FAK proteins are known to be localized at focal adhesions and to aggregate to the cytoplasmic tails of integrins (Parsons, 2003). As expected, a distribution of FAK in the

cytosol as well as in the region of the plasma membrane was observed in the non-adherent condition (Fig. 4.14a). In contrast, FAK was detected mainly close to the plasma membrane at adherent conditions (Fig. 4.14b). A significant increase in loose clustering was observed after adhesion of the cells. The number of spots per cluster increased from 6.3 (BSA-coated slides) in comparison to 8 (BSA-PLL-coated slides) (Fig. 4.14c). A significant increase in the mean radius from 44 nm to 50 nm could also be observed and calculated for the size of the spots of tight clusters from BSA-coated slides in comparison to PLL-coated slides (Fig. 4.14d).

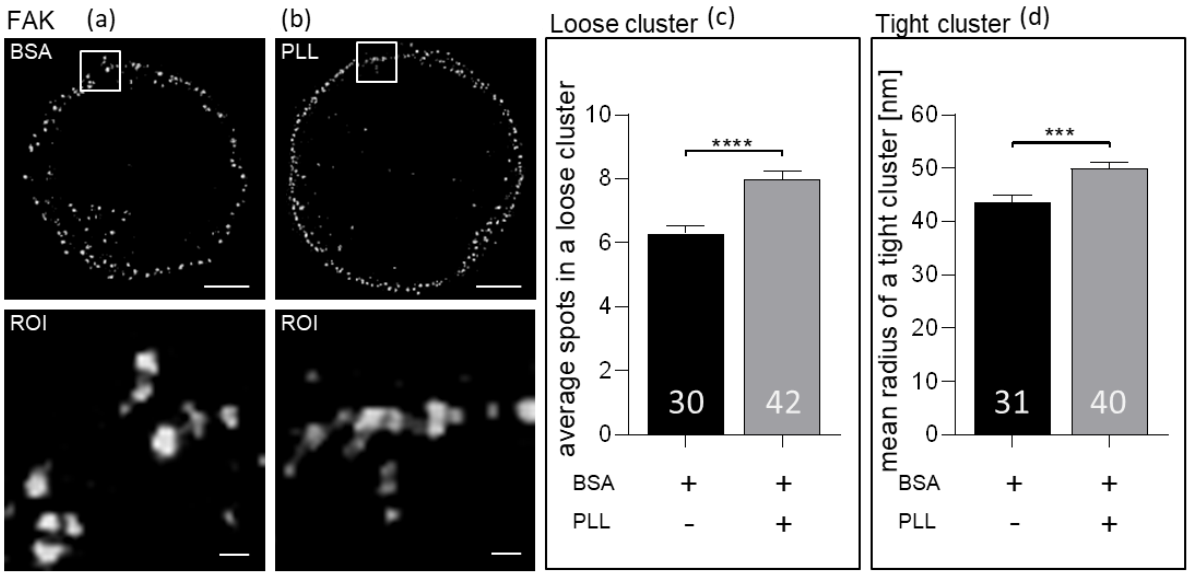

Figure 4.14: Analysis of cluster formation and mean radius of FAK protein spots in primary murine T cells.

The distribution of FAK proteins was determined by super resolution STED microscopy, at approx. 40 nm spatial resolution. Cells were fixed on slides coated with (a) BSA or (b) PLL and the (c) average cluster formation and (d) mean size of the individual spots were determined. Representative primary murine T cells after weka (Waikato environment for knowledge analysis) segmentation are shown. Upper row: Distribution of FAK proteins throughout the cell; scale bar: 2 µm. Lower row: Magnification (ROI) of a region of the plasma membrane, showing an average distribution; scale bar: 100 nm. The bar charts show the statistical analysis of the (c) average loose cluster formation (BSA: n=30, PLL: n=42) and (d) the average mean value of the spot size of tight clusters (BSA: n=31, PLL: n=40). Statistical test: two-tailed Mann-Whitney U-test, ***: $p<0.001$, ****: $p<0.0001$.

The last proteins to be analyzed downstream of FAK signalling were the three IP_3R isoforms. Like the STIM proteins, the IP_3Rs are located in the ER membrane (Yoshida and Imai, 1997). STED microscopy was used to determine the distribution of the

clustering of IP_3R1 (Fig. 4.15a+b), IP_3R2 (Fig. 4.15e+f) and IP_3R3 (Fig. 4.15i+j) proteins near the plasma membrane under non-adherent (Fig. 4.15a+e+i) and adherent conditions (Fig. 4.15b+f+j). Considering loose cluster formation, a significant increase from 6.9 spots per cluster using BSA-coated slides in comparison to 8.7 spots per cluster on PLL-coated slides was observed for IP_3R1 proteins (Fig. 4.15c). In contrast, the loose clustering of the IP_3R2 (Fig. 4.15g) and IP_3R3 (Fig. 4.15k) proteins remained unchanged in both conditions (BSA-coated slides: IP_3R2, 7.8 spots per cluster; IP_3R3, 7.4 spots per cluster; PLL-coated slides: IP_3R2, 7.9 spots per cluster; IP_3R3, 7.7 spots per cluster). No significant differences were observed in the size of the spots of tight clusters in all three isotypes under different conditions (Fig. 15d+h+l). For BSA-coated slides, the spots in the images of IP_3R1 had a radius of 49 nm, for IP_3R2 a radius of 46 nm and for IP_3R3 45 nm. Similar numbers for PLL-coated slides, here the spots of tight clusters in the IP_3R1 images had a radius of 49 nm, in IP_3R2 a radius of 47 nm and in IP_3R3 44 nm.

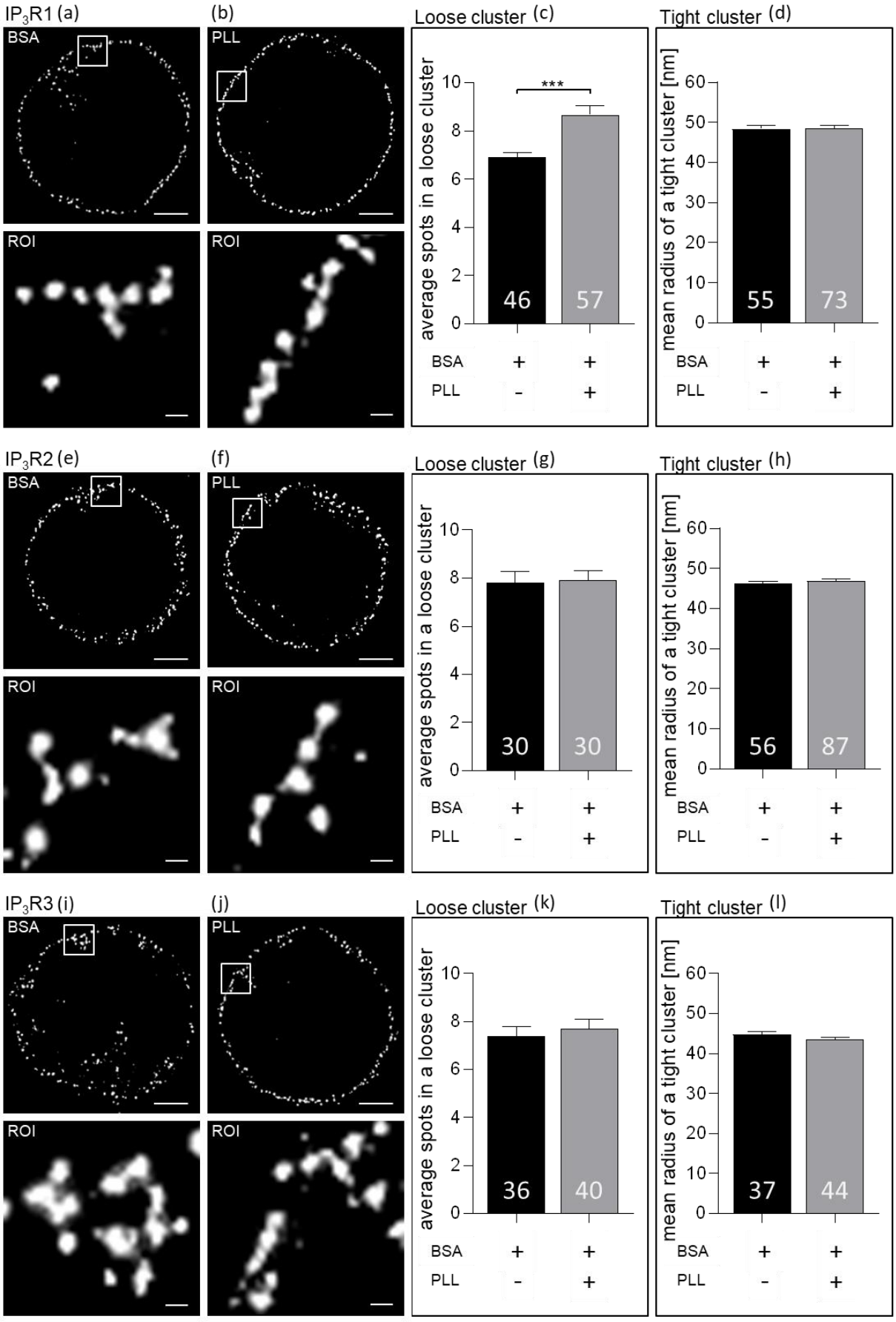
IP3R1 (a)
(b)
Loose cluster (c)
Tight cluster (d)
BSA
PLL
ROI
average spots in a loose cluster
mean radius of a tight cluster [nm]
***
46
57
55
73
BSA + +
PLL - +
IP3R2 (e)
(f)
Loose cluster (g)
Tight cluster (h)
30
30
56
87
IP3R3 (i)
(j)
Loose cluster (k)
Tight cluster (l)
36
40
37
44

Figure 4.15: Analysis of cluster formation and mean radius of the IP_3R protein spots in primary murine T cells.

The distribution of the IP_3R proteins was determined by super resolution STED microscopy, at approx. 40 nm spatial resolution. Cells were fixed on slides coated with (a+e+i) BSA or (b+f+j) PLL and the (c+g+k) average cluster formation and (d+h+l) mean size of the individual spots were determined. Representative primary murine T cells after weka (Waikato environment for knowledge analysis) segmentation are shown. Upper row: Distribution of the IP_3R proteins throughout the cell; scale bar: 2 µm. Lower row: Magnification (ROI) of a region of the plasma membrane, showing an average distribution; scale bar: 100 nm. The bar charts show the statistical analysis of the (c+g+k) average loose cluster formation and (d+h+l) the average mean value of the spot size of tight clusters. Statistical test: two-tailed Mann-Whitney U-test, ***: $p<0.001$.

To sum up, the proteins ORAI1, STIM1 and IP_3R1 showed a significant increase in cluster formation and single spot size from non-adherent to adherent conditions, indicating an adhesion-dependent activation of the proteins. In contrast, no adhesion-related change was observed in STIM2, IP_3R2 and IP_3R3.

4.2.2 Co-localization between ORAI1 and proteins involved in adhesion-dependent signalling

In the last part of the work, the co-localization between ORAI1 and the proteins involved in adhesion-dependent activation was investigated. For this experiment, primary murine T cells were fixed on coated slides, stained and imaged by STED microscopy to determine the co-localization between ORAI1 and FAK or ORAI1 and the three IP_3R isoforms, respectively.

In the first step, the interaction between ORAI1 and FAK was investigated. Co-localization was observed on BSA as well as PLL coating in the region of the PM (Fig. 4.16a+b). It was determined that 18.8 % of ORAI1 proteins co-localized with FAK in non-adherent conditions (BSA-coated slides). In adherent conditions using PLL-coated slides, a strong significant increase in co-localization to 32.7 % was detected (Fig. 4.16c).

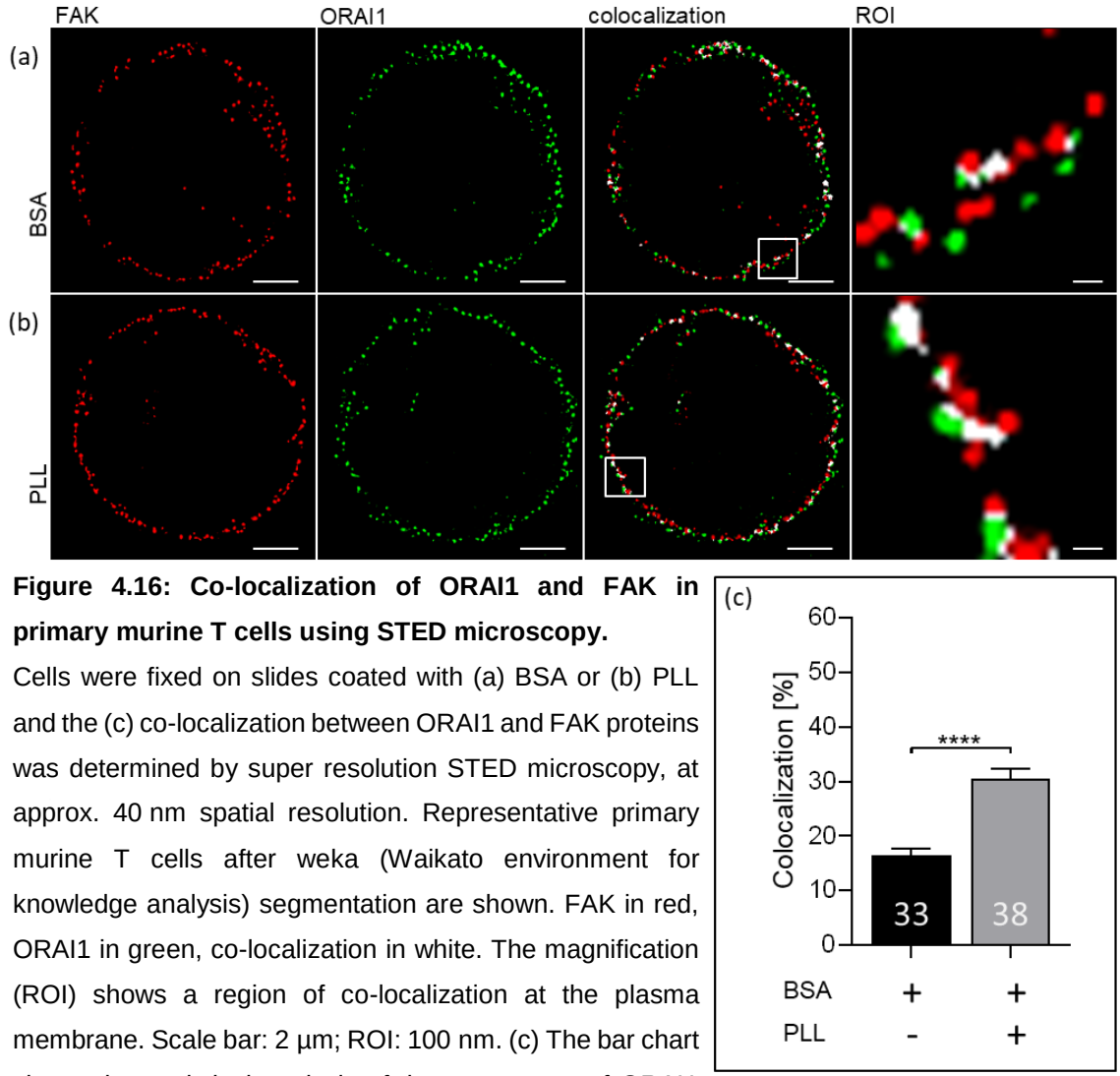

Figure 4.16: Co-localization of ORAI1 and FAK in primary murine T cells using STED microscopy.
Cells were fixed on slides coated with (a) BSA or (b) PLL and the (c) co-localization between ORAI1 and FAK proteins was determined by super resolution STED microscopy, at approx. 40 nm spatial resolution. Representative primary murine T cells after weka (Waikato environment for knowledge analysis) segmentation are shown. FAK in red, ORAI1 in green, co-localization in white. The magnification (ROI) shows a region of co-localization at the plasma membrane. Scale bar: 2 µm; ROI: 100 nm. (c) The bar chart shows the statistical analysis of the percentage of ORAI1 proteins that co-localize with FAK. Statistical test: two-tailed Mann-Whitney U-test, ****: p<0.0001.

When co-localization between ORAI1 and IP_3R1, IP_3R2 and IP_3R3 was examined, an interaction was observed in all three isotypes (Fig. 4.17a-f). 43.6 % of ORAI1 spots co-localize with IP_3R1 in non-adherent conditions. A significant increase to 49.6 % of co-localization was observed at adherent conditions (Fig. 4.17g). In contrast, only a marginal difference was observed in co-localization between ORAI1 and the IP_3R2 and IP_3R3 isotypes under non-adherent and adherent conditions (Fig. 4.17h+i). The co-localization between ORAI1 and IP_3R2 is 26.9 % for BSA-coated slides and 26 % for PLL-coated slides. A co-localization of 26.1 % was observed between ORAI1 and IP_3R3 for BSA-coated slides and 29 % for PLL-coated slides.

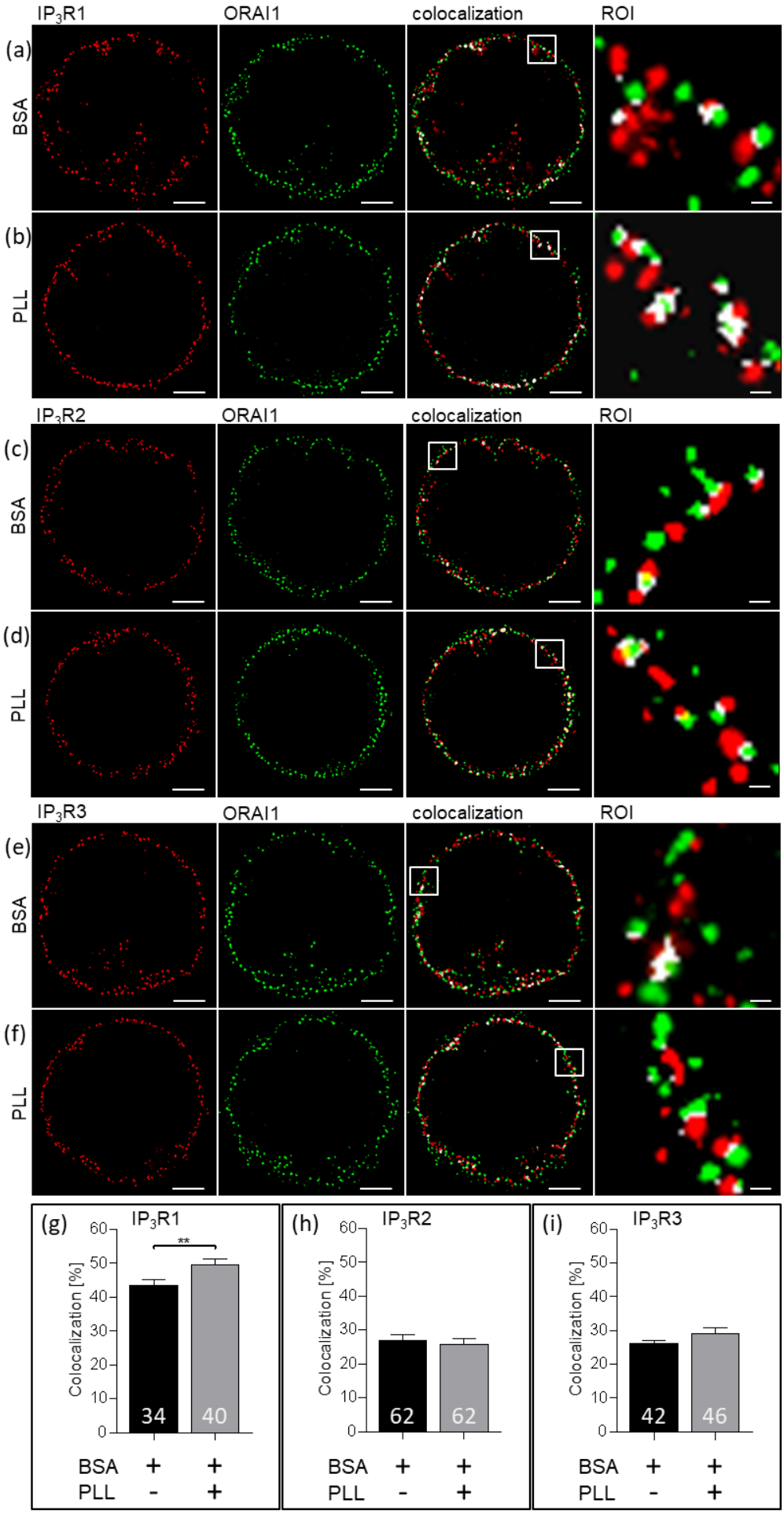
IP3R1
ORAI1
colocalization
ROI
(a)
BSA
(b)
PLL
IP3R2
ORAI1
colocalization
ROI
(c)
BSA
(d)
PLL
IP3R3
ORAI1
colocalization
ROI
(e)
BSA
(f)
PLL
(g)
IP3R1
Colocalization [%]
60
50
40
30
20
10
0
**
34
40
BSA + +
PLL - +
(h)
IP3R2
Colocalization [%]
62
62
BSA + +
PLL - +
(i)
IP3R3
Colocalization [%]
42
46
BSA + +
PLL - +

Figure 4.17: Co-localization of ORAI1 and the three IP_3R isoforms in primary murine T cells using STED microscopy.

Cells were fixed on slides coated with (a+c+e) BSA or (b+d+f) PLL and the (g+h+i) co-localization between ORAI1 and the IP_3R proteins was determined by super resolution STED microscopy, at approx. 40 nm spatial resolution. Representative primary murine T cells after weka (Waikato environment for knowledge analysis) segmentation are shown. IP_3R isoforms in red, ORAI1 in green, co-localization in white. The magnification (ROI) shows a region of co-localization at the plasma membrane. Scale bar: 2 µm; ROI: 100 nm. (g-i) The bar charts show the statistical analysis of the percentage of ORAI1 proteins that co-localize with IP_3R2 (BSA: n=62, PLL: n=62). Statistical test: two-tailed Mann-Whitney U-test.

Taken together co-localization of FAK and IP_3R1 with ORAI1 increased significantly on PLL coated slides, while this was not the case for IP_3R2 and IP_3R3. Indicating that FAK and IP_3R1 are responsible for adhesion dependent signalling.

5. Discussion

T cell activation is initiated by the formation of local Ca^{2+} signals called Ca^{2+} microdomains (Diercks et al., 2018). After stimulation of the TCR/CD3 complex, Ca^{2+} is released from ER Ca^{2+} stores and subsequently leads to Ca^{2+} influx via Ca^{2+} channels localized in the plasma membrane. A recent study by our group demonstrated formation of small infrequent Ca^{2+} microdomains in T cells in the absence of TCR/CD3 stimulation (Diercks et al., 2018). Furthermore, we observed that adhesion of T cells to PLL or ECM proteins is essential for the formation of Ca^{2+} microdomains in the absence of TCR stimulation (communicated by Dr. Mariella Weiß, Department of Biochemistry and Molecular Cell Biology, University Medical Center Hamburg-Eppendorf, unpublished data).

The aim of this study was to analyse the adhesion mediated signalling pathway activated by the binding of T cells to PLL.

Therefore, we wanted to (i) find the optimal advanced optical method to determine the localization of proteins, to (ii) analyse the distribution and (iii) interaction by adhesion versus non-adhesion conditions of ORAI1, STIM1 and 2, FAK and the IP_3R isoforms that are likely to be involved in adhesion dependent signalling.

5.1 Comparison of advanced optical method to determine co-localization of proteins

The co-localization of two proteins can be described when they are in close proximity and interact with each other. To detect co-localization between ORAI1 and the STIM proteins as accurately as possible, FRET on a confocal system, as well as SoRa and STED microscopy experiments were performed. In general, all three methods have their advantages and disadvantages, which will be described in the following.

In terms of co-localization, FRET can only provide limited information. A FRET signal is detectable if two fluorescence molecules are physically interconnected i.e. when both molecules are at a distance of 10 nm or below from each other (Forster, 1946). When two fluorescence molecules are further apart (>10 nm), the FRET signal is negligible and no information about co-localization would be detectable. In other words, a FRET signal indicates strong co-localization and inter-molecular interaction, while no

FRET signal indicates no intra-molecular interaction. However, this does not imply that there is no co-localization. Consequently, in the absence of FRET signals, it is not possible to distinguish whether the proteins are not co-localized or only more than 10 nm apart.

There are many studies in which FRET microscopy has been used to analyse the interaction or oligomerisation of STIM1 and ORAI1 after cell activation (Covington et al., 2010; Emrich et al., 2021; Liou et al., 2007; Wang et al., 2014). However, here we analysed the interaction between STIM1 and ORAI1 in adhesion mediated activation, compared to non-adhesive conditions, which showed no difference (Fig. 4.2, 4.4a). As mentioned above, the use of FRET in optical microscopy can provide information at the molecular level when the FRET pair molecules interact with each other. This leads, however, to an average FRET signal (Selvin, 1995) that is influenced by the size of the PSF of the microscope. The bigger the PSF, the higher the number of FRET pairs that are excited. In this thesis, STIM-CFP and ORAI1-YFP were transfected into cells leading to an overexpression. This resulted in an accumulation of fluorophores, which could only be observed as one signal as the available resolution did not allow for the detection of isolated molecular pairs. Thus, using FRET microscopy does not appear to be sensitive enough to detect small changes in single molecule interactions which seem to occur on adhesive coating. Increasing the resolution of the microscope (reducing the emission PSF) used for FRET measurements would lead to the detection of information closer to the single FRET pair level. For example, performing STED, FRET microscopy would allow the acquisition of the FRET signal to a resolution 100 times smaller than the one typical for confocal FRET microscopy (Szalai et al., 2021).

Using SoRa microscopy, a spatial resolution of around 120 nm can be achieved (Azuma and Kei, 2015). The increase in spatial resolution would allow a more precise analysis of the protein's interaction between STIM1 and ORAI1. And indeed, a slight increase in co-localization between STIM1 and ORAI1 on PLL slides compared to BSA slides was observed (Fig. 4.5, 4.7a). If the spatial resolution is further increased by STED microscopy, the percentage of co-localization is lower (due to the smaller size of the spots), but the comparison of adhesion-dependent Ca^{2+} microdomains obtained on BSA or PLL becomes significant (Fig. 4.8, 4.10a). Measuring the co-localization in

fixed cells, STED microscopy is currently the best available method (available at the UKE) because of its high lateral resolution (theoretically, a spatial resolution up to 20 nm is possible) (Hell and Wichmann, 1994). However, the SoRa based microscope was the best to determine molecular interaction in living cells. The advantage of the SoRa microscopy is that the images can be generated at a high frame rate due to the spinning disk (Azuma and Kei, 2015) that cannot be achieved by using STED microscopy. Indeed, the limited scan acquisition speed and the high intensities involved during frame recording were still hindering to perform live STED imaging. In the future, however, this approach might be very promising for visualizing events that occur in volumes of few cubic micro meters.

Another limiting factor related to immunofluorescence (IF) microscopy is the size of a typical antibody that binds the fluorophore to the target protein. To perform IF staining, classically two antibodies are used (primary and secondary antibodies), where each one has a specific size of 15 nm (Tan et al., 2008). Due to the size, the antibodies cannot reach every binding site of the target molecules. Alternatively, nanobodies (4 nm) (Bannas et al., 2017; Van Audenhove and Gettemans, 2016) or aptamers (up to 2 nm) (Zhou and Rossi, 2017) can be used, which are almost 10 times smaller than antibodies and therefore small enough to be used in super resolution based experiments that possess a resolution power of about 20 nm (Dhar et al., 2020). However, one disadvantage is that the production of aptamers and nanobodies is challenging: e.g. the heavy chain antibodies from which nanobodies are developed can only be obtained from camelids and sharks. Therefore, nanobody development requires greater and more complicated housing and animal husbandry to obtain the desired nanobody (Bannas et al., 2017). The production of aptamers is very time and labor consuming as well, since purified target molecules (by affine chromatography) are required for generations (Lakhin et al., 2013). The smaller size due to direct coupling of fluorophores to aptamers or nanobodies also has disadvantages in terms of signal intensity. In the indirect staining method, multiple secondary antibodies can bind to a primary antibody, resulting in signal enhancement compared to direct methods (Im et al., 2019).

The use of nanobodies or aptamers for protein staining together with the setting of a smaller pixel size are the conditions necessary for achieving higher optical resolution.

Moreover, using a novel super resolution technique named MINFLUX microscopy up to 1-3 nm resolution can be achieved. MINFLUX microscopy combines the strengths of the two highest resolution fluorescence nanoscopy techniques to date: Stochastic optical reconstruction microscopy (STORM) and STED microscopy. In this technique, a probing doughnut-shaped excitation beam is used to determine the localization of individual switchable fluorophores (Balzarotti et al., 2017; Gwosch et al., 2020). Hence, MINFLUX microscopy could be a plausible solution for quantitative analysis of protein-protein interactions and clusters with resolution up to single molecule level. However, at present, this microscopy technique is not yet available at our institute and more effort on optimisation for sample preparation would still be needed for successful MINFLUX acquisition.

5.1.1 Formation of clustering during adhesion

Clustering is defined as an accumulation of spots. Thereby, all spots within a certain radius (radius of a spot multiplied by 1.3) are part of one cluster (described in fig 5.1b). Due to the high resolution of STED microscopy, it is possible to define cluster formation more precisely.

In STED microscopy experiments, a pixel size of 20 nm was used which resulted in a resolution of about 40-50 nm. To detect proteins on an individual level, the proteins need to be at least 60 nm apart due to the size of the antibodies. If intramolecular distance is less than 60 nm, the labelling of the fluorophores would be closer than the maximum optical resolution achievable and would be detected as a single spot. Hence, to detect individual proteins, they have to be at least 40 nm in size and 60 nm apart. However, since proteins often form clusters, it is not always possible to distinguish between each individual protein.

The IP_3R is the largest protein studied in this thesis with an edge length of 20 nm (Ludtke et al., 2011). Since the proteins were detected by classical antibody staining, the IP_3R-antibody-complex had a size of approx. 50 nm, which is within the range of detectable resolution of the STED microscopy. The proteins ORAI1, FAK and the STIM isoforms, on the other hand, are significantly smaller, so individual proteins could not be detected. However, all the protein clusters analysed have an average spot diameter

in the range of 80-100 nm (Fig. 4.12-4.15), suggesting that each spot consists of few proteins possibly closely packed.

In general, due to the limited optical resolution the number of proteins in one spot can only be estimated. In addition, the STED microscopy images were created in two dimensions, meaning that the bond along the Z-axis cannot be detected. To provide more specific information, additional images along the Z-axis would be necessary. Based on these data, in turn, a statement about the strength of the interaction between proteins is possible. Hence, due to the high resolution provided by STED microscopy, a separation between tight and loose clustering may be achieved. Individual spots can be defined as a tight protein clustering location. Clustering between multiple spots, on the other hand, reflects a loose interaction, as the distance between the spots is large enough to be recognised as individual spots. The definition of tight and loose clustering is shown in figure 4.11.

5.2 Proteins involved in adhesion induced T cell priming

T cell activation is initiated via TCR/CD3/CD28 complex stimulation and is immediately followed by Ca^{2+} signalling events, resulting in the increase of $[Ca^{2+}]_i$. Under physiological conditions, a naive T cell circulates in the bloodstream of a large vessel, without contact with APCs or adhesive structures like surface receptors of other cells, cytokines (such as interleukins), as well as components of the ECM. After infectious organisms have entered the body, T cells are stimulated via their TCR and recruited to the inflamed tissue. During migration, the they make contact with adhesive structures or other cells (Ley et al., 2007). Interestingly, non-TCR/CD3/CD28 dependent increase in clustering and co-localization of ORAI1 and STIM1, FAK or IP_3R1 by adherence to PLL was observed (Fig. 4.8, 4.10a, 4.12(a-c)-4.15(a-c), 4.16, 4.17a+b+g). These experiments of this thesis are in line with other data from our group showing that PLL-induced local Ca^{2+} microdomains were observed near the PM. Whereby these Ca^{2+} microdomains were significantly reduced by blocking the downstream integrin signalling pathway. To block the pathway, FAK was inhibited by PF562,271, PLC-γ was suppressed with U73122 or IP_3R subtypes were knocked down by deletion (communicated by Dr. Mariella Weiß, Department of Biochemistry and Molecular Cell Biology, University Medical Center Hamburg-Eppendorf, unpublished

data). So far, not much is known about the effect of adhesion on the formation of Ca^{2+} microdomains. PLL is generally used for adhesion of cells to slides, as it was assumed to be inert. However, it was shown that attachment to PLL triggers Ca^{2+} signalling such as stimulation of the TCR in T cells (Jurkat T cells, primary mouse T cells) (Randriamampita et al., 2003), which is consistent with the results of clustering and co-localization in the figures (4.8, 4.10a, 4.12(a-c)-4.15(a-c), 4.16, 4.17a+b+g). In contrast, super resolution microscopy showed that the organisation of TCRs were different on adhesive slides compared to cells suspended in hydrogel. PLL-coated glass cover slips evoked increased clustering of TCRs (Ponjavic et al., 2018; Santos et al., 2018). Likewise, in 2003, Randriamampita and colleagues observed an increase in the amplitude of the Ca^{2+} response by performing spectrofluorimetry with adherent compared to suspended T cells. This adhesion-triggered T cell priming occurred via interaction with other cells, as well as by binding to artificial substrates. Furthermore, increased replenishment of intracellular Ca^{2+} stores was observed as a result of adhesion (Randriamampita et al., 2003).

All these data indicate the activation of a signalling pathway due to adhesion of T cells to PLL.

5.2.1 Function of FAK during T cell adhesion

STED imaging of tight and loose FAK clustering demonstrated a significant increase on PLL-coated slides compared to slides with BSA (Fig. 4.14). Likewise, co-localization of FAK with ORAI1 displayed an increase due to adhesion to PLL (Fig. 4.16). These results confirm that the signalling pathway initiated by PLL results in FAK activation. For around 30 years, it has been known that FAK plays an important role in integrin signalling (Guan et al., 1991; Hanks et al., 1992; Kornberg et al., 1992; Schaller et al., 1992). Increased intracellular Ca^{2+} concentration, was also observed by binding to ECM proteins such as laminin-1 and collagen IV. The involvement of PKC and PLC-γ was determined by inhibition of these proteins, leading to a selective blocking of global Ca^{2+} response (Schöttelndreier et al., 1999). Activation of integrins leads to autophosphorylation of FAK, which directly mediates interaction with PLC-γ (Zhang et al., 1999). This indicates a key function of FAK in adhesion-dependent signalling.

Focal adhesion is required for cell migration, with FAK playing an essential role in the dynamics of these adhesion (Wagner et al., 2008). FAK activates a signalling pathway, whereby phosphorylation of PLC-γ leads to Ca^{2+} release via IP_3Rs and subsequently Ca^{2+} influx by SOCE activation. Therefore, Ciccimaro and colleagues investigated whether the role of ORAI1 and ORAI2 in cell migration could be due to the regulation of FAK autophosphorylation. Here, the phosphorylation was used as an indicator of FAK activation (Ciccimaro et al., 2006; Golubovskaya et al., 2012). Silencing of ORAI1 and 2 was found to reduce the migratory ability of HL60 (myelioid leukemia cell line) (Diez-Bello et al., 2017). Moreover, FAK phosphorylation induced by fMLP was almost completely inhibited in cells transfected with shRNA ORAI1 or with siRNA ORAI2. These findings suggest that ORAI1 and ORAI2 are required for the tyrosine phosphorylation of FAK, which may explain the role of these proteins in the migration of HL60 cells.

Comparing these results with the studies on FAK and ORAI1 performed in this thesis, similarities can be observed. As a result of adhesion to PLL, increased co-localization between FAK and ORAI1 was observed (Fig. 4.16), which may indicate that ORAI1 has an effect on adhesion-triggered activation of FAK. Here, the increased clustering of FAK (Fig. 4.14) is an indicator of its adhesion-triggered activation.

5.2.2 Role of IP_3Rs during T cell adhesion

Looking at the adhesion-dependent signalling pathway in T cells, the clustering of IP_3R isoforms, as well as co-localization with ORAI1 demonstrated the essential function of IP_3R1 (Fig. 4.15, 4.17). No difference was observed in co-localization and clustering of IP_3R2 and 3 on BSA slides compared to PLL slides, while a significant increase was detected for IP_3R1. This suggests not only an accumulation of ORAI1 and STIM1 proteins, but also an IP_3R1 accumulation at the ER-PM junctions as an indication of a pre-activation state induced by adhesion. Already in 1994, Sugiyama and colleagues demonstrated the expression of the three IP_3R isoforms in T cells. Furthermore, in naïve $CD4^+$ T cells, it was observed that the expression of IP_3R2 and 3, but not IP_3R1, is down regulated (Nagaleekar et al., 2008). This was in line with the observed crucial role of IP_3R1 in adhesion-dependent T cell priming.

There have been other studies investigating the interaction between IP_3R and STIM1 proteins in HEK (Sampieri et al., 2018) as well as in HeLa cells (Thillaiappan et al.,

2017) after store depletion. Measuring FRET signals using confocal microscopy and performing co-IP experiments, Sampieri and colleagues observed an increased binding after TCR stimulation, but not after incubation with Tg. This indicates the crucial role of IP_3R1 in TCR/CD3-depnendent T cell activation (Sampieri et al., 2018). Looking at the clustering experiments of STIM1 and IP_3R1 (Fig. 4.13(a-d), 4.15(a-d)), a correlation with the results of Sampieri et al. can be observed. Both proteins showed a significantly higher clustering from non-adherent to adherent conditions. Since increased co-localization on PLL slides was detected between ORAI1 and IP_3R1 (Fig. 4.17a+b+g) as well, this indicates an association of ORAI1, STIM1 and IP_3R1 due to adhesion. In contrast, using total internal reflection fluorescence microscopy (TIRFM), Thilaiappan and colleagues (Jahr) determined no significant co-localization between STIM1 and IP_3R1 puncta after store depletion. It is known that activation of IP_3Rs generates Ca^{2+} puffs, that are building blocks for local and global Ca^{2+} signalling (Tovey et al., 2001). In this study, Thilaiappan et al. claim that IP_3R1s are responsible for Ca^{2+} puffs to occur almost exclusively at immobile puncta adjacent to, but not coincident with ER-PM junctions where ORAI1 and STIM1 accumulate (Thillaiappan et al., 2017). This might be due to the fact that IP_3Rs are not small enough (20 nm) to fit into the gap between ER and PM (9-12 nm) (Fernández-Busnadiego et al., 2015; Lur et al., 2009; Várnai et al., 2007). The observed accumulation of IP_3R1 at ER-PM junctions due to increased co-localization between ORAI1 and IP_3R1 during PLL adhesion (Fig. 4.17a+b+g) may be related to the use of antibodies for protein staining. As mentioned above (see chapter 5.1), the antibodies (primary + secondary antibody) have a total size of 30 nm. This indicates co-localization, although there may be a distance of up to 60 nm between proteins. The region of ER-PM junctions has a length of only approximately 200 nm (Wu et al., 2006), which enables the IP_3R1 proteins to locate outside this region and still showed a co-localization with ORAI1.

Looking at the spots of the IP_3R, the average size on BSA and PLL slides had a value of around 90 nm (Fig. 4.15d+h+l). Based on the theoretical size of the IP_3R-antibody complex (50 nm) one spot could consist of 1.5 - 2 IP_3R proteins having a tight interaction (tight cluster formation). In turn, the spots in the detection of IP_3R1 form a cluster of around 9 spots due to adhesion. Since there are 1-2 IP_3Rs in a spot, this indicates an accumulation of 13 to 18 IP_3R1 proteins in loose and/or tight clusters.

Wiltgen and colleagues established a variant of STORM microscopy called stochastic Ca^{2+} channel resolution at the nanoscale (SCCaNR), which allows simultaneous monitoring of function and super-resolution localization (within < 50 nm) of active IP_3Rs in intact cells by imaging Ca^{2+} flux. They determined in Human neuroblastoma SH-SY5Y cells the localization from Ca^{2+} puffs over a range of around 400 nm, assuming that IP_3Rs at these sites form clusters that have a diameter of 400 nm (Wiltgen et al., 2010). Since approximately 6 channels open simultaneously after store depletion in SH-SY5Y cells (Smith and Parker, 2009), the mean distance between IP_3Rs is >100 nm. This suggests relatively loose coupling between IP_3Rs via Ca^{2+} diffusion and CICR, similar to the results of adhesion-induced IP_3R1 channel opening, showing 9 spots in a loose cluster (Fig. 4.15(a-c)).

Furthermore, stimulation-dependent clustering of IP_3R1 has already been shown in different cell types as well: for example, using endogenous IP_3R1 with EGFP, the distribution of IP_3R1 in the ER membrane was determined by TIRFM, as well as STORM microscopy. Thereby, a clustering of around 8 IP_3R1 tetramers was observed in HeLa cells (Thillaiappan et al., 2017). In SH-SY5Y cells, using single-particle tracking of overexpressed mEos2-IP_3R1 from Ca^{2+} puffs, 2-9 receptors were determined within most puff sites (Dickinson et al., 2012), while in immature Xenopus oocytes around 20 channels are involved (Shuai et al., 2006).

Altogether, the number of IP_3Rs in a cluster depends on both, the cell type and the method used for determination. In addition, only the stimulation-dependent clustering of cells has been studied so far, whereas in this work the adhesion-dependent clustering of IP_3Rs was determined. However, the results are not directly comparable.

5.2.3 Adhesion mediated interaction between ORAI1 and the STIM proteins in T cells

Here, for the first time, adhesion-dependent effects for the STIM proteins and ORAI1 were investigated. A significant increase in clustering and co-localization of ORAI1 and STIM1 proteins in T cells due to adhesion to PLL compared to no adhesion was observed (Fig. 4.8, 4.10). These results correlated with the already established data that STIM1 activates ORAI1 after stores are depleted by TCR stimulation (Covington et al., 2010; Fahrner et al., 2017; Liou et al., 2007; Luik et al., 2008; Wang et al., 2014; Yeung et al., 2020; Zhou et al., 2017, 2019). Related to adhesion-induced ORAI1-

STIM1 interaction, Diercks et al. observed spontaneous Ca^{2+} microdomains on PLL-coated slides that were dependent on SOCE, but not on RYR1 (Diercks et al., 2018). In contrast, the interaction between ORAI1 and STIM2, as well as the clustering of STIM2 remained unchanged with and without adhesion (Fig. 4.9, 4.10b). Based on the already established data, the function of STIM2 is controversial. STIM2 was identified by siRNA screen as the strongest positive regulator of basal Ca^{2+}, keeping basal cytosolic and ER Ca^{2+} concentration within tight limits (Brandman et al., 2007). STIM2 is reported to be the main regulator of Ca^{2+} oscillation (Ong et al., 2015; Thiel et al., 2013). Furthermore, STIM2 clusters with ORAI1 in ER-PM junctions at minimal depletion of the ER and recruits and remodels STIM1 to its active conformation when the ER Ca^{2+} concentration is not low enough to stimulate STIM1 (Son et al., 2020; Subedi et al., 2018). In a recent study from Emrich and colleagues in HEK cells, all isoforms of STIM and ORAI are non-redundant and together with the IP_3Rs ensure diverse Ca^{2+} signalling in mammals. Thereby, both STIM isoforms are always required together for SOCE activation (Emrich et al., 2021). These data support the conclusion of the adhesion-related ORAI-STIM interaction, suggesting the crucial role of SOCE activation by STIM1 after adhesion to PLL. STIM2 serves to regulate Ca^{2+} levels in adherent as well as non-adherent conditions. Both STIM isoforms are always present in the ER-PM junctions at basal state as well as during pre-activation up to the complete activation of T cells. Here, the percentage of STIM2 proteins remains unchanged, while the number of STIM1 proteins rises significantly with increasing activation.

Contrary to this, in HEK cells, STIM2 was identified as a strong SOCE inhibitor. This was established by Ca^{2+} measurements after Tg stimulation with overexpression of STIM2, where an almost complete inhibition of SOCE was observed (Soboloff et al., 2006). Further reports claim that only STIM1 is required for Ca^{2+} oscillation when low concentrations of the agonist was used (Bird et al., 2009; Wedel et al., 2007).

Regarding the clustering of ORAI1 proteins, a significantly increased accumulation of spots (loose clustering), as well as an enlargement of the individual spots themselves (tight clustering) through adhesion to PLL was observed (Fig. 4.12). The adhesion-related tight clusters had a size of about 100 nm, while the loose clusters consisted of an average of 9 spots. In 2012, Hou and colleagues determined the crystal structure of the ORAI channel hexamer of Drosophila melanogaster (Hou et al., 2012).

Controversially, different information about the diameter of the crystal structure have been described: 6 nm (Perni et al., 2015) and 8 nm (Zhou et al., 2018). Based on the theoretical size of an ORAI1 channel (size of an ORAI1-antibody complex: 36-38 nm), the amount of proteins located in the different clusters can be estimated. Hence, a tight cluster consists of 2-3, whereas in a loose cluster 18-27 channels are located.

Using a morphological approach with transmission and freeze-fracture electron microscopy, Perni and colleagues determined the distribution of individual ORAI1 channels on the cell surface in HEK cells (Perni et al., 2015). A diameter of 7.6 nm was observed for the individual channels. In cells expressing sufficient amounts of STIM1 and ORAI1 and exposed to Tg, a clustering effect was observed, whereas without stimulation, ORAI1 clustering was very rarely detected. The majority of spots are in the medium range of 200-300 particles (ORAI1 channels), but larger spots are not uncommon.

When comparing the cluster formation, the number of ORAI1 channels in a cluster is significantly higher than the one calculated in this thesis. However, it should be noted that Perni et al. used a morphological approach. In addition, the surface of a cell was analysed, whereas in the experiments presented here, a cross-section of the cell was examined. Another important difference is the stage of the cell as well as the cell type. Here, pre-activation of T cells by adhesion were studied while in HEK cells the fully activated state was analysed.

5.2.4 Three-dimensional model of adhesion dependent T cell signalling

In parallel to the experimental studies of adhesion-dependent T cell stimulation, a mathematical model was created in our working group (Gil et al., 2021). Here, the relationship between IP_3R1 and ORAI/STIM complexes, as well as the spatiotemporal characteristics of the observed Ca^{2+} responses were investigated. This model is based on a mathematical three dimensional (3D) description of the junction created by McIvor et al. (2018), which was modified by using the acquired data from Diercks et al. (2018) on the formation of non-TCR/CD3-dependent Ca^{2+} microdomains and further optimised using unpublished data of our group. Based on the simulation, it could be determined that the activity of IP_3R1 and ORAI1 channels are responsible for the non-TCR/CD3-dependent Ca^{2+} microdomains in T cells. The simulation suggested that cell attachment induces Ca^{2+} microdomains that are generated by clusters of five ORAI1

channels in the ER-PM junctions. Activation of these channels results from ER-store depletion by the opening of IP_3R1s located next the junction. The computational results showed that local ER depletion mediated by stimulation of the FAK-PLC-y pathway first induced Ca^{2+} entry through STIM2/ORAI1 complexes by clustering of 2-6 IP_3R1s, which further favours the opening of ORAI1 through STIM1/2 SOCE and the formation of clusters including 5-7 IP_3R1 proteins.

The adhesion of T cells to PLL, causes a clustering of 13-18 IP_3R1 proteins (described in 5.2.3). This number is significantly higher than described in the model. However, due to the size of the antibodies, as well as the resolution not being high enough to distinguish individual receptors, only an estimate of the number of IP_3R1s in one clusters can be made (described in 5.1.1). Furthermore, the mathematical model based on the clustering of IP_3R1s was extracted from experiments using HeLa cells (Thillaiappan et al., 2017). Hence, the results are not directly comparable. Another difference between the mathematical model and the data analysed in the thesis was the activation of SOCE by STIM proteins. An interaction of STIM1 and STIM2 was permanently observed during the transition from a quiescent state to a fully activated T cell.

5.3 Summary

The results of this thesis indicate a non-TCR/CD3-dependent low-level activation of T cells. Adhesion of T cells to PLL triggers the FAK-PLC-y pathway, where Ca^{2+} release via IP_3R1 leads to activation of STIM proteins and Ca^{2+} entry by opening ORAI1 channels. Thus, three different T cell activation states can be described (Fig. 5.2): (i) quiescent state: T cells circulate in the bloodstream without adhesion (Fig. 5.2a). (ii) adhesion pre-activated state: here T cells bind to adhesive structures as they migrate to the inflamed tissue. This leads to a slight pre-activation of T cells by integrin-mediated stimulation of the FAK-PLC-y pathway (Fig. 5.2b). (iii) fully activated state: The TCR is stimulated by presented antigen, leading to Ca^{2+} release via IP_3Rs and RYRs as well as a strong Ca^{2+} entry by SOCE activation (Fig. 5.2c).

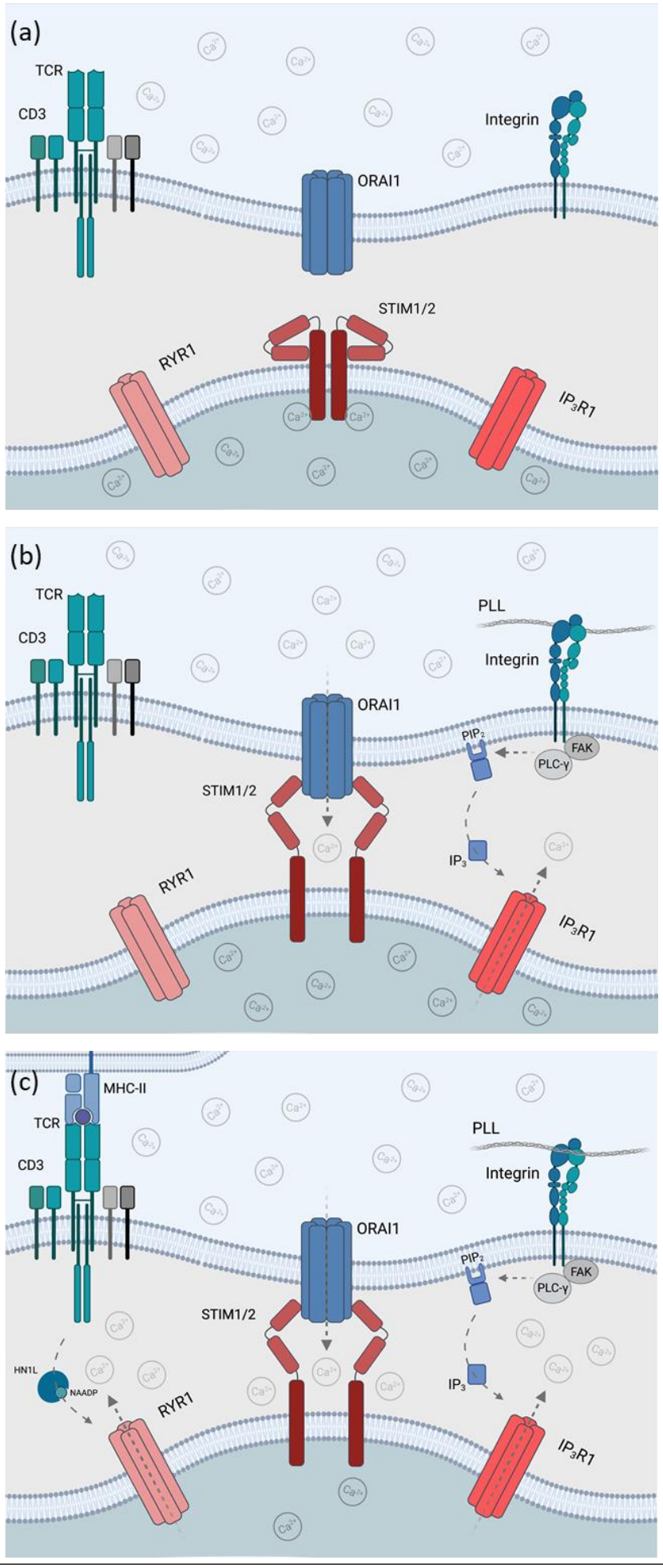
(a)
TCR
CD3
Integrin
ORAI1
STIM1/2
RYR1
IP3R1
(b)
TCR
CD3
PLL
Integrin
ORAI1
PIP2
FAK
PLC-γ
STIM1/2
IP3
RYR1
IP3R1
(c)
MHC-II
TCR
CD3
PLL
Integrin
ORAI1
PIP2
FAK
PLC-γ
STIM1/2
HN1L
NAADP
IP3
RYR1
IP3R1

Figure 5.1: Model of different activation states in T cells.

The figure shows a schematic model of a T cell in transition from a quiescent to a fully activated state. (a) A resting state of a T cell is shown, in which the cell migrates in the bloodstream without getting in contact with adherent structures. (b) The adhesion pre-activated state describes the migration of T cells into the inflamed tissue, where the cells bind to adherent structures. The adhesion leads to activation of the FAK-PLC-γ pathway and subsequent formation of small local Ca^{2+} microdomains. (c) In the fully activated state, an antigen is presented to the T cell via APCs. TCR stimulation causes Ca^{2+} release from the Ca^{2+}-ER store and subsequently a strong Ca^{2+} entry via ORAI1 activation. Created with Biorender.com.

5.4 Outlook

The results of this thesis suggest a non-TCR/CD3-dependent T cell activation involving the formation of small local Ca^{2+} microdomains via activation of the FAK-PLC-γ pathway. However, the detailed molecular mechanism of adhesion-dependent activation of T cells is not yet fully elucidated. To study this in detail more sensitive methods of measurements would be needed.

Of special interest is the region of T cells that attach to ECM proteins. Therefore, measurements could be performed using TIRF microscopy, as this method examines the outer layer from 100-200 nm (Axelrod, 1981). If nanobodies or aptamers are available, their use could provide more precise information on the localization and number of proteins involved in clustering or interactions. To achieve a higher optical resolution, the measurements could be performed on the MINFLUX system. Moreover, this method can only analyse a segment of the cell and not the interaction of proteins in relation to the cell in its entirety. For the detection of dynamic interactions of proteins in living cells and at higher resolution, STED FRET microscopy could be a suitable option.

Furthermore, to determine a dynamic interaction between more than two proteins in real time (e.g. ORAI1 and the STIM isoforms), a three-fluorophore protein FRET analysis could also be performed. A three-color FRET experiment has already been performed (Lee et al., 2010; Sun et al., 2010; Yoo et al., 2020). However, establishing optimal working conditions and parameters for this method is difficult. The major limitations of three colour FRET could be for example, is that the different fluorophores used would need to be close in wavelength to ensure energy transfer, and high

resolution and accurate lasers would be needed to avoid a strong overlap of the signals. In addition, plasmid constructs (including the fluorophore coupled to the protein of interest) with a strong signal would be needed to ensure optimal energy transfer between the fluorophores for FRET to occur so that the signal is detectable.

Additionally, in this work, the localization of different proteins in T cells during adhesion to PLL was determined. This adhesion to PLL is meant to mimic the migration of T cells into the inflamed tissue. Typically, a cascade of adhesive interactions between T cells and endothelial cells or proteins of the ECM is initiated during migration from blood vessels to inflamed tissue (Ley et al., 2007). The interaction of T cells with the endothelium is triggered by a short, weak binding between the integrins of T cells and their associated endothelial ligands (e.g. ICAM-1, VCAM-1) (Block et al., 2012; Sriramarao and Broide, 1996; Stadtmann et al., 2011; Zarbock et al., 2008). After transmigration through the endothelium, T cells attach to ECM proteins of the basement membrane (e.g., laminin-1 and collagen-IV) and the interstitium (e.g., collagen-VI or fibronectin) via integrins before migrating to the site of inflammation (Paulsson, 1992). To perform more physiological experiments, the different associated ligands of T cells like ICAM1, laminin-1 or collagen-IV could be used for cell adhesion.

In addition, T cell activation leads to an increased ATP concentration, which causes, besides other things, the activation of P2X4 receptors. In our group, significantly decreased Ca^{2+} microdomains were observed by *P2rx4*$^{-/-}$ on PLL-coated slides (Brock et al., 2022). These were similar to *Orai1*$^{-/-}$ published by Diercks et al. (2018). Inhibition of Ca^{2+} entry by blocking the P2X4 receptor was observed already in 2010, suggesting that P2X4 controls ORAI1 and T-cell activation (Woehrle et al., 2010). Another important question to be answered would be to understand how ORAI1 and P2X4 relate to each other in the absence of adhesion in comparison to adhesion or fully activated state of T cells.

6. References

Aarhus, R., Graeff, R.M., Dickey, D.M., Walseth, T.F., and Lee, H.C. (1995). ADP-ribosyl cyclase and CD38 catalyze the synthesis of a calcium-mobilizing metabolite from NADP. J Biol Chem *270*, 30327–30333.

Abraham, R.T., and Weiss, A. (2004). Jurkat T cells and development of the T-cell receptor signalling paradigm. Nat Rev Immunol *4*, 301–308.

Acuto, O., and Michel, F. (2003). CD28-mediated co-stimulation: a quantitative support for TCR signalling. Nat Rev Immunol *3*, 939–951.

Åhlgren, J., and Voikar, V. (2019). Experiments done in Black-6 mice: what does it mean? Lab Animal *48*.

Akagi, T., Murata, K., Shishido, T., and Hanafusa, H. (2002). v-Crk activates the phosphoinositide 3-kinase/AKT pathway by utilizing focal adhesion kinase and H-Ras. Mol Cell Biol *22*, 7015–7023.

Alon, R., and Feigelson, S.W. (2009). Chemokine signaling to lymphocyte integrins under shear flow. Microcirculation *16*, 3–16.

Alzayady, K.J., Wang, L., Chandrasekhar, R., Wagner, L.E., Van Petegem, F., and Yule, D.I. (2016). Defining the stoichiometry of inositol 1,4,5-trisphosphate binding required to initiate Ca^{2+} release. Sci Signal *9*, ra35.

Ambudkar, I.S., de Souza, L.B., and Ong, H.L. (2017). TRPC1, Orai1, and STIM1 in SOCE: Friends in tight spaces. Cell Calcium *63*, 33–39.

Axelrod, D. (1981). Cell-substrate contacts illuminated by total internal reflection fluorescence. Journal of Cell Biology *89*, 141–145.

Azuma, T., and Kei, T. (2015). Super-resolution spinning-disk confocal microscopy using optical photon reassignment. Opt. Express, OE *23*, 15003–15011.

Baba, Y., Hayashi, K., Fujii, Y., Mizushima, A., Watarai, H., Wakamori, M., Numaga, T., Mori, Y., Iino, M., Hikida, M., et al. (2006). Coupling of STIM1 to store-operated

Ca^{2+} entry through its constitutive and inducible movement in the endoplasmic reticulum. Proc Natl Acad Sci U S A *103*, 16704–16709.

Bajar, B.T., Wang, E.S., Zhang, S., Lin, M.Z., and Chu, J. (2016). A Guide to Fluorescent Protein FRET Pairs. Sensors (Basel) *16*, 1488.

Balzarotti, F., Eilers, Y., Gwosch, K.C., Gynnå, A.H., Westphal, V., Stefani, F.D., Elf, J., and Hell, S.W. (2017). Nanometer resolution imaging and tracking of fluorescent molecules with minimal photon fluxes. Science *355*, 606–612.

Bannas, P., Hambach, J., and Koch-Nolte, F. (2017). Nanobodies and Nanobody-Based Human Heavy Chain Antibodies As Antitumor Therapeutics. Front Immunol *8*, 1603.

Beeson, K., Potasek, M., and Parilov, E. (2015). Optimizing experimental conditions for stimulated emission depletion microscopy in biophotonics. Proceedings of SPIE - The International Society for Optical Engineering *9369*.

Ben-Kasus Nissim, T., Zhang, X., Elazar, A., Roy, S., Stolwijk, J.A., Zhou, Y., Motiani, R.K., Gueguinou, M., Hempel, N., Hershfinkel, M., et al. (2017). Mitochondria control store-operated Ca^{2+} entry through Na^{+} and redox signals. EMBO J *36*, 797–815.

Berridge, M.J. (1993). Inositol trisphosphate and calcium signalling. Nature *361*, 315–325.

Berridge, M.J. (2006). Calcium microdomains: organization and function. Cell Calcium *40*, 405–412.

Berridge, M.J. (2016). The Inositol Trisphosphate/Calcium Signaling Pathway in Health and Disease. Physiol Rev *96*, 1261–1296.

Berridge, M.J., Lipp, P., and Bootman, M.D. (2000). The versatility and universality of calcium signalling. Nat Rev Mol Cell Biol *1*, 11–21.

Berridge, M.J., Bootman, M.D., and Roderick, H.L. (2003). Calcium signalling: dynamics, homeostasis and remodelling. Nat Rev Mol Cell Biol *4*, 517–529.

Bird, G.S., Hwang, S.-Y., Smyth, J.T., Fukushima, M., Boyles, R.R., and Putney, J.W. (2009). STIM1 is a Calcium Sensor Specialized for Digital Signaling. Curr Biol *19*, 1724–1729.

Bittar, E.E., Bittar, N., and ScienceDirect (Online service) (1996). Immunobiology (Greenwich, Conn.: JAI Press).

Block, H., Herter, J., Rossaint, J., Stadtmann, A., Kliche, S., Lowell, C., and Zarbock, A. (2012). Crucial role of SLP-76 and ADAP for neutrophil recruitment in mouse kidney ischemia-reperfusion injury. The Journal of Experimental Medicine *209*, 407–421.

Bourguignon, L.Y., Chu, A., Jin, H., and Brandt, N.R. (1995). Ryanodine receptor-ankyrin interaction regulates internal Ca^{2+} release in mouse T-lymphoma cells. J Biol Chem *270*, 17917–17922.

Brandman, O., Liou, J., Park, W.S., and Meyer, T. (2007). STIM2 is a feedback regulator that stabilizes basal cytosolic and endoplasmic reticulum Ca^{2+} levels. Cell *131*, 1327–1339.

Brock, V.J., Wolf, I.M.A., Er-Lukowiak, M., Lory, N., Stähler, T., Woelk, L.-M., Mittrücker, H.-W., Müller, C.E., Koch-Nolte, F., Rissiek, B., et al. (2022). P2X4 and P2X7 are essential players in basal T cell activity and Ca^{2+} signaling milliseconds after T cell activation. Sci Adv *8*, eabl9770.

Broere, F., Apasov, S.G., Sitkovsky, M.V., and van Eden, W. (2011). A2 T cell subsets and T cell-mediated immunity. In Principles of Immunopharmacology: 3rd Revised and Extended Edition, F.P. Nijkamp, and M.J. Parnham, eds. (Basel: Birkhäuser), pp. 15–27.

Broussard, J.A., and Green, K.J. (2017). Research Techniques Made Simple: Methodology and Applications of Förster Resonance Energy Transfer (FRET) Microscopy. J Invest Dermatol *137*, e185–e191.

Brown, E.M. (1991). Extracellular Ca^{2+} sensing, regulation of parathyroid cell function, and role of Ca^{2+} and other ions as extracellular (first) messengers. Physiol Rev *71*, 371–411.

Cahalan, M.D., and Chandy, K.G. (2009). The functional network of ion channels in T lymphocytes. Immunol Rev *231*, 59–87.

Cai, X., Wang, X., Patel, S., and Clapham, D.E. (2015). Insights into the early evolution of animal calcium signaling machinery: a unicellular point of view. Cell Calcium *57*, 166–173.

Calalb, M.B., Polte, T.R., and Hanks, S.K. (1995). Tyrosine phosphorylation of focal adhesion kinase at sites in the catalytic domain regulates kinase activity: a role for Src family kinases. Mol Cell Biol *15*, 954–963.

Calì, T., Brini, M., and Carafoli, E. (2017). Regulation of Cell Calcium and Role of Plasma Membrane Calcium ATPases. Int Rev Cell Mol Biol *332*, 259–296.

Chemaly, E.R., Troncone, L., and Lebeche, D. (2018). SERCA control of cell death and survival. Cell Calcium *69*, 46–61.

Chen, H.C., and Guan, J.L. (1994). Association of focal adhesion kinase with its potential substrate phosphatidylinositol 3-kinase. Proc Natl Acad Sci U S A *91*, 10148–10152.

Chen, H.C., Appeddu, P.A., Isoda, H., and Guan, J.L. (1996). Phosphorylation of tyrosine 397 in focal adhesion kinase is required for binding phosphatidylinositol 3-kinase. J Biol Chem *271*, 26329–26334.

Ciccimaro, E., Hevko, J., and Blair, I.A. (2006). Analysis of phosphorylation sites on focal adhesion kinase using nanospray liquid chromatography/multiple reaction monitoring mass spectrometry. Rapid Commun Mass Spectrom *20*, 3681–3692.

Clapper, D.L., Walseth, T., Dargie, P.J., and Lee, H. (1987). Pyridine nucleotide metabolites stimulate calcium release from sea urchin egg microsomes desensitized to inositol trisphosphate. The Journal of Biological Chemistry *262*, 9561–9568.

Constantin, G., Majeed, M., Giagulli, C., Piccio, L., Kim, J.Y., Butcher, E.C., and Laudanna, C. (2000). Chemokines trigger immediate beta2 integrin affinity and mobility changes: differential regulation and roles in lymphocyte arrest under flow. Immunity *13*, 759–769.

Courtney, A.H., Lo, W.-L., and Weiss, A. (2018). TCR Signaling: Mechanisms of Initiation and Propagation. Trends Biochem Sci *43*, 108–123.

Covington, E.D., Wu, M.M., and Lewis, R.S. (2010). Essential role for the CRAC activation domain in store-dependent oligomerization of STIM1. Mol Biol Cell *21*, 1897–1907.

Darbellay, B., Arnaudeau, S., Bader, C.R., Konig, S., and Bernheim, L. (2011). STIM1L is a new actin-binding splice variant involved in fast repetitive Ca^{2+} release. Journal of Cell Biology *194*, 335–346.

De Stefani, D., Rizzuto, R., and Pozzan, T. (2016). Enjoy the Trip: Calcium in Mitochondria Back and Forth. Annu Rev Biochem *85*, 161–192.

Derler, I., Jardin, I., and Romanin, C. (2016). Molecular mechanisms of STIM/Orai communication. Am J Physiol Cell Physiol *310*, C643–C662.

Dhar, P., Samarasinghe, R.M., and Shigdar, S. (2020). Antibodies, Nanobodies, or Aptamers—Which Is Best for Deciphering the Proteomes of Non-Model Species? International Journal of Molecular Sciences *21*, 2485.

Dickinson, G.D., Swaminathan, D., and Parker, I. (2012). The Probability of Triggering Calcium Puffs Is Linearly Related to the Number of Inositol Trisphosphate Receptors in a Cluster. Biophys J *102*, 1826–1836.

Diercks, B.-P., Werner, R., Weidemüller, P., Czarniak, F., Hernandez, L., Lehmann, C., Rosche, A., Krüger, A., Kaufmann, U., Vaeth, M., et al. (2018). ORAI1, STIM1/2, and RYR1 shape subsecond Ca^{2+} microdomains upon T cell activation. Sci Signal *11*, eaat0358.

Dixit, N., and Simon, S.I. (2012). Chemokines, selectins and intracellular calcium flux: temporal and spatial cues for leukocyte arrest. Front Immunol *3*, 188.

Dolmetsch, R.E., and Lewis, R.S. (1994). Signaling between intracellular Ca2+ stores and depletion-activated Ca^{2+} channels generates $[Ca^{2+}]_i$ oscillations in T lymphocytes. J Gen Physiol *103*, 365–388.

Donnadieu, E., Bismuth, G., and Trautmann, A. (1994). Antigen recognition by helper T cells elicits a sequence of distinct changes of their shape and intracellular calcium. Curr Biol *4*, 584–595.

Drake, T.M., and Gupta, V. (2021). Calcium (StatPearls Publishing).

Dziadek, M.A., and Johnstone, L.S. (2007). Biochemical properties and cellular localisation of STIM proteins. Cell Calcium *42*, 123–132.

Echevarría, W., Leite, M.F., Guerra, M.T., Zipfel, W.R., and Nathanson, M.H. (2003). Regulation of calcium signals in the nucleus by a nucleoplasmic reticulum. Nat Cell Biol *5*, 440–446.

Emrich, S.M., Yoast, R.E., Xin, P., Arige, V., Wagner, L.E., Hempel, N., Gill, D.L., Sneyd, J., Yule, D.I., and Trebak, M. (2021). Omnitemporal choreographies of all five STIM/Orai and IP_3Rs underlie the complexity of mammalian Ca^{2+} signaling. Cell Rep *34*, 108760.

Fahrner, M., Schindl, R., Muik, M., Derler, I., and Romanin, C. (2017). The STIM-Orai Pathway: The Interactions Between STIM and Orai. Adv Exp Med Biol *993*, 59–81.

Fang, C., Li, T., Li, Y., Xu, G.J., Deng, Q.W., Chen, Y.J., Hou, Y.N., Lee, H.C., and Zhao, Y.J. (2018). CD38 produces nicotinic acid adenosine dinucleotide phosphate in the lysosome. J Biol Chem *293*, 8151–8160.

Fernández-Busnadiego, R., Saheki, Y., and De Camilli, P. (2015). Three-dimensional architecture of extended synaptotagmin-mediated endoplasmic reticulum-plasma membrane contact sites. Proc Natl Acad Sci U S A *112*, E2004-2013.

Feske, S. (2007). Calcium signalling in lymphocyte activation and disease. Nat Rev Immunol *7*, 690–702.

Feske, S., Gwack, Y., Prakriya, M., Srikanth, S., Puppel, S.-H., Tanasa, B., Hogan, P.G., Lewis, R.S., Daly, M., and Rao, A. (2006). A mutation in Orai1 causes immune deficiency by abrogating CRAC channel function. Nature *441*, 179–185.

Feske, S., Skolnik, E.Y., and Prakriya, M. (2012). Ion channels and transporters in lymphocyte function and immunity. Nat Rev Immunol *12*, 532–547.

Feske, S., Wulff, H., and Skolnik, E.Y. (2015). Ion channels in innate and adaptive immunity. Annu Rev Immunol *33*, 291–353.

Finch, E.A., Turner, T.J., and Goldin, S.M. (1991). Calcium as a Coagonist of Inositol 1,4,5-Trisphosphate-Induced Calcium Release. Science.

Förster, Th. (1946). Energiewanderung und Fluoreszenz. Naturwissenschaften *33*, 166–175.

Foskett, J.K., White, C., Cheung, K.-H., and Mak, D.-O.D. (2007). Inositol trisphosphate receptor Ca^{2+} release channels. Physiol Rev *87*, 593–658.

Fox, G.L., Rebay, I., and Hynes, R.O. (1999). Expression of DFak56, a Drosophila homolog of vertebrate focal adhesion kinase, supports a role in cell migration in vivo. Proc Natl Acad Sci U S A *96*, 14978–14983.

Furuichi, T., Yoshikawa, S., Miyawaki, A., Wada, K., Maeda, N., and Mikoshiba, K. (1989). Primary structure and functional expression of the inositol 1,4,5-trisphosphate-binding protein P400. Nature *342*, 32–38.

Galione, A. (2019). NAADP Receptors. Cold Spring Harb Perspect Biol *11*, a035071.

Gallagher, S.R. (2012). One-dimensional SDS gel electrophoresis of proteins. Curr Protoc Mol Biol *Chapter 10*, Unit 10.2A.

Gasser, A., Bruhn, S., and Guse, A.H. (2006). Second messenger function of nicotinic acid adenine dinucleotide phosphate revealed by an improved enzymatic cycling assay. J Biol Chem *281*, 16906–16913.

Gil, D., Guse, A.H., and Dupont, G. (2021). Three-Dimensional Model of Sub-Plasmalemmal Ca^{2+} Microdomains Evoked by the Interplay Between ORAI1 and InsP3 Receptors. Front. Immunol. *12*, 659790.

Girault, J.A., Labesse, G., Mornon, J.P., and Callebaut, I. (1999). The N-termini of FAK and JAKs contain divergent band 4.1 domains. Trends Biochem Sci *24*, 54–57.

Golubovskaya, V.M., Figel, S., Ho, B.T., Johnson, C.P., Yemma, M., Huang, G., Zheng, M., Nyberg, C., Magis, A., Ostrov, D.A., et al. (2012). A small molecule focal

adhesion kinase (FAK) inhibitor, targeting Y397 site: 1-(2-hydroxyethyl) -3, 5, 7-triaza-1-azoniatricyclo [3.3.1.13,7]decane; bromide effectively inhibits FAK autophosphorylation activity and decreases cancer cell viability, clonogenicity and tumor growth in vivo. Carcinogenesis *33*, 1004–1013.

Gowans, J.L. (1996). The lymphocyte--a disgraceful gap in medical knowledge. Immunol Today *17*, 288–291.

Graeff, R.M., Franco, L., De Flora, A., and Lee, H.C. (1998). Cyclic GMP-dependent and -independent effects on the synthesis of the calcium messengers cyclic ADP-ribose and nicotinic acid adenine dinucleotide phosphate. J Biol Chem *273*, 118–125.

Gu, F., Krüger, A., Roggenkamp, H.G., Alpers, R., Lodygin, D., Jaquet, V., Möckl, F., Hernandez C, L.C., Winterberg, K., Bauche, A., et al. (2021). Dual NADPH oxidases DUOX1 and DUOX2 synthesize NAADP and are necessary for Ca^{2+} signaling during T cell activation. Sci Signal *14*, eabe3800.

Guan, J.L. (1997). Role of focal adhesion kinase in integrin signaling. Int J Biochem Cell Biol *29*, 1085–1096.

Guan, J.L., Trevithick, J.E., and Hynes, R.O. (1991). Fibronectin/integrin interaction induces tyrosine phosphorylation of a 120-kDa protein. Cell Regul *2*, 951–964.

Gunaratne, G.S., Brailoiu, E., He, S., Unterwald, E.M., Patel, S., Slama, J.T., Walseth, T.F., and Marchant, J.S. (2021). Essential requirement for JPT2 in NAADP-evoked Ca^{2+} signaling. Sci Signal *14*, eabd5605.

Guse, A.H. (1999). Cyclic ADP-ribose: A Novel Ca^{2+}-Mobilising Second Messenger. Cellular Signalling *11*, 309–316.

Guse, A.H. (2012). Linking NAADP to Ion Channel Activity: A Unifying Hypothesis. Science Signaling *5*, pe18–pe18.

Gwosch, K.C., Pape, J.K., Balzarotti, F., Hoess, P., Ellenberg, J., Ries, J., and Hell, S.W. (2020). MINFLUX nanoscopy delivers 3D multicolor nanometer resolution in cells. Nat Methods *17*, 217–224.

Hanks, S.K., Calalb, M.B., Harper, M.C., and Patel, S.K. (1992). Focal adhesion protein-tyrosine kinase phosphorylated in response to cell attachment to fibronectin. Proc Natl Acad Sci U S A *89*, 8487–8491.

Hell, S.W. (2009). Microscopy and its focal switch. Nat Methods *6*, 24–32.

Hell, S.W., and Wichmann, J. (1994). Breaking the diffraction resolution limit by stimulated emission: stimulated-emission-depletion fluorescence microscopy. Opt Lett *19*, 780–782.

Henry, C.A., Crawford, B.D., Yan, Y.L., Postlethwait, J., Cooper, M.S., and Hille, M.B. (2001). Roles for zebrafish focal adhesion kinase in notochord and somite morphogenesis. Dev Biol *240*, 474–487.

Herter, J., and Zarbock, A. (2013). Integrin Regulation during Leukocyte Recruitment. J Immunol *190*, 4451–4457.

Hogan, P.G., Lewis, R.S., and Rao, A. (2010). Molecular basis of calcium signaling in lymphocytes: STIM and ORAI. Annu Rev Immunol *28*, 491–533.

Hoover, P.J., and Lewis, R.S. (2011). Stoichiometric requirements for trapping and gating of Ca^{2+} release-activated Ca^{2+} (CRAC) channels by stromal interaction molecule 1 (STIM1). Proc Natl Acad Sci U S A *108*, 13299–13304.

Hoth, M., and Penner, R. (1992). Depletion of intracellular calcium stores activates a calcium current in mast cells. Nature *355*, 353–356.

Hou, X., Pedi, L., Diver, M.M., and Long, S.B. (2012). Crystal structure of the calcium release-activated calcium channel Orai. Science *338*, 1308–1313.

Hsu, S., O'Connell, P.J., Klyachko, V.A., Badminton, M.N., Thomson, A.W., Jackson, M.B., Clapham, D.E., and Ahern, G.P. (2001). Fundamental Ca^{2+} Signaling Mechanisms in Mouse Dendritic Cells: CRAC Is the Major Ca^{2+} Entry Pathway. The Journal of Immunology *166*, 6126–6133.

Hynes, R.O. (1992). Integrins: versatility, modulation, and signaling in cell adhesion. Cell *69*, 11–25.

Im, K., Mareninov, S., Diaz, M.F.P., and Yong, W.H. (2019). An Introduction to Performing Immunofluorescence Staining. In Biobanking: Methods and Protocols, W.H. Yong, ed. (New York, NY: Springer), pp. 299–311.

Inoué, S. (2006). Foundations of Confocal Scanned Imaging in Light Microscopy. In Handbook Of Biological Confocal Microscopy, J.B. Pawley, ed. (Boston, MA: Springer US), pp. 1–19.

Iwai, M., Michikawa, T., Bosanac, I., Ikura, M., and Mikoshiba, K. (2007). Molecular basis of the isoform-specific ligand-binding affinity of inositol 1,4,5-trisphosphate receptors. J Biol Chem *282*, 12755–12764.

Jaffe, E.A., Ruggiero, J.T., and Falcone, D.J. (1985). Monocytes and macrophages synthesize and secrete thrombospondin. Blood *65*, 79–84.

Johnson, M., and Trebak, M. (2019). ORAI channels in cellular remodeling of cardiorespiratory disease. Cell Calcium *79*, 1–10.

Kaboord, B., and Perr, M. (2008). Isolation of proteins and protein complexes by immunoprecipitation. Methods Mol Biol *424*, 349–364.

Klar, T.A., and Hell, S.W. (1999). Subdiffraction resolution in far-field fluorescence microscopy. Opt Lett *24*, 954–956.

Kornberg, L., Earp, H.S., Parsons, J.T., Schaller, M., and Juliano, R.L. (1992). Cell adhesion or integrin clustering increases phosphorylation of a focal adhesion-associated tyrosine kinase. J Biol Chem *267*, 23439–23442.

Kummerow, C., Junker, C., Kruse, K., Rieger, H., Quintana, A., and Hoth, M. (2009). The immunological synapse controls local and global calcium signals in T lymphocytes. Immunol Rev *231*, 132–147.

Laemmli, U.K. (1970). Cleavage of structural proteins during the assembly of the head of bacteriophage T4. Nature *227*, 680–685.

Lakhin, A.V., Tarantul, V.Z., and Gening, L.V. (2013). Aptamers: Problems, Solutions and Prospects. Acta Naturae *5*, 34–43.

Lam, A.J., St-Pierre, F., Gong, Y., Marshall, J.D., Cranfill, P.J., Baird, M.A., McKeown, M.R., Wiedenmann, J., Davidson, M.W., Schnitzer, M.J., et al. (2012). Improving FRET dynamic range with bright green and red fluorescent proteins. Nat Methods *9*, 1005–1012.

Langhorst, M.F., Schwarzmann, N., and Guse, A.H. (2004). Ca^{2+} release via ryanodine receptors and Ca^{2+} entry: major mechanisms in NAADP-mediated Ca^{2+} signaling in T-lymphocytes. Cellular Signalling *16*, 1283–1289.

Lazar, T. (2002). Immunology of Infectious Diseases. Emerg Infect Dis *8*, 1362–1363.

Le Deist, F., Hivroz, C., Partiseti, M., Thomas, C., Buc, H.A., Oleastro, M., Belohradsky, B., Choquet, D., and Fischer, A. (1995). A primary T-cell immunodeficiency associated with defective transmembrane calcium influx. Blood *85*, 1053–1062.

Leavesley, S.J., and Rich, T.C. (2016). Overcoming Limitations of FRET Measurements. Cytometry A *89*, 325–327.

Lee, H.C. (2001). Physiological functions of cyclic ADP-ribose and NAADP as calcium messengers. Annu Rev Pharmacol Toxicol *41*, 317–345.

Lee, H.C. (2011). Cyclic ADP-ribose and NAADP: fraternal twin messengers for calcium signaling. Sci. China Life Sci. *54*, 699–711.

Lee, H.C., and Aarhus, R. (1995). A Derivative of NADP Mobilizes Calcium Stores Insensitive to Inositol Trisphosphate and Cyclic ADP-ribose (∗). Journal of Biological Chemistry *270*, 2152–2157.

Lee, H.C., Walseth, T.F., Bratt, G.T., Hayes, R.N., and Clapper, D.L. (1989). Structural Determination of a Cyclic Metabolite of NAD+ with Intracellular Ca^{2+}-mobilizing Activity. Journal of Biological Chemistry *264*, 1608–1615.

Lee, S., Lee, J., and Hohng, S. (2010). Single-molecule three-color FRET with both negligible spectral overlap and long observation time. PLoS One *5*, e12270.

Lewis, R.S. (2001). Calcium signaling mechanisms in T lymphocytes. Annu Rev Immunol *19*, 497–521.

Lewis, R.S., and Cahalan, M.D. (1989). Mitogen-induced oscillations of cytosolic Ca^{2+} and transmembrane Ca^{2+} current in human leukemic T cells. Cell Regul *1*, 99–112.

Ley, K., Laudanna, C., Cybulsky, M.I., and Nourshargh, S. (2007). Getting to the site of inflammation: the leukocyte adhesion cascade updated. Nat Rev Immunol *7*, 678–689.

Lin, A., and Loré, K. (2017). Granulocytes: New Members of the Antigen-Presenting Cell Family. Front Immunol *8*, 1781.

Liou, J., Kim, M.L., Heo, W.D., Jones, J.T., Myers, J.W., Ferrell, J.E., and Meyer, T. (2005). STIM is a Ca^{2+} sensor essential for Ca2+-store-depletion-triggered Ca^{2+} influx. Curr Biol *15*, 1235–1241.

Liou, J., Fivaz, M., Inoue, T., and Meyer, T. (2007). Live-cell imaging reveals sequential oligomerization and local plasma membrane targeting of stromal interaction molecule 1 after Ca^{2+} store depletion. Proc Natl Acad Sci U S A *104*, 9301–9306.

Lis, A., Peinelt, C., Beck, A., Parvez, S., Monteilh-Zoller, M., Fleig, A., and Penner, R. (2007). CRACM1, CRACM2, and CRACM3 are store-operated Ca^{2+} channels with distinct functional properties. Curr Biol *17*, 794–800.

Liu, J., Zhao, Y.J., Li, W.H., Hou, Y.N., Li, T., Zhao, Z.Y., Fang, C., Li, S.L., and Lee, H.C. (2017). Cytosolic interaction of type III human CD38 with CIB1 modulates cellular cyclic ADP-ribose levels. Proc Natl Acad Sci U S A *114*, 8283–8288.

Ludtke, S.J., Tran, T.P., Ngo, Q.T., Moiseenkova-Bell, V.Yu., Chiu, W., and Serysheva, I.I. (2011). Flexible Architecture of IP_3R1 by Cryo-EM. Structure *19*, 1192–1199.

Luik, R.M., Wu, M.M., Buchanan, J., and Lewis, R.S. (2006). The elementary unit of store-operated Ca^{2+} entry: local activation of CRAC channels by STIM1 at ER-plasma membrane junctions. J Cell Biol *174*, 815–825.

Luik, R.M., Wang, B., Prakriya, M., Wu, M.M., and Lewis, R.S. (2008). Oligomerization of STIM1 couples ER calcium depletion to CRAC channel activation. Nature *454*, 538–542.

Lur, G., Haynes, L.P., Prior, I.A., Gerasimenko, O.V., Feske, S., Petersen, O.H., Burgoyne, R.D., and Tepikin, A.V. (2009). Ribosome-free Terminals of Rough ER Allow Formation of STIM1 Puncta and Segregation of STIM1 from IP_3 Receptors. Curr Biol *19*, 1648–1653.

Marchant, J.S., and Taylor, C.W. (1997). Cooperative activation of IP_3 receptors by sequential binding of IP_3 and Ca^{2+} safeguards against spontaneous activity. Curr Biol *7*, 510–518.

Martin, K.H., Boerner, S.A., and Parsons, J.T. (2002). Regulation of focal adhesion targeting and inhibitory functions of the FAK related protein FRNK using a novel estrogen receptor “switch.” Cell Motility and the Cytoskeleton *51*, 76-88.

McIvor, E., Coombes, S., and Thul, R. (2018). Three-dimensional spatio-temporal modelling of store operated Ca^{2+} entry: insights into ER refilling and the spatial signature of Ca^{2+} signals. Cell Calcium *73*, 11-24.

Mercer, J.C., Dehaven, W.I., Smyth, J.T., Wedel, B., Boyles, R.R., Bird, G.S., and Putney, J.W. (2006). Large store-operated calcium selective currents due to co-expression of Orai1 or Orai2 with the intracellular calcium sensor, Stim1. J Biol Chem *281*, 24979–24990.

Miederer, A.-M., Alansary, D., Schwär, G., Lee, P.-H., Jung, M., Helms, V., and Niemeyer, B.A. (2015). A STIM2 splice variant negatively regulates store-operated calcium entry. Nat Commun *6*, 6899.

Mignery, G.A., and Südhof, T.C. (1990). The ligand binding site and transduction mechanism in the inositol-1,4,5-triphosphate receptor. EMBO J *9*, 3893–3898.

Mikoshiba, K. (2007). IP_3 receptor/Ca^{2+} channel: from discovery to new signaling concepts. J Neurochem *102*, 1426–1446.

Miyawaki, A. (2011). Development of probes for cellular functions using fluorescent proteins and fluorescence resonance energy transfer. Annu Rev Biochem *80*, 357–373.

Morgan, A.J., Davis, L.C., Ruas, M., and Galione, A. (2015). TPC: the NAADP discovery channel? Biochem Soc Trans *43*, 384–389.

Moritz, C.P. (2020). 40 years Western blotting: A scientific birthday toast. J Proteomics *212*, 103575.

Muik, M., Frischauf, I., Derler, I., Fahrner, M., Bergsmann, J., Eder, P., Schindl, R., Hesch, C., Polzinger, B., Fritsch, R., et al. (2008). Dynamic coupling of the putative coiled-coil domain of ORAI1 with STIM1 mediates ORAI1 channel activation. J Biol Chem *283*, 8014–8022.

Müller, C.B., and Enderlein, J. (2010). Image Scanning Microscopy. Phys. Rev. Lett. *104*, 198101.

Murphy, K.M., and Weaver, C. (2018). Janeway Immunologie (Springer Spektrum).

Nagaleekar, V.K., Diehl, S.A., Juncadella, I., Charland, C., Muthusamy, N., Eaton, S., Haynes, L., Garrett-Sinha, L.A., Anguita, J., and Rincon, M. (2008). IP_3 RECEPTOR-MEDIATED Ca^{2+}-RELEASE IN NAIVE CD4 T CELLS DICTATES THEIR CYTOKINE PROGRAM. J Immunol *181*, 8315–8322.

Nauth, T., Huschka, F., Schweizer, M., Bosse, J.B., Diepold, A., Failla, A.V., Steffen, A., Stradal, T.E.B., Wolters, M., and Aepfelbacher, M. (2018). Visualization of translocons in Yersinia type III protein secretion machines during host cell infection. PLoS Pathog *14*, e1007527.

Neumann, E., Schaefer-Ridder, M., Wang, Y., and Hofschneider, P.H. (1982). Gene transfer into mouse lyoma cells by electroporation in high electric fields. EMBO J *1*, 841–845.

Nikiforov, A., Kulikova, V., and Ziegler, M. (2015). The human NAD metabolome: Functions, metabolism and compartmentalization. Crit Rev Biochem Mol Biol *50*, 284–297.

Oh-Hora, M., Yamashita, M., Hogan, P.G., Sharma, S., Lamperti, E., Chung, W., Prakriya, M., Feske, S., and Rao, A. (2008). Dual functions for the endoplasmic reticulum calcium sensors STIM1 and STIM2 in T cell activation and tolerance. Nat Immunol *9*, 432–443.

Ong, H.L., de Souza, L.B., Zheng, C., Cheng, K.T., Liu, X., Goldsmith, C.M., Feske, S., and Ambudkar, I.S. (2015). STIM2 enhances receptor-stimulated Ca^{2+} signaling by promoting recruitment of STIM1 to the endoplasmic reticulum-plasma membrane junctions. Sci Signal *8*, ra3.

Palty, R., Silverman, W.F., Hershfinkel, M., Caporale, T., Sensi, S.L., Parnis, J., Nolte, C., Fishman, D., Shoshan-Barmatz, V., Herrmann, S., et al. (2010). NCLX is an essential component of mitochondrial Na^{+}/Ca^{2+} exchange. Proc Natl Acad Sci U S A *107*, 436–441.

Parekh, A.B., and Penner, R. (1997). Store depletion and calcium influx. Physiol Rev *77*, 901–930.

Parekh, A.B., and Putney, J.W. (2005). Store-operated calcium channels. Physiol Rev *85*, 757–810.

Parker, I., and Smith, I.F. (2010). Recording single-channel activity of inositol trisphosphate receptors in intact cells with a microscope, not a patch clamp. J Gen Physiol *136*, 119–127.

Parsons, J.T. (2003). Focal adhesion kinase: the first ten years. Journal of Cell Science *116*, 1409–1416.

Partiseti, M., Le Deist, F., Hivroz, C., Fischer, A., Korn, H., and Choquet, D. (1994). The calcium current activated by T cell receptor and store depletion in human lymphocytes is absent in a primary immunodeficiency. J Biol Chem *269*, 32327–32335.

Patterson, R.L., Boehning, D., and Snyder, S.H. (2004). Inositol 1,4,5-trisphosphate receptors as signal integrators. Annual Review of Biochemistry *73*, 437–465.

Paulsson, M. (1992). Basement membrane proteins: structure, assembly, and cellular interactions. Crit Rev Biochem Mol Biol *27*, 93–127.

Perni, S., Dynes, J.L., Yeromin, A.V., Cahalan, M.D., and Franzini-Armstrong, C. (2015). Nanoscale patterning of STIM1 and Orai1 during store-operated Ca^{2+} entry. Proc Natl Acad Sci U S A *112*, E5533-5542.

Phillipson, M., Heit, B., Parsons, S.A., Petri, B., Mullaly, S.C., Colarusso, P., Gower, R.M., Neely, G., Simon, S.I., and Kubes, P. (2009). Vav1 is essential for mechanotactic crawling and migration of neutrophils out of the inflamed microvasculature. J Immunol *182*, 6870–6878.

Pizzo, P., Lissandron, V., Capitanio, P., and Pozzan, T. (2011). Ca^{2+} signalling in the Golgi apparatus. Cell Calcium *50*, 184–192.

Ponjavic, A., McColl, J., Carr, A.R., Santos, A.M., Kulenkampff, K., Lippert, A., Davis, S.J., Klenerman, D., and Lee, S.F. (2018). Single-Molecule Light-Sheet Imaging of Suspended T Cells. Biophys J *114*, 2200–2211.

Prakriya, M., and Lewis, R.S. (2001). Potentiation and inhibition of Ca^{2+} release-activated Ca^{2+} channels by 2-aminoethyldiphenyl borate (2-APB) occurs independently of IP3 receptors. J Physiol *536*, 3–19.

Prakriya, M., and Lewis, R.S. (2015). Store-Operated Calcium Channels. Physiol Rev *95*, 1383–1436.

Preissner, K.T. (1991). Structure and biological role of vitronectin. Annu Rev Cell Biol *7*, 275–310.

Prole, D.L., and Taylor, C.W. (2011). Identification of intracellular and plasma membrane calcium channel homologues in pathogenic parasites. PLoS One *6*, e26218.

Prole, D.L., and Taylor, C.W. (2019). Structure and Function of IP3 Receptors. Cold Spring Harb Perspect Biol *11*, a035063.

Putney, J.W. (1986). A model for receptor-regulated calcium entry. Cell Calcium *7*, 1–12.

Putney, J.W. (1990). Capacitative calcium entry revisited. Cell Calcium *11*, 611–624.

Putney, J.W. (2007). Recent breakthroughs in the molecular mechanism of capacitative calcium entry (with thoughts on how we got here). Cell Calcium *42*, 103–110.

Qoronfleh, M.W., Ren, L., Emery, D., Perr, M., and Kaboord, B. (2003). Use of Immunomatrix Methods to Improve Protein-Protein Interaction Detection. J Biomed Biotechnol *2003*, 291–298.

Raffaello, A., Mammucari, C., Gherardi, G., and Rizzuto, R. (2016). Calcium at the Center of Cell Signaling: Interplay between Endoplasmic Reticulum, Mitochondria, and Lysosomes. Trends Biochem Sci *41*, 1035–1049.

Rana, A., Yen, M., Sadaghiani, A.M., Malmersjö, S., Park, C.Y., Dolmetsch, R.E., and Lewis, R.S. (2015). Alternative splicing converts STIM2 from an activator to an inhibitor of store-operated calcium channels. J Cell Biol *209*, 653–670.

Randriamampita, C., Boulla, G., Revy, P., Lemaitre, F., and Trautmann, A. (2003). T cell adhesion lowers the threshold for antigen detection. Eur J Immunol *33*, 1215–1223.

Raugi, G.J., Mumby, S.M., Abbott-Brown, D., and Bornstein, P. (1982). Thrombospondin: synthesis and secretion by cells in culture. J Cell Biol *95*, 351–354.

Renart, J., Reiser, J., and Stark, G.R. (1979). Transfer of proteins from gels to diazobenzyloxymethyl-paper and detection with antisera: a method for studying antibody specificity and antigen structure. PNAS *76*, 3116–3120.

Rodríguez-Prados, M., Rojo-Ruiz, J., Aulestia, F.J., García-Sancho, J., and Alonso, M.T. (2015). A new low-Ca^{2+} affinity GAP indicator to monitor high Ca^{2+} in organelles by luminescence. Cell Calcium *58*, 558–564.

Rogers, T.B., Inesi, G., Wade, R., and Lederer, W.J. (1995). Use of thapsigargin to study Ca^{2+} homeostasis in cardiac cells. Biosci Rep *15*, 341–349.

Roggenkamp, H.G., Khansahib, I., Hernandez C, L.C., Zhang, Y., Lodygin, D., Krüger, A., Gu, F., Möckl, F., Löhndorf, A., Wolters, V., et al. (2021). HN1L/JPT2: A signaling

protein that connects NAADP generation to Ca^{2+} microdomain formation. Sci Signal *14*, eabd5647.

Roos, J., DiGregorio, P.J., Yeromin, A.V., Ohlsen, K., Lioudyno, M., Zhang, S., Safrina, O., Kozak, J.A., Wagner, S.L., Cahalan, M.D., et al. (2005). STIM1, an essential and conserved component of store-operated Ca^{2+} channel function. J Cell Biol *169*, 435–445.

Rudd, C.E., Taylor, A., and Schneider, H. (2009). CD28 and CTLA-4 coreceptor expression and signal transduction. Immunol Rev *229*, 12–26.

Sage, E.H., and Bornstein, P. (1991). Extracellular proteins that modulate cell-matrix interactions. SPARC, tenascin, and thrombospondin. J Biol Chem *266*, 14831–14834.

Sampieri, A., Santoyo, K., Asanov, A., and Vaca, L. (2018). Association of the IP_3R to STIM1 provides a reduced intraluminal calcium microenvironment, resulting in enhanced store-operated calcium entry. Scientific Reports *8*, 13252

Santos, A.M., Ponjavic, A., Fritzsche, M., Fernandes, R.A., de la Serna, J.B., Wilcock, M.J., Schneider, F., Urbančič, I., McColl, J., Anzilotti, C., et al. (2018). Capturing resting T cells: the perils of PLL. Nat Immunol *19*, 203–205.

Saüc, S., Bulla, M., Nunes, P., Orci, L., Marchetti, A., Antigny, F., Bernheim, L., Cosson, P., Frieden, M., and Demaurex, N. (2015). STIM1L traps and gates Orai1 channels without remodeling the cortical ER. J Cell Sci *128*, 1568–1579.

Schaller, M.D., Borgman, C.A., Cobb, B.S., Vines, R.R., Reynolds, A.B., and Parsons, J.T. (1992). pp125FAK a structurally distinctive protein-tyrosine kinase associated with focal adhesions. Proc Natl Acad Sci U S A *89*, 5192–5196.

Schaller, M.D., Hildebrand, J.D., Shannon, J.D., Fox, J.W., Vines, R.R., and Parsons, J.T. (1994). Autophosphorylation of the focal adhesion kinase, pp125FAK, directs SH2-dependent binding of pp60src. Mol Cell Biol *14*, 1680–1688.

Schaller, M.D., Otey, C.A., Hildebrand, J.D., and Parsons, J.T. (1995). Focal adhesion kinase and paxillin bind to peptides mimicking beta integrin cytoplasmic domains. J Cell Biol *130*, 1181–1187.

Schneider, U., Schwenk, H.U., and Bornkamm, G. (1977). Characterization of EBV-genome negative “null” and “T” cell lines derived from children with acute lymphoblastic leukemia and leukemic transformed non-Hodgkin lymphoma. Int J Cancer *19*, 621–626.

Schöttelndreier, H., Mayr, G.W., and Guse, A.H. (1999). Beta1-integrins mediate Ca^{2+}-signalling and T cell spreading via divergent pathways. Cell Signal *11*, 611–619.

Schwarzmann, N., Kunerth, S., Weber, K., Mayr, G.W., and Guse, A.H. (2002). Knock-down of the type 3 ryanodine receptor impairs sustained Ca^{2+} signaling via the T cell receptor/CD3 complex. J Biol Chem *277*, 50636–50642.

Seder, R.A., and Paul, W.E. (1994). Acquisition of lymphokine-producing phenotype by CD4+ T cells. Annu Rev Immunol *12*, 635–673.

Sekler, I. (2015). Standing of giants shoulders the story of the mitochondrial $Na^{+}Ca^{2+}$ exchanger. Biochem Biophys Res Commun *460*, 50–52.

Selvin, P.R. (1995). Fluorescence resonance energy transfer. Methods Enzymol *246*, 300–334.

Shaw, P.J., and Feske, S. (2012). Regulation of lymphocyte function by ORAI and STIM proteins in infection and autoimmunity. J Physiol *590*, 4157–4167.

Sheppard, C. (1988). Super-resolution in confocal imaging. Optik - International Journal for Light and Electron Optics *80*, 53.

Sheppard, C.J.R., Mehta, S.B., and Heintzmann, R. (2013). Superresolution by image scanning microscopy using pixel reassignment. Opt. Lett., OL *38*, 2889–2892.

Shi, J., Ma, Y., Zhu, J., Chen, Y., Sun, Y., Yao, Y., Yang, Z., and Xie, J. (2018). A Review on Electroporation-Based Intracellular Delivery. Molecules *23*, 3044.

Shuai, J., Rose, H.J., and Parker, I. (2006). The Number and Spatial Distribution of IP_3 Receptors Underlying Calcium Puffs in Xenopus Oocytes. Biophys J *91*, 4033–4044.

Sieg, D.J., Hauck, C.R., Ilic, D., Klingbeil, C.K., Schaefer, E., Damsky, C.H., and Schlaepfer, D.D. (2000). FAK integrates growth-factor and integrin signals to promote cell migration. Nat Cell Biol *2*, 249–256.

Smith, I.F., and Parker, I. (2009). Imaging the quantal substructure of single IP_3R channel activity during Ca^{2+} puffs in intact mammalian cells. Proc Natl Acad Sci U S A *106*, 6404–6409.

Smith, A., Carrasco, Y.R., Stanley, P., Kieffer, N., Batista, F.D., and Hogg, N. (2005). A talin-dependent LFA-1 focal zone is formed by rapidly migrating T lymphocytes. J Cell Biol *170*, 141–151.

Soboloff, J., Spassova, M.A., Hewavitharana, T., He, L.-P., Xu, W., Johnstone, L.S., Dziadek, M.A., and Gill, D.L. (2006). STIM2 is an inhibitor of STIM1-mediated store-operated Ca^{2+} Entry. Curr Biol *16*, 1465–1470.

Soboloff, J., Rothberg, B.S., Madesh, M., and Gill, D.L. (2012). STIM proteins: dynamic calcium signal transducers. Nat Rev Mol Cell Biol *13*, 549–565.

Son, G.-Y., Subedi, K.P., Ong, H.L., Noyer, L., Saadi, H., Zheng, C., Bhardwaj, R., Feske, S., and Ambudkar, I.S. (2020). STIM2 targets Orai1/STIM1 to the AKAP79 signaling complex and confers coupling of Ca^{2+} entry with NFAT1 activation. PNAS *117*, 16638–16648.

Spassova, M.A., Soboloff, J., He, L.-P., Xu, W., Dziadek, M.A., and Gill, D.L. (2006). STIM1 has a plasma membrane role in the activation of store-operated Ca^{2+} channels. Proc Natl Acad Sci U S A *103*, 4040–4045.

Sriramarao, P., and Broide, D.H. (1996). Differential regulation of eosinophil adhesion under conditions of flow in vivo. Ann N Y Acad Sci *796*, 218–225.

Stadtmann, A., Brinkhaus, L., Mueller, H., Rossaint, J., Bolomini-Vittori, M., Bergmeier, W., Van Aken, H., Wagner, D.D., Laudanna, C., Ley, K., et al. (2011). Rap1a activation by CalDAG-GEFI and p38 MAPK is involved in E-selectin-dependent slow leukocyte rolling. Eur J Immunol *41*, 2074–2085.

Stafford, N., Wilson, C., Oceandy, D., Neyses, L., and Cartwright, E.J. (2017). The Plasma Membrane Calcium ATPases and Their Role as Major New Players in Human Disease. Physiol Rev *97*, 1089–1125.

Stathopulos, P.B., Li, G.-Y., Plevin, M.J., Ames, J.B., and Ikura, M. (2006). Stored Ca^{2+} depletion-induced oligomerization of stromal interaction molecule 1 (STIM1) via the EF-SAM region: An initiation mechanism for capacitive Ca^{2+} entry. J Biol Chem *281*, 35855–35862.

Stathopulos, P.B., Zheng, L., Li, G.-Y., Plevin, M.J., and Ikura, M. (2008). Structural and mechanistic insights into STIM1-mediated initiation of store-operated calcium entry. Cell *135*, 110–122.

Streb, H., Irvine, R.F., Berridge, M.J., and Schulz, I. (1983). Release of Ca^{2+} from a nonmitochondrial intracellular store in pancreatic acinar cells by inositol-1,4,5-trisphosphate. Nature *306*, 67–69.

Stryer, L., and Haugland, R.P. (1967). Energy transfer: a spectroscopic ruler. Proc Natl Acad Sci U S A *58*, 719–726.

Subedi, K.P., Ong, H.L., Son, G.-Y., Liu, X., and Ambudkar, I.S. (2018). STIM2 Induces Activated Conformation of STIM1 to Control Orai1 Function in ER-PM Junctions. Cell Rep *23*, 522–534.

Sun, C.-X., Robb, V.A., and Gutmann, D.H. (2002). Protein 4.1 tumor suppressors: getting a FERM grip on growth regulation. J Cell Sci *115*, 3991–4000.

Sun, Y., Wallrabe, H., Booker, C.F., Day, R.N., and Periasamy, A. (2010). Three-Color Spectral FRET Microscopy Localizes Three Interacting Proteins in Living Cells. Biophys J *99*, 1274–1283.

Szalai, A.M., Siarry, B., Lukin, J., Giusti, S., Unsain, N., Cáceres, A., Steiner, F., Tinnefeld, P., Refojo, D., Jovin, T.M., et al. (2021). Super-resolution Imaging of Energy Transfer by Intensity-Based STED-FRET. Nano Lett. *21*, 2296–2303.

Takemura, H., Hughes, A.R., Thastrup, O., and Putney, J.W. (1989). Activation of calcium entry by the tumor promoter thapsigargin in parotid acinar cells. Evidence that

an intracellular calcium pool and not an inositol phosphate regulates calcium fluxes at the plasma membrane. J Biol Chem *264*, 12266–12271.

Tan, Y.H., Liu, M., Nolting, B., Go, J.G., Gervay-Hague, J., and Liu, G. (2008). A nanoengineering approach for investigation and regulation of protein immobilization. ACS Nano *2*, 2374–2384.

Taylor, C.W., Genazzani, A.A., and Morris, S.A. (1999). Expression of inositol trisphosphate receptors. Cell Calcium *26*, 237–251.

Thiel, M., Lis, A., and Penner, R. (2013). STIM2 drives Ca^{2+} oscillations through store-operated Ca^{2+} entry caused by mild store depletion. J Physiol *591*, 1433–1445.

Thillaiappan, N.B., Chavda, A.P., Tovey, S.C., Prole, D.L., and Taylor, C.W. (2017). Ca^{2+} signals initiate at immobile IP3 receptors adjacent to ER-plasma membrane junctions. Nat Commun *8*, 1505.

Tovey, S.C., de Smet, P., Lipp, P., Thomas, D., Young, K.W., Missiaen, L., De Smedt, H., Parys, J.B., Berridge, M.J., Thuring, J., et al. (2001). Calcium puffs are generic InsP(3)-activated elementary calcium signals and are downregulated by prolonged hormonal stimulation to inhibit cellular calcium responses. J Cell Sci *114*, 3979–3989.

Trebak, M., and Kinet, J.-P. (2019). Calcium signalling in T cells. Nat Rev Immunol *19*, 154–169.

Tu, H., Wang, Z., and Bezprozvanny, I. (2005). Modulation of Mammalian Inositol 1,4,5-Trisphosphate Receptor Isoforms by Calcium: A Role of Calcium Sensor Region. Biophysical Journal *88*, 1056–1069.

Uchida, K., Miyauchi, H., Furuichi, T., Michikawa, T., and Mikoshiba, K. (2003). Critical regions for activation gating of the inositol 1,4,5-trisphosphate receptor. J Biol Chem *278*, 16551–16560.

Vaeth, M., Yang, J., Yamashita, M., Zee, I., Eckstein, M., Knosp, C., Kaufmann, U., Karoly Jani, P., Lacruz, R.S., Flockerzi, V., et al. (2017). ORAI2 modulates store-operated calcium entry and T cell-mediated immunity. Nat Commun *8*, 14714.

Van Audenhove, I., and Gettemans, J. (2016). Nanobodies as Versatile Tools to Understand, Diagnose, Visualize and Treat Cancer. EBioMedicine *8*, 40–48.

Várnai, P., Tóth, B., Tóth, D.J., Hunyady, L., and Balla, T. (2007). Visualization and manipulation of plasma membrane-endoplasmic reticulum contact sites indicates the presence of additional molecular components within the STIM1-Orai1 Complex. J Biol Chem *282*, 29678–29690.

Vermassen, E., Parys, J.B., and Mauger, J.-P. (2004). Subcellular distribution of the inositol 1,4,5-trisphosphate receptors: functional relevance and molecular determinants. Biol Cell *96*, 3–17.

Vig, M., and Kinet, J.-P. (2009). Calcium signaling in immune cells. Nat Immunol *10*, 21–27.

Vig, M., Peinelt, C., Beck, A., Koomoa, D.L., Rabah, D., Koblan-Huberson, M., Kraft, S., Turner, H., Fleig, A., Penner, R., et al. (2006). CRACM1 is a plasma membrane protein essential for store-operated Ca^{2+} entry. Science *312*, 1220–1223.

Wagner, S., Storbeck, C.J., Roovers, K., Chaar, Z.Y., Kolodziej, P., McKay, M., and Sabourin, L.A. (2008). FAK/src-family dependent activation of the Ste20-like kinase SLK is required for microtubule-dependent focal adhesion turnover and cell migration. PLoS One *3*, e1868.

Wang, X., Wang, Y., Zhou, Y., Hendron, E., Mancarella, S., Andrake, M.D., Rothberg, B.S., Soboloff, J., and Gill, D.L. (2014). Distinct Orai-coupling domains in STIM1 and STIM2 define the Orai-activating site. Nat Commun *5*, 3183.

Weaver, C.T., Harrington, L.E., Mangan, P.R., Gavrieli, M., and Murphy, K.M. (2006). Th17: an effector CD4 T cell lineage with regulatory T cell ties. Immunity *24*, 677–688.

Wedel, B., Boyles, R.R., Putney, J.W., and Bird, G.S. (2007). Role of the store-operated calcium entry proteins Stim1 and Orai1 in muscarinic cholinergic receptor-stimulated calcium oscillations in human embryonic kidney cells. J Physiol *579*, 679–689.

Wei, L., and Min, W. (2013). What can stimulated emission do for bioimaging?: What can stimulated emission do for bioimaging? Ann. N.Y. Acad. Sci. *1293*, 1–7.

Weismann, M., Guse, A.H., Sorokin, L., Bröker, B., Frieser, M., Hallmann, R., and Mayr, G.W. (1997). Integrin-mediated intracellular Ca^{2+} signaling in Jurkat T lymphocytes. The Journal of Immunology *158*, 1618–1627.

Weiss, A., Wiskocil, R.L., and Stobo, J.D. (1984). The role of T3 surface molecules in the activation of human T cells: a two-stimulus requirement for IL 2 production reflects events occurring at a pre-translational level. J Immunol *133*, 123–128.

Westphal, V., Rizzoli, S.O., Lauterbach, M.A., Kamin, D., Jahn, R., and Hell, S.W. (2008). Video-rate far-field optical nanoscopy dissects synaptic vesicle movement. Science *320*, 246–249.

Wiltgen, S.M., Smith, I.F., and Parker, I. (2010). Superresolution Localization of Single Functional IP3R Channels Utilizing Ca^{2+} Flux as a Readout. Biophys J *99*, 437–446.

Woehrle, T., Yip, L., Elkhal, A., Sumi, Y., Chen, Y., Yao, Y., Insel, P.A., and Junger, W.G. (2010). Pannexin-1 hemichannel-mediated ATP release together with P2X1 and P2X4 receptors regulate T-cell activation at the immune synapse. Blood *116*, 3475–3484.

Wong, A.K.C., Capitanio, P., Lissandron, V., Bortolozzi, M., Pozzan, T., and Pizzo, P. (2013). Heterogeneity of Ca^{2+} handling among and within Golgi compartments. J Mol Cell Biol *5*, 266–276.

Wu, M.M., Buchanan, J., Luik, R.M., and Lewis, R.S. (2006). Ca2+ store depletion causes STIM1 to accumulate in ER regions closely associated with the plasma membrane. J Cell Biol *174*, 803–813.

Xing, Z., Chen, H.C., Nowlen, J.K., Taylor, S.J., Shalloway, D., and Guan, J.L. (1994). Direct interaction of v-Src with the focal adhesion kinase mediated by the Src SH2 domain. Mol Biol Cell *5*, 413–421.

Xiong, J., and Zhu, M.X. (2016). Regulation of lysosomal ion homeostasis by channels and transporters. Sci. China Life Sci. *59*, 777–791.

Xu, H., and Ren, D. (2015). Lysosomal physiology. Annu Rev Physiol *77*, 57–80.

Yang, Z., Samanta, S., Yan, W., Yu, B., and Qu, J. (2021). Super-resolution Microscopy for Biological Imaging. Adv Exp Med Biol *3233*, 23–43.

Yeung, P.S.-W., Yamashita, M., and Prakriya, M. (2020). Molecular basis of allosteric Orai1 channel activation by STIM1. J Physiol *598*, 1707–1723.

Yoo, J., Kim, J.-Y., Louis, J.M., Gopich, I.V., and Chung, H.S. (2020). Fast three-color single-molecule FRET using statistical inference. Nat Commun *11*, 3336.

York, A.G., Chandris, P., Nogare, D.D., Head, J., Wawrzusin, P., Fischer, R.S., Chitnis, A., and Shroff, H. (2013). Instant super-resolution imaging in live cells and embryos via analog image processing. Nat Methods *10*, 1122–1126.

Yoshida, Y., and Imai, S. (1997). Structure and Function of Inositol 1, 4, 5-Trisphosphate Receptor. The Japanese Journal of Pharmacology *74*, 125–137.

Yoshikawa, F., Morita, M., Monkawa, T., Michikawa, T., Furuichi, T., and Mikoshiba, K. (1996). Mutational analysis of the ligand binding site of the inositol 1,4,5-trisphosphate receptor. J Biol Chem *271*, 18277–18284.

Yoshikawa, F., Iwasaki, H., Michikawa, T., Furuichi, T., and Mikoshiba, K. (1999). Cooperative formation of the ligand-binding site of the inositol 1,4, 5-trisphosphate receptor by two separable domains. J Biol Chem *274*, 328–334.

Yu, E., and Sharma, S. (2021). Physiology, Calcium (StatPearls Publishing).

Zarbock, A., Abram, C.L., Hundt, M., Altman, A., Lowell, C.A., and Ley, K. (2008). PSGL-1 engagement by E-selectin signals through Src kinase Fgr and ITAM adapters DAP12 and FcRγ to induce slow leukocyte rolling. J Exp Med *205*, 2339–2347.

Zhang, J., Guan, X., Shah, K., and Yan, J. (2021). Lsm12 is an NAADP receptor and a two-pore channel regulatory protein required for calcium mobilization from acidic organelles. Nat Commun *12*, 4739.

Zhang, S.L., Yu, Y., Roos, J., Kozak, J.A., Deerinck, T.J., Ellisman, M.H., Stauderman, K.A., and Cahalan, M.D. (2005). STIM1 is a Ca^{2+} sensor that activates CRAC channels and migrates from the Ca^{2+} store to the plasma membrane. Nature *437*, 902–905.

Zhang, S.L., Yeromin, A.V., Zhang, X.H.-F., Yu, Y., Safrina, O., Penna, A., Roos, J., Stauderman, K.A., and Cahalan, M.D. (2006). Genome-wide RNAi screen of Ca^{2+} influx identifies genes that regulate Ca^{2+} release-activated Ca^{2+} channel activity. Proc Natl Acad Sci U S A *103*, 9357–9362.

Zhang, X., Chattopadhyay, A., Ji, Q.S., Owen, J.D., Ruest, P.J., Carpenter, G., and Hanks, S.K. (1999). Focal adhesion kinase promotes phospholipase C-gamma1 activity. Proc Natl Acad Sci U S A *96*, 9021–9026.

Zheng, S., Ma, G., He, L., Zhang, T., Li, J., Yuan, X., Nguyen, N.T., Huang, Y., Zhang, X., Gao, P., et al. (2018). Identification of molecular determinants that govern distinct STIM2 activation dynamics. PLoS Biol *16*, e2006898.

Zhou, J., and Rossi, J. (2017). Aptamers as targeted therapeutics: current potential and challenges. Nat Rev Drug Discov *16*, 181–202.

Zhou, Y., Cai, X., Nwokonko, R.M., Loktionova, N.A., Wang, Y., and Gill, D.L. (2017). The STIM-Orai coupling interface and gating of the Orai1 channel. Cell Calcium *63*, 8–13.

Zhou, Y., Nwokonko, R.M., Cai, X., Loktionova, N.A., Abdulqadir, R., Xin, P., Niemeyer, B.A., Wang, Y., Trebak, M., and Gill, D.L. (2018). Cross-linking of Orai1 channels by STIM proteins. PNAS *115*, E3398–E3407.

Zhou, Y., Nwokonko, R.M., Baraniak, J.H., Trebak, M., Lee, K.P.K., and Gill, D.L. (2019). The remote allosteric control of Orai channel gating. PLoS Biol *17*, e3000413.

Zweifach, A., and Lewis, R.S. (1993). Mitogen-regulated Ca2+ current of T lymphocytes is activated by depletion of intracellular Ca^{2+} stores. Proc Natl Acad Sci U S A *90*, 6295–6299.

7. Publications and poster presentations

Publications

Gu, F.*, Krüger, A.*, Roggenkamp, H.*, Alpers, R., Dmitri Lodygin[2], Vincent Jaquet[3], Möckl, F., **Hernandez L.**, Winterberg, K., Bauche, A., Rosche, A., Flügel, A., Diercks, B.P., Guse, A. 2021 “Dual NADPH oxidases DUOX1 and DUOX2 synthesize NAADP and are necessary for Ca^{2+} signaling during T cell activation”. Sci Signal 14, eabe3800.

* These authors contributed equally to this work.

Roggenkamp, H.G.*, Khansahib, I.*, **Hernandez, L.C**.*, Zhang, Y.*, Lodygin, D., Krüger, A., Gu, F., Möckl, F., Löhndorf, A., Wolters, V. 2021 “HN1L/JPT2: A signaling protein that connects NAADP generation to Ca^{2+} microdomain formation”. Sci. Signal. 14, eabd5647

* These authors contributed equally to this work.

Diercks, B.-P., Werner, R., Weidemüller, P., Czarniak, F., **Hernandez, L.**, Lehmann, C., Rosche, A., Krüger, A., Kaufmann, U., Vaeth, M. 2018 “ORAI1, STIM1/2, and RYR1 shape subsecond Ca^{2+} microdomains upon T cell activation”. Sci Signal 11, eaat0358.

Poster Presentations

Lola Hernandez[1], Antonio Virgilio Failla[2], Andreas H. Guse[1], Björn-Ph. Diercks[1] (**2021**) Comparison of advanced optical method to determine localization of proteins. Junior *European Calcium Society* (ECS) board, 23-24 November 2021, virtual participation

Lola Hernandez[1], Antonio Virgilio Failla[2], Andreas H. Guse[1], Björn-Ph. Diercks[1](**2021**)

Adhesion-dependent T cell priming via FAK-PLC-γ pathway and SOCE activation demonstrated by advanced optical methods. Federation of American Societies (FASEB), 26-28 October 2021, virtual participation

Lola Hernandez[1], Mariella Kessler[1], Anke Löhndorf[1], Antonio Virgilio Failla[2], Andreas H. Guse[1], Björn-Ph. Diercks[1] (**2021**) Adhesion-dependent T cell priming via FAK-PLC-γ pathway and SOCE activation demonstrated by advanced optical methods. 74th Annual Society of General Physiologists (SGP) Symposium, 22-26 September 2021, Woods Hole, Massachusetts, USA (virtual participation)

Lola Hernandez[1], Marie Bischof[1], Anette Rosche[1], Antonio Virgilio Failla[2], Bernd Zobiak[2], Andreas H. Guse[1], Björn-Ph. Diercks[1] Diercks (**2020**) ORAI1, STIM1/2 *and* RYR *form functional clusters already before T cell activation*. *India-EMBO Symposium*, 26-29 January 2020, Bangalore, India

Lola Hernandez[1], Marie Bischof[1], Anette Rosche[1], Antonio Virgilio Failla[2], Bernd Zobiak[2], Andreas H. Guse[1], Björn-Ph. Diercks[1] (**2018**) ORAI1 and STIM1 form functional clusters already before T cell activation. *Conference of European Calcium Society*, September 2018, Hamburg

Eidesstattliche Versicherung

Name: Hernandez Cabrera Vorname: Lola Carmen

Hiermit erkläre ich an Eides statt, dass ich die vorliegende Dissertationsschrift selbst verfasst und keine anderen als die angegebenen Quellen und Hilfsmittel benutzt habe.

Hamburg, 09.02.2022

Ort, Datum Unterschrift

Acknowledgements

First of all, my special thanks go to Prof. Dr. Andreas H. Guse, who, as head of the Department of Biochemistry and Molecular Cell Biology, made it possible for me to complete this thesis. Furthermore, I would like to thank him for the motivating and always excellent supervision and active support.

I would like to thank Prof. Dr. Hans Will Mitrücker for the evaluation of my thesis.

Moreover, I would like to thank our collaboration partner Dr. Antonio Virgilio Failla for the opportunity to perform the STED experiments in his core-facility. Especially I would like to thank Virgilio for his support.

I thank all my colleagues of the Calcium Signalling Group, especially Björn-Philipp Diercks, Mariella Weiß, and Ralf Fliegert for their everlasting willingness to help, for their kind support and discussion of scientific, experimental and other problems. My thanks also go to Markus Heine, who provided me with spleens and lymph nodes for my experiments. Last but not least, I would like to thank the whole group for the excellent and very motivating working atmosphere, which made time fly in no time.

Finally, a very big thank you goes to my mother for her constant support in my private and working life. Without her, I would never have made it this far.